NOVEL STRATEGIES TO ENHANCE LPL ACTIVITY *IN VIVO*

Aspen Rene Gutgsell

A dissertation submitted to the faculty of the University of North Carolina at Chapel Hill in partial fulfillment of the requirements of the degree of Doctor of Philosophy in the Department of Biochemistry and Biophysics.

Chapel Hill
2020

Approved by:

Saskia Neher

Albert Bowers

Sharon Campbell

Brian Kuhlman

Gary Pielak

ABSTRACT

Aspen Rene Gutgsell: Novel Strategies to Enhance LPL Activity *In Vivo*
(Under the direction of Saskia Neher)

Lipoprotein lipase (LPL) is required for the clearance of triglycerides (TG) from the bloodstream. LPL is anchored to the walls of blood vessels where it undergoes conformational changes to engage TG-rich lipoprotein particles, hydrolyze TG within the particle, and release free fatty acids. LPL activity is tightly regulated in a nutrient-dependent manner to coordinate the delivery of free fatty acids to specific tissues. The unique ability of LPL to directly control plasma TG levels makes it a good target for specific TG-lowering therapeutics. However, directly targeting LPL may be a difficult as it has several regulatory partners and disruption of activators or its endothelial anchor will abolish LPL activity. Alternatively, pharmacologic modulation of proteins that regulate LPL has been shown to dramatically lower plasma TG levels in both preclinical animal models and human clinical trials. One approach is to inactivate a subset of LPL inhibitory proteins, known as angiopoietin-like protein 3 or 4 (ANGPTL3, 4). Despite not knowing the molecular mechanism for how ANGPTL3 inhibits LPL, anti-ANGPTL3 monoclonal antibodies have shown great promise in clinical trials for severe HTG. The molecular mechanism for ANGPTL4-mediated inhibition of LPL has been more thoroughly investigated; however, therapeutic strategies that result in complete loss of ANGPTL4 have not been successful in preclinical animal models.

This thesis aims to better understand the molecular mechanism of LPL inhibition by ANGPTL3 and ANGPTL4 and use this information to enhance the activity of LPL *in vivo*. To better understand the molecular mechanisms of ANGPTL-mediated inhibition of LPL, we i)

performed biophysical experiments to compare ANGPTL3 and ANGPTL4 *in vitro*, ii) looked for differences in LPL inhibition and iii) identified ANGPTL4 binding sites on LPL. Lastly, we sought to improve upon existing ANGPTL4 inhibitors by generating a domain-specific inhibitor of ANGPTL4 to prevent LPL inhibition. Overall, we have identified LPL variants with ANGPTL4 resistance and an anti-ANGPTL4 single domain antibody for inactivation of the N-terminal domain of ANGPTL4. These results could have implications for future biologic-based therapeutics for hypertriglyceridemia and acute pancreatitis.

ACKNOWLEDGEMENTS

I would like to sincerely thank everyone who has made the work described in this dissertation possible. First and foremost, I want to thank Saskia Neher for giving me the tremendous opportunity to work in her lab. Saskia has been instrumental in this journey and my gratitude for her support and excellent mentorship cannot be properly summarized in words. Her belief in me has enabled me to achieve more than I thought possible. Thank you to my colleagues in the Neher lab who have given me the great privilege of working in a welcoming, supportive, and joyful environment. I want to especially thank Albert Bowers and my colleagues in his laboratory for their gracious support and brilliant mentorship. My time in the Bowers lab is something I will always cherish as it was a tremendous learning opportunity that truly shaped my scientific training. I also want to express gratitude to Brian Kuhlman and my colleagues in his laboratory. It is amazing that no matter how busy the Kuhlman lab is, they have always taken the time to help me. Time is one of the most valuable things you can give someone and my gratitude for the time that Saskia Neher, Albert Bowers, Brian Kuhlman, Sharon Campbell, Gary Pielak, my colleagues at UNC, and my family is more than can be expressed in words. With my greatest sincerity, thank you to everyone who in their own way has contributed to the success of this work.

PREFACE

Part of this work were done in collaboration with other talented scientists. The work described in chapter 2 was originally published in the Journal of Biological Chemistry on 22 February 2019 and has been modified slightly for this dissertation. Aspen Gutgsell performed all molecular cloning, protein purification, biochemical characterization, and data analysis. Swapnil Ghodge synthesized, purified, and performed mass spectrometry analysis on all peptides described in this work. Hydrogen deuterium exchange mass spectrometry experiments were performed by Saskia Neher and Eric Soderblom at the Duke University Proteomics and Metabolomics Core Facility. This work was guided and funded by Saskia Neher and Albert Bowers.

The work described in chapter three covers our unpublished and ongoing efforts to develop an inhibitor of the N-terminal coiled-coil domain of ANGPTL4. Steven Fleming and Albert Bowers aided in the design and implementation of all mRNA display experiments. Stephan Kudlacek, David Thieker, and Brian Kuhlman aided in the design and implementation of all yeast display experiments. This work was funded by and performed under the direction of Saskia Neher, Albert Bowers, and Brian Kuhlman.

The work described in chapter four covers our ongoing efforts to compare ANGPTL3 and ANGPTL4 from a biochemical and mechanistic perspective. Kathryn Gunn performed all molecular cloning, purification, and biochemical experiments using ANGPTL3. Aspen Gutgsell performed purification and biochemical experiments involving ANGPTL4 and LPL chimeric mutants. Caitlin Johnson performed the heparin LPL activity assays. Yongmei Xu synthesized and prepared all heparin fragments. The work was overseen and funded by Saskia Neher and Jian Liu.

TABLE OF CONTENTS

LIST OF TABLES

LIST OF FIGURES

LIST OF ABBREVIATIONS

ANGPTL	Angiopoietin-like protein
ApoA-V	Apolipoprotein A-V
ApoB-48	Apolipoprotein B-48
ApoB-100	Apolipoprotein B-100
ApoC-I	Apolipoprotein CI
ApoCII	Apolipoprotein CII
ApoCIII	Apolipoprotein CIII
ApoE	Apolipoprotein E
ASO	Antisense oligonucleotide
BSA	Bovine serum albumin
DGGR	1,2-Di-O-lauryl-rac-glycero-3-(glutaric acid 6-methylresorufin ester)
DMSO	Dimethyl sulfoxide
EDTA	Ethylenediaminetetraacetic acid
EL	Endothelial lipase
ER	Endoplasmic reticulum
FBS	Fetal bovine serum
FCS	Familial chylomicronemia syndrome
FFA	Free fatty acids
FITC	Fluorescein isothiocyanate
GPIHBP1	Glycosylphosphatidylinositol anchored high density lipoprotein binding protein 1
HA	Hemagglutinin
HDL	High density lipoprotein
HDX-MS	Hydrogen deuterium exchange mass spectrometry
HEK	Human embryonic kidney cells

HL	Hepatic lipase
HoFH	Homozygous familial hypercholesterolemia
HSPG	Heparan sulfate proteoglycan
HTG	Hypertriglyceridemia
IDL	Intermediate-density lipoprotein
LDL	Low-density lipoprotein
LDLR	Low-density lipoprotein receptor
LMF1	Lipase maturation factor 1
LPL	Lipoprotein lipase
LRP1	LDL receptor-related protein
MACS	Magnetic activated cell sorting
MALS	Multiangle light scattering
MTP	Microsomal triglyceride transfer protein
NEM	N-ethylmaleimide
PCSK9	Proprotein convertase subtilisin kexin type 9
PPI	Protein-protein interaction
SAXS	Small angle x-ray scattering
SEC	Size exclusion chromatography
TAMRA	Tetramethylrhodamine
TCEP	Tris(2-carboxyethyl)phosphine hydrochloride
TG	Triglycerides
VLDL	Very-low-density-lipoprotein

CHAPTER 1

Mechanistic review of lipoprotein lipase and emerging strategies for treating hypertriglyceridemia

1.1 Overview of triglyceride metabolism

Fatty acids contained within a glycerol backbone, or triglycerides (TG), are a vital source of energy. The chemical properties of TG molecules make them an extremely efficient moiety for long term energy storage. However, these same properties make them difficult to store and transport within water-based systems (1). Fortunately, vertebrates have evolved elegant mechanisms for storing and transporting these extremely hydrophobic molecules. TG are solubilized in specialized tissues within dedicated organelles and transported within specific plasma lipoprotein particles (1).

Chylomicrons and VLDL production - TG are sourced for metabolism from two pathways: exogenous (dietary) and endogenous (hepatic) (2). Dietary TG are first emulsified by bile salts within the small intestine and hydrolyzed into free fatty acids (FFA) by pancreatic lipase. FFA are absorbed by enterocytes and transported to the ER for esterification into TG (Figure 1.1A). Within the ER, microsomal triglyceride transfer protein (MTP) assembles TG, cholesterol esters, and apolipoprotein B-48 (apoB-48) into nascent chylomicrons (3). Chylomicrons are transported to the Golgi for secretion into lymphatic circulation and enter the bloodstream through the subclavian vein (Figure 1.1A) (3). In circulation, chylomicrons mature by acquiring apolipoprotein C-II (apoC-II) and apolipoprotein E (apoE) from high-density lipoprotein (HDL) particles (3).

The second pathway assembles endogenous TG into very-low-density lipoprotein (VLDL) particles and secretes them directly into circulation from the liver. In a similar process as enterocytes, hepatocytes esterify FFA into TG using diacylglycerol O-acyltransferases within the ER membrane (4). MTP assembles apolipoprotein B-100 (apoB-100), cholesterol esters, and TG into VLDL particles

(Figure 1.1B). Nascent VLDL particles are secreted from the liver directly into the bloodstream and mature by acquiring apoC-II and apoE from HDL. Unlike enterocytes, hepatocytes can obtain FFA from three different sources: i) direct absorption of FFA from the plasma, ii) uptake of remnant chylomicrons and iii) uptake of dietary medium-chain fatty acids (2).

Chylomicron and VLDL clearance – TG-rich lipoproteins are large particles that cannot be removed from circulation without being broken down. Lipoprotein lipase (LPL) is the rate-limiting enzyme in plasma TG clearance (5). LPL is primarily produced in the parenchymal cells of the skeletal muscle, heart, and adipose tissue whereby its transcription, secretion, and post-secretory activity are tightly regulated in a nutrition-dependent manner (6, 7). Heparan sulfate proteoglycans (HSPGs) anchor freshly secreted LPL to the cell surface of parenchymal cells in the interstitial space. Glycosylphosphatidylinositol-anchored high-density lipoprotein binding protein 1 (GPIHBP1) preferentially displaces LPL from cell surface HSPGs and shuttles LPL into the capillary endothelium where it anchors it to the vessel walls (8). GPIHBP1-anchored LPL hydrolyzes TG within circulating VLDL and chylomicrons to release FFA into the plasma and surrounding tissues (Figure 1.1C) (9). In the vasculature, LPL activity is spatially and temporally regulated by several partner proteins to control the delivery of fatty acids to specific tissues. The mechanism of LPL regulation by each of these partner proteins will be discussed in detail in sections 1.1.2 and 1.1.3.

As LPL hydrolyzes TG within VLDL and chylomicron particles, the vesicles shrink to form intermediate-density lipoprotein particles (IDL) and chylomicron remnants, respectively (Figure 1.1C). These remnant lipoprotein particles are cleared from circulation upon binding to the

surface of the liver by HSPGs and internalized by the low-density lipoprotein receptor (LDLR) and LDL receptor-related protein 1 (LRP1) (Figure 1.1D). Alternatively, IDL can be further metabolized by hepatic lipase to form low-density lipoprotein particles (LDL). Interestingly, LPL has been shown to have a second role in TG metabolism that is independent of its catalytic activity. Enzymatically inactive LPL associates with remnant lipoprotein particles and facilitates hepatic uptake by directly binding LDLR and LRP1 (10, 11). The precise mechanism for how LPL becomes catalytically inactive and dissociates from GPIHBP1 is not entirely understood; however fatty acids and other LPL partner proteins have been shown to dissociate LPL from GPIHBP1 (12). Nonetheless, LPL-mediated uptake of remnant lipoproteins can significantly affect plasma TG levels as humans with an LPL gain of function mutation, S447X, have enhanced remnant lipoprotein uptake and lower average TG levels (11, 13).

Hypertriglyceridemia – Dyslipidemia occurs when the balance between lipoprotein production and lipoprotein clearance is altered or impaired. One of the most common forms of dyslipidemia is hypertriglyceridemia (HTG), or elevated plasma TG levels. HTG is an independent risk factor for cardiovascular disease (14). There are several drivers of HTG that contribute to its prevalence in ~27% of the general population (15). Drivers of HTG include obesity, metabolic disease, renal disease, autoimmune disease, and genetic mutations. Despite its association with cardiovascular disease, treatment for the majority of HTG cases is limited to adopting a low-fat diet with regular exercise (16). Pharmacologic intervention, in the form of fibrates or statins, is only considered for cases of very high HTG or if the patient has additional risk factors for cardiovascular disease (17). Current treatment options are not effective for everyone and the need for additional therapeutics has motivated several independent research groups to develop novel TG-lowering therapeutics. This chapter will provide an overview of our current structural and mechanistic understanding of LPL in TG metabolism and emerging biologic therapeutics for the treatment of HTG for the prevention of cardiovascular disease.

1.1.1 LPL structure

Historically, structural and biophysical studies of LPL have been limited by an inability to produce large quantities of catalytically active enzyme. Five intramolecular disulfide bonds and two N-linked glycosylation sites restrict LPL production to mammalian cell culture, where the overall purification yield is notoriously poor (18). LPL contains a furin protease cleavage site between its N- and C-terminal domain that inactivates it and diminishes the overall yield of enzymatically active lipase by several-fold. Therefore, our group generated a furin-resistant mutant of LPL (R324N) and found that co-expression with its ER-resident partner protein, lipase maturation factor 1 (LMF1), increased the overall quality and yield of LPL by over 20-fold (18). Since then, others have improved the yield of LPL such that two independent groups were able to produce enough LPL to solve the crystal structure of LPL in complex with GPIHBP1 (19, 20).

Birrane and colleagues produced up to 15 mg of furin-resistant LPL (R324A) upon co-expression with LMF1 in CHO cells and mixed with a two-fold molar excess of GPIHBP1 for crystallization (19). Their 2.8 Å resolution structure (PDB: 6E7K) revealed GPIHBP1 binds LPL in a 1:1 stoichiometry primarily through hydrophobic contacts at the C-terminal domain (Figure 1.2A). The N-terminal domain of LPL contains an α/β hydrolase fold, commonly found in lipases, with a serine protease-like catalytic triad, an oxyanion hole to coordinate fatty acid tails of the lipid substrate for hydrolysis, and an unresolved lid domain that covers the active site (Figure 1.2A). The 6E7K structure is missing electron densities for the first four amino acids of the mature protein (residues 28-31), residues 249-258 of the lid domain, residues 414-421 within the C-terminal tryptophan-rich lipid-binding region, and the last five amino acids of LPL (residues 471-475). Two LPL-GPIHBP1 complexes were arranged in a head-to-tail orientation within a crystallographic unit. The unresolved C-terminal tryptophan-rich lipid-binding region of one LPL molecule was predicted to interact with the catalytic pocket in the N-terminal domain of another LPL molecule. Although they could not resolve electron density at the proposed dimer interface, the authors conclude the 6E7K structure is consistent with previous studies suggesting LPL is a homodimer (19).

Arora and colleagues co-expressed wild type LPL with LMF1 and glycosylation deficient GPIHBP1 (N78D/N82D) in HEK293 Freestyle suspension cells (20). Although both groups had a slightly different approach for generating LPL-GPIHBP1 complexes, the resulting structures were very similar. However, Arora and colleagues were able to solve an additional 2.8 Å resolution structure that included the entire lid domain and lipid-binding region after soaking a novel inhibitor in the active site (PDB: 6OB0) (Figure 1.2B) (20). The 6OB0 structure revealed the lid and lipid-binding region create hydrophobic patches on the surface of LPL. The authors determined that none of their LPL-GPIHBP1 structures (PDB: 6OAZ, 6OAU, 6OB0) indicate the presence of a physiological LPL-LPL protein interface and conclude the LPL-GPIHBP1 complex is monomeric and provide biochemical evidence that this complex is enzymatically active (20).

LPL, purified from bovine milk by heparin-sepharose, was first described as a homodimeric enzyme by sedimentation equilibrium ultracentrifugation and analytical gel chromatography (21). Since then, nearly a dozen publications have supported the notion that enzymatically active LPL is a homodimer (22–32). This notion has only recently come into question with evidence that monomeric LPL in complex with GPIHBP1 is enzymatically active from three publications by two different research groups (20, 33, 34). Beigneux and colleagues performed sedimentation ultracentrifugation experiments and enzyme activity assays on LPL alone and in complex with GPIHBP1 and determined that catalytically active LPL exists as a monomer.

1.1.2 LPL enzymatic activation

Apolipoprotein C-II – The first activator of LPL was identified as apolipoprotein C-II (apoC-II) in 1970 (35, 36). ApoC-II is a small, α-helical protein that is almost exclusively expressed in the liver and small intestine (2). In circulation, apoC-II avidly binds to lipid surfaces of lipoprotein particles. TG-rich lipoproteins, like chylomicrons and VLDL particles, are hydrolyzed by apoC-II-activated LPL and form remnant lipoprotein particles. As the surface pressure on the lipoprotein

particle increases, apoC-II desorbs from the lipoprotein surface and transfers onto high-density lipoproteins (HDL) (37).

The crystal structure for apoC-II has not be solved, but secondary structure prediction and nuclear magnetic resonance analysis reveal that apoC-II is made up of three α-helices in the presence of lipid (38, 39). The first N-terminal α-helix is an amphipathic A-type helix that strongly associates with lipoproteins (37, 39, 40). The second helix is short and mostly appears to form random coils. The third C-terminal helix is a G-type helix that does not bind lipid as tightly as the N-terminal α-helix (37). Site-directed mutagenesis and synthetic peptide analysis suggest this C-terminal helix is primarily responsible for binding LPL at a 1:1 stoichiometry (41–43). The precise binding site for apoC-II on LPL is not known, but cross-linking studies suggest apoC-II binds near the lid domain of LPL and may displace the lid to facilitate TG entry to the catalytic site (44). Kinetically, apoC-II enhances LPL activity on TG-rich lipoprotein substrates with an estimated K_d of 22 nM (44, 45).

Genetic mutations resulting in apoC-II deficiency result in a rare, but severe form of HTG known as familial chylomicronemia syndrome (FCS). The most common cause of FCS is LPL deficiency, but loss of LPL partner proteins like LMF1, GPIHBP1, apoC-II, and apoA-V also cause FCS (46). Several apoC-II mutations are missense mutations within the first N-terminal α-helix that are predicted to abolish its ability to bind lipoproteins (2). Mutations in the third C-terminal helix likely abolish binding and activation of LPL (2). Unfortunately, the consequences of loss of LPL activity are severe as there are limited treatment options for patients with FCS (47).

Apolipoprotein A-V – Apolipoprotein A-V (apoA-V) is produced and secreted from the liver at sub-lipoprotein concentrations where just 4% of VLDL particles are estimated to carry one apoA-V molecule (48). Although apoA-V exists at low plasma concentrations, apoA-V deficiency results in severe HTG. Similar to other apolipoproteins, apoA-V is predicted to be primarily α-helical and has a high affinity for lipid membranes (49). *In vitro* and *in vivo* studies suggest apoA-V indirectly promotes LPL-mediated hydrolysis of TG-rich lipoproteins by forming a ternary

complex between the lipoprotein particle, endothelial cell surface HSPGs, and LPL (50). Additional evidence suggests apoA-V also stimulates the remnant lipoprotein uptake through interactions with LDLR and HSPG (51). Interestingly, LPL is known to also interact with LDLR to mediate remnant lipoprotein uptake but it is not known if apoA-V is involved in LPL-mediated lipoprotein uptake processes. Overall, the precise mechanism of apoA-V is not well understood but *in vitro* studies have shown that apoA-V alone does not activate LPL at physiological concentrations (45, 50).

1.1.3 LPL enzymatic inhibition

Apolipoprotein C-I – Apolipoprotein C-I (apoC-I) is a 6.6 kDa protein that is primarily expressed in the liver and, to some extent, expressed in the lung, skin, spleen, adipose, and brain tissues (52). Circulating apoC-I associates with chylomicrons, VLDL, and HDL and is present at a relatively high concentration of 10 mg/dL (53). Although, studies in both humans and mice have shown that increased expression of apoC-I results in HTG, loss of apoC-I in mice does not affect plasma lipid concentrations. Overexpression of the *APOC1* gene was shown to primarily increase VLDL concentrations by primarily inhibiting LPL activity and, to a lesser extent, inhibiting hepatic VLDL receptor-mediated uptake of VLDL particles (53). Using *in vitro* LPL activity assays, Larsson and colleagues demonstrated that the addition of exogenous apoC-I displaces LPL from both rat chylomicrons and Intralipid emulsions in a dose-dependent manner (54). The authors estimate that roughly 10-20% of the Intralipid substrate was covered with apoC-I, therefore, LPL expulsion from the substrate is unlikely attributed to steric effects. Rather, apoC-I is predicted to modify the surface properties of the lipid particles such that LPL can no longer bind (54).

Genetic variants in *APOC1* identified in human population studies are associated with TG levels, as well as, total cholesterol and LDL cholesterol. Hypomorphisms in the *APOC1* promotor, HpaI, have been shown to increase apoC-I expression by ~57% and, concomitantly, increase TG levels.

Angiopoietin-like protein 3-4-8 – Angiopoietin-like proteins (ANGPTL) are a family of proteins with similar domain architecture to angiopoietins (ANG) and have a diverse set of biological roles. Both ANG and ANGPTL share an N-terminal coiled-coil domain and a C-terminal fibrinogen-like domain. The ANG family are primarily involved in angiogenesis via their well-documented interactions with tyrosine kinase receptors, Tie1 and Tie2 (55). ANGPTL proteins are involved in lipid metabolism, inflammation, and angiogenesis independent of the Tie1 and Tie2 receptors (56). ANGPTL3, 4, and 8 have a prominent role in triglyceride metabolism as known inhibitors of LPL (57).

ANGPTL3 (54 kDa) and ANGPTL8 (22 kDa) are secreted glycoproteins that are almost exclusively expressed in the liver. ANGPTL3 expression is independent of nutritional status and it circulates in the blood in a full-length and a proteolytically cleaved N-terminal coiled-coil domain and a C-terminal fibrinogen-like domain. The C-terminal fibrinogen-like domain has been shown to interact with $\alpha_v\beta_3$ integrin and promotes angiogenesis in endothelial cells (58). Concomitantly, both full-length and the N-terminal coiled-coil domain are primarily responsible for LPL inhibition, giving ANGPTL3 a role in both TG metabolism and angiogenesis (59). ANGPTL8, to date, has only been shown to have a role in TG metabolism as its expression is specifically upregulated after feeding (60). Although ANGPTL3 is capable of inhibiting LPL on its own *in vitro,* its ability to inhibit LPL *in vivo* is largely dependent on the presence of ANGPTL8 after feeding. For example, the hypertriglyceridemic effect of ANGPTL3 overexpression in ANGPTL8 knockout mice is blunted and, likewise, the hypertriglyceridemic effect of ANGPTL8 overexpression in ANGPTL3 knockout mice is attenuated in the absence of ANGPTL3 (60–62). Furthermore, co-immunoprecipitation experiments suggest ANGPTL8 primarily circulates in complex with ANGPTL3 within the plasma (60). However, the molecular mechanism of ANGPTL3/8 complex formation and LPL inhibition is not well understood.

Even though ANGPTL3 alone can inhibit LPL *in vitro*, several independent studies report the potency of LPL inhibition is significantly enhanced in complex with ANGPTL8 (61–63). Multiple

groups have reported that ANGPTL3 and ANGPTL8 only form a complex when they are co-expressed *in vivo* or denatured and refolded together *in vitro* (61, 63). Given that both ANGPTL3 and ANGPTL8 are almost exclusively expressed in the liver, the dependence on co-expression for complex formation and LPL inhibition may explain why ANGPTL3 alone does not inhibit LPL. Before the discovery of ANGPTL8 in 2012, Ono and colleagues determined that the ability of ANGPTL3 to inhibit LPL both *in vitro* and *in vivo* was dependent on its heparin-binding motif within the N-terminal coiled-coil domain. Mutations within the heparin-binding motif inactivated ANGPTL3 and resulted in enhanced LPL activity and lower plasma TG levels in mice (59). The authors suggested the *in vivo* activity of ANGPTL3 may be suppressed when bound to proteoglycans and activated by interacting with another protein (59).

Human population and animal studies have been an important resource for understanding of the overall role of ANGPTL3/8 on lipid metabolism. Humans with loss of function mutations in ANGPTL3 have familial combined hypolipidemia with 17-27% lower TG levels, 9-12% lower LDL cholesterol levels, 0-4% lower HDL levels, and a 34-39% lower risk for coronary artery disease in heterozygous carriers (64–66). Hypolipidemia is replicated in mice and nonhuman primates treated with anti-ANGPTL3 monoclonal antibodies or ANGPTL3 targeted antisense oligonucleotides (64, 67, 68). Human ANGPTL8 variants have a slightly different lipid profile with increased plasma HDL cholesterol levels and decreased TG levels (69). The human phenotype is also replicated in animal studies where ANGPTL8 knockout mice or anti-ANGPTL8 antibody-treated nonhuman primates have lower plasma TG by ~65% and increased HDL cholesterol by ~30% (70). The difference in HDL levels after loss of ANGPTL3 versus ANGPTL8 is likely due to the fact that ANGPTL3 is an inhibitor of endothelial lipase (EL) and ANGPTL8 is not (68). EL has lipolytic activity against phospholipids and primarily hydrolyzes HDL particles (71). Overall, mouse knockout and overexpression studies suggest that after feeding ANGPTL8, in complex with ANGPTL3, inhibit LPL in oxidative tissues to direct dietary fatty acids to white adipose tissue for storage (70).

ANGPTL4 is a 45 kDa secreted glycoprotein whose expression is detected in several types of tissues but is most abundantly expressed in adipose and the liver (72). Unlike ANGPTL3 and ANGPTL8, ANGPTL4 is capable of inhibiting LPL on its own and its expression is specifically upregulated during periods of fasting (73). Similar to ANGPTL3, ANGPTL4 is secreted into the plasma as both full-length and a proteolytically cleaved N-terminal coiled-coil domain and a C-terminal fibrinogen-like domain. The C-terminal fibrinogen-like domain binds $\alpha_v\beta_3$, β_1, and β_5 integrins, fibronectin, and vitronectin with roles in regulating endothelial cell adhesion, migration, and angiogenesis (74–76). Both the full length and the cleaved N-terminal coiled-coil domain are responsible for LPL inhibition (77). The multitude of ANGPTL4 partner proteins make it the most physiologically versatile among its ANGPTL family members (56).

There is some controversy surrounding the molecular mechanism of ANGPTL4-mediated inhibition of LPL. Sukonina and colleagues first reported that the cleaved N-terminal coiled-coil domain of ANGPTL4, herein referred to as nANGPTL4, is an irreversible inhibitor of LPL that dissociates active LPL dimers into inactive, unfolded monomers (78). In 2013, Lafferty and colleagues expressed concern over this mechanism (79). The concern surrounded the fact that on its own, purified LPL is prone to thermal unfolding and inactivation (25). Purified LPL requires additives for stabilization to effectively measure its kinetic activity *in vitro* (80, 81). Sukonina *et al*. used heparin to stabilize LPL and Lafferty *et al.* used deoxycholate. The authors were not convinced that LPL was sufficiently stabilized in a number of the assays performed by Sukonina *et al.* and suggested that this may have resulted in the misinterpretation of the molecular mechanism for inhibition. Lafferty and colleagues found that deoxycholate-stabilized LPL is reversibly, noncompetitively inhibited by nANGPTL4 (79). Both mechanisms have been supported by additional studies and between the different models, the concentration of nANGPTL4 required for LPL inhibition is nearly an order of magnitude different where heparin-stabilized LPL is inhibited by low nanomolar concentrations of nANGPTL4 and deoxycholate-stabilized LPL is inhibited by low micromolar concentrations (11, 18, 82–85). In 2009, it was shown

that GPIHBP1 protects LPL from nANGPTL4 inhibition, however, the highest concentration tested was just 20 nM of nANGPTL4 (82). In contrast, Hayne and colleagues found that even in the absence of deoxycholate, GPIHBP1 did not protect LPL from nANGPTL4 inhibition at low micromolar concentrations (11). Overall, conflicting data surrounding the mechanism of ANGPTL4 inhibition of LPL may largely depend on the method for LPL stabilization and the answer to the actual mechanism will likely be found in physiologically-relevant assay conditions.

GPIHBP1 has largely been demonstrated to be the most physiologically relevant stabilizer of LPL (82, 86). Within the vasculature, the vast majority of catalytically active LPL is bound to GPIHBP1. The most recent proposed molecular mechanism of ANGPTL4 inhibition of LPL was published in 2015 where Chi and colleagues revealed that both full-length and nANGPTL4 bind LPL and dissociate it from GPIHBP1. This work was recently supported with compelling evidence by Nimonkar and co-workers showing an LPL-GPIHBP1 covalent fusion protein is resistant to inhibition of full-length ANGPTL4. Both Chi and Nimonkar show strong evidence that ANGPTL4 binds LPL where previous studies using heparin-stabilized LPL were unable to observe evidence of nANGPTL4-LPL complex formation (78, 87). Nimonkar and colleagues revealed ANGPTL4 out competes GPIHBP1 for binding LPL. However, we do not know if ANGPTL4 remains bound to LPL after dissociation or if this mechanism of inhibition is reversible. Interestingly, ANGPTL4 is present in LPL-bound LDL fractions in plasma of mice overexpressing ANGPTL4 (88). Perhaps ANGPTL4 remains bound to LPL following GPIHBP1 dissociation to temporally alter LPL-mediated uptake of apoB-containing lipoproteins.

Similar to ANGPTL8, genetic mutations resulting in loss ANGPTL4 confer a cardioprotective lipid profile with decreased TG levels and increased HDL levels (89, 90). Human carriers of inactivating ANGPTL4 mutations have a decreased risk of coronary artery disease (89). ANGPTL4 knockout mice and anti-ANGPTL4 monoclonal antibody-treated nonhuman primates replicate human lipid phenotypes and are protected from coronary artery disease (89, 91). However, the complete loss of ANGPTL4 in animal models results in severe mesenteric

lymphadenopathy when maintained on a high-fat diet (89, 91, 92). To date, no humans with complete loss of ANGPTL4 have been reported (90, 93, 94). All variants are either heterozygous or homozygous for missense mutations that do not abolish ANGPTL4 expression or secretion (93). Overall, a combination of human and mouse knockout/overexpression studies suggest ANGPTL4 acts as a local inhibitor of LPL during periods of fasting to direct TG-rich lipoproteins away from white adipose tissue for oxidative catabolism (88, 95–97). Additional studies support the notion that ANGPTL4 acts as a local inhibitor of LPL such that during cold exposure, ANGPTL4 expression is downregulated in brown adipose tissue by AMPK and concomitantly upregulated in the white adipose tissue (98). During periods of exercise, human studies have shown that ANGPTL4 is upregulated in nonexercising muscle or liver to potentially direct TG lipolysis to the exercising muscle (99, 100). In concert ANGPTL3/8 and ANGPTL4 precisely regulate LPL in a tissue-specific manner to ensure that energy-rich TG are utilized efficiently as an important source of fuel (57).

1.2 Emerging biologic therapeutics for the prevention of cardiovascular disease

1.2.1 Overview of current biologics for dyslipidemia

Biologics are defined as a class of therapeutics sourced from a living system, meaning they are either nucleic acid or amino acid-based (101). The market is primarily composed of monoclonal antibodies, vaccines, recombinant proteins, antisense oligonucleotides, and RNA interference molecules for indications in infectious disease, oncology, immunology, and autoimmune disease (102). In 2018, the biologics market was valued at $251.5 million and the market value is projected to grow by nearly 12% by 2026 (102).

The area of dyslipidemia has interesting roots in the biologics market as the first-ever approved gene therapy in 2012 was for the treatment of LPL deficiency, or FCS (103). Since then, only five biologics have come to market for the treatment of dyslipidemia. Mipomersen is an antisense oligonucleotide targeted against apo-B100 mRNA that was approved by the FDA in 2013 for the treatment homozygous familial hypercholesterolemia (HoFH) (104). However, is only

available to a restricted group of patients because preventing the translation of apoB-100 and secretion of VLDL particles seriously increases the risk for hepatic steatosis and hepatotoxicity. Sebelipase alfa, an enzyme replacement therapy for the treatment of a rare lysosomal acid lipase deficiency, was approved by the FDA in 2015 (103). Evolocumab and alirocumab are two monoclonal antibodies for the treatment of hypercholesterolemia that were approved by the FDA in 2015 (105). Both antibodies target proprotein convertase subtilisin kexin type 9 (PCSK9) and concomitantly reduce LDL cholesterol levels by up to 60% (104). PCSK9 is a protease responsible for the degradation of LDLR, therefore, PCSK9 inhibitors are an effective strategy for increasing LDLR recycling and enhance LDL clearance (106).

1.2.1 Investigational biologics for hypertriglyceridemia

Volanesorsen – Apolipoprotein C-III (apoC-III) is an 8.8 kDa glycoprotein produced in the liver and small intestine. Like other apolipoproteins, it circulates in the plasma on the surface of chylomicrons, VLDL, LDL and HDL particles (107). Plasma concentrations of apoC-III are positively associated with plasma TG levels and risk for coronary artery disease, such that humans with loss of function variants have low TGs concomitant with a lower risk for coronary artery disease than noncarriers (107, 108). Given the clinical benefit of genetic loss apoC-III, Ionis Pharmaceuticals and Akcea Therapeutics developed volanesorsen, a second-generation antisense oligonucleotide (ASO) against apoC-III mRNA for the treatment of severe HTG.

The mechanism for apoC-III-mediated HTG has been somewhat controversial over the years. ApoC-III seems to have multiple roles in TG metabolism, but early *in vitro* studies suggested apoC-III primarily increase TG levels by inhibiting LPL. The proposed mechanism for LPL inhibition was similar to that of apoC-I, where apoC-III displace LPL from TG-rich lipoproteins in a dose-dependent manner (54). Although this mechanism could be true, ASO studies suggest that the primary effect of apoC-III on TG metabolism is independent of LPL inhibition. Volanesorsen was tested in patients with severe HTG resulting from loss-of-function mutations in LPL (109). The treated subjects experienced 71-90% reductions in apoC-III

concomitant with 56 – 86% decrease in TG levels (110). Therefore, it was hypothesized that apoC-III primary mode of action may be by inhibition of hepatic VLDL uptake. This model was tested by administering volanesorsen to mice lacking the *Ldlr* and *Lrp1* genes. The lipid-lowering effect of the ASO was abolished in mice lacking LDLR and LRP1, suggesting apoC-III primarily increase plasma TG by inhibiting hepatic uptake of VLDL particles, rather than LPL inhibition (111).

Volanesorsen is a gapmer family ASO where the core nucleotides are deoxynucleotides and the flanking nucleotides are 2'-O-2-methoxyethyl-modified nucleotides (112). Furthermore, all cytidine residues are modified with 5-methyl groups. This formulation enhances the ASO half-life by preventing degradation from nucleases and allows pairing at the 3' untranscribed region of *APOC3* mRNA and causes duplex degradation by ribonuclease H1 (112). To date, volanesorsen has completed two phase III clinical trials in patients with severe HTG or FCS. Both studies administered volanesorsen as a subcutaneous injection once weekly. In the FCS cohort, 62% of the subjects had LPL mutations and after 12 weeks of treatment patients experienced an 84% decrease in apoC-III levels concomitant with 77% decrease in plasma TG levels (110). The most common adverse outcomes in the study was injection site reaction (61%) and thrombocytopenia, or low platelet count (45%) (109). Five subjects left the trial due to increased bleeding risk from thrombocytopenia, others also experienced decreased platelet count but were able to continue in the trial.

Overall, the successful completion of phase III clinical trials for volanesorsen resulted in approval for the treatment of FCS in Europe by the European Medicines Agency (EMA). However, the FDA rejected volanesorsen for the treatment of FCS due to increased risk of bleeding from thrombocytopenia in September 2018. The precise cause of thrombocytopenia is not entirely known. Population studies have revealed that humans with loss of function mutations in apoC-III have not been observed to have an increased risk for thrombocytopenia,

rather, thrombocytopenia has been reported as an adverse side effect with other ASO therapeutics (113, 114).

Evinacumab – A monoclonal antibody targeted against ANGPTL3, evinacumab, is a promising therapeutic for hypercholesterolemia and HTG. After successful completion of phase II clinical trials in homozygous familial hypercholesterolemia (HoFH), the EPA designated evinacumab as a breakthrough therapy for HoFH (110). The majority of HoFH patients are intensively treated with combinations of statins, PCSK9 inhibitors, and other approved cholesterol-lowering medications but still have high levels of LDL cholesterol due to loss of function mutations in LDLR (115). Current cholesterol-lowering therapeutics block LDL production, dietary absorption, or enhance LDL clearance via LDLR. However, these therapies are not usually enough to lower cholesterol in patients with HoFH as clearance of LDL cholesterol is severely impaired without LDLR.

Fortunately, evinacumab lowered LDL cholesterol levels by a mean of 49%, TG decreased by 47%, and HDL cholesterol decreased by 36% after four weeks of treatment in phase II clinical trials in HoFH patients (115). From preclinical animal studies, we know that loss of ANGPTL3 results in a dramatic decrease in TG and HDL cholesterol levels due to reduced hepatic secretion of VLDL and enhanced activity of LPL and EL (116, 117). The mechanism for reduced LDL cholesterol is less clear but may be due to increased clearance of LDL precursor lipoproteins through a pathway independent of LDLR, LRP1, apoE, or syndecan-1 (117). Herein to date, evinacumab has successfully completed phase III clinical trials for HoFH and is in phase II clinical trials for severe HTG (118). Regeneron is expected to submit its clinical trial results to regulatory agencies and bring evinacumab to market pending FDA approval (118).

AKCEA-ANGPTL3-L$_{RX}$ - Ionis Pharmaceuticals and Akcea Therapeutics have developed a second-generation GalNAc-conjugated ASO against ANGPTL3 mRNA (67). GalNAc conjugation enhances ASO uptake in hepatocytes by ~10 fold via the asialoglycoprotein receptor (119). Phase I clinical trials of ANGPTL3-L$_{RX}$ lowered TG by ~55% and LDL cholesterol

decreased by ~30% (67). The ASO was well-tolerated and animal studies suggest an ANGPTL3 targeted ASO differs in some respects to anti-ANGPTL3 antibodies. ANGPTL3-L_{RX} treated mice were protected from mipomersen- induced hepatic steatosis (67). Therefore, Ionis is currently testing ANGPTL3-L_{RX} in phase II clinical trials for non-alcoholic fatty liver disease, FCS, familial partial lipodystrophy, type 2 diabetes, and HTG.

D6PV peptide - Remaley and colleagues developed a peptide mimetic of apoC-II for the potential treatment of HTG (120). As mentioned in section 1.1.2, apoC-II is composed of three α-helices where the N-terminal helix is responsible for binding to the surface of lipoproteins, the middle contains a random coil, and the C-terminal helix binds LPL. Their apoC-II mimetic, D6PV, contains the random coil region and the C-terminal helix (residues 40-79) with modifications at 8 positions (120). Preclinical *in vitro* and mouse studies revealed that D6PV binds VLDL and HDL particles, activates LPL, and antagonizes the ability of apoC-III to increase TG. Circulating lipoprotein particles typically contain both apoC-II and apoC-III molecules on their surface. D6PV competes apoC-III and full-length apoC-II off VLDL and HDL particles, resulting in reduced apoC-III concentrations by up to 80% (120). The D6PV peptide has enhanced potency to activate LPL over native full-length apoC-II and, therefore, treatment with D6PV effectively lowered TG by more than 80% in two different mouse models by two distinct mechanisms (120).

Although peptide therapeutics typically have short plasma half-lives, D6PV circulates on HDL particles, which extended its half-life to ~42-50 hours in nonhuman primates (120, 121). To date, the long-term safety and efficacy of the D6PV peptide has not been tested in nonhuman primates. Therefore, it is unclear if D6PV will be developed into a TG-lowering therapeutic for humans, but the preclinical data looks promising.

1.2.2 Future perspectives

Despite the widespread success of statin therapy, cardiovascular disease is still the number one cause of death worldwide (14). Biologics have enormous potential to improve lipid-

lowering regimes and lower the occurrence of cardiovascular disease. In the coming years, the repertoire for treating HTG is expected to expand with an array of promising biologics in preclinical and clinical development (110).

When it comes to developing TG-lowering therapeutics, there are three possible mechanisms to target: i) block dietary absorption, ii) prevent VLDL secretion, or iii) enhance TG-rich lipoprotein clearance. Some approaches inherently come with more risks than others. Blocking TG absorption or secretion can result in oily/fatty stool or the development of hepatic steatosis and toxicity (122, 123). Several promising pharmacologic approaches that modulate LPL partner proteins safely lower TG via enhanced LPL activity in preclinical and clinical trials (68, 70, 120, 124). However, it remains to be seen if prolonged enhancement of LPL activity, either systemically or in localized tissues, will lead to adverse outcomes after long-term treatment.

1.3 Figures

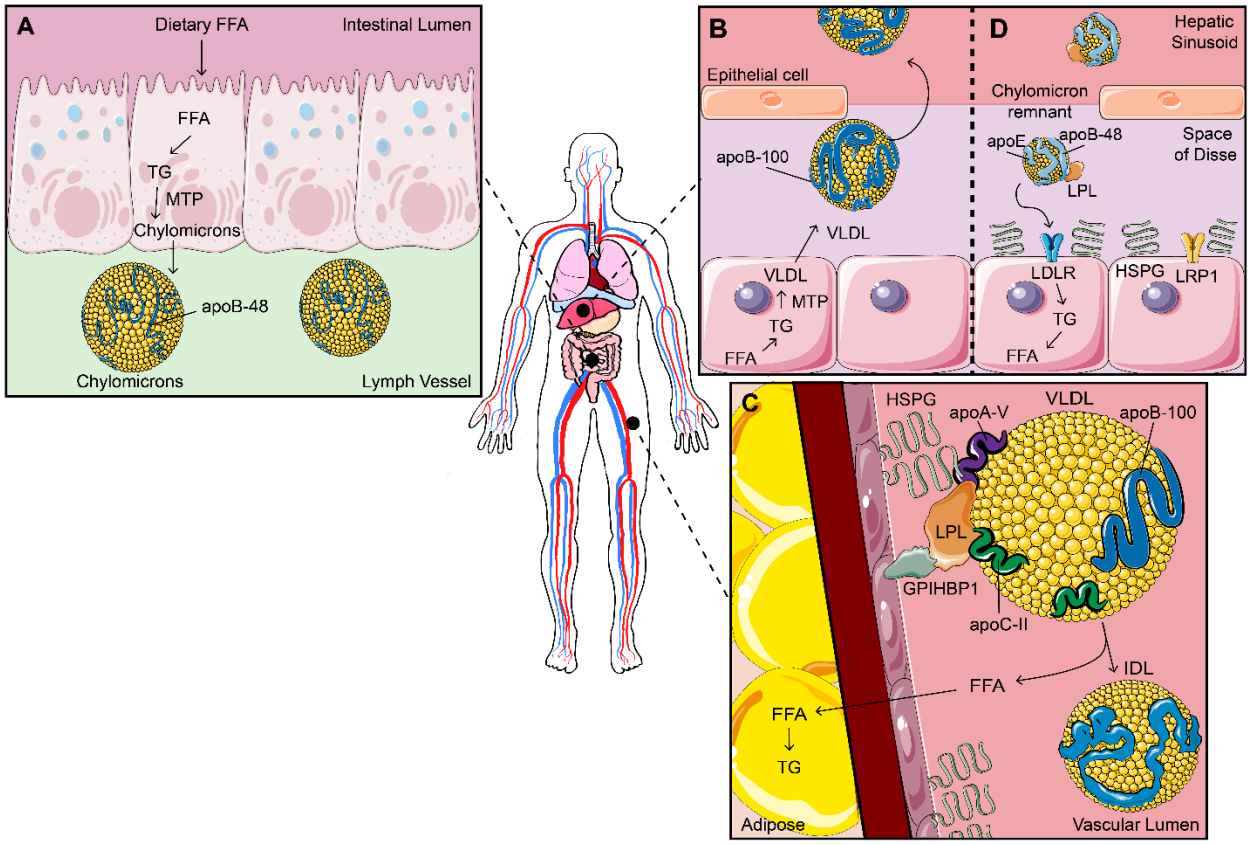

Figure 1.1 Overview of triglyceride metabolism. A) Dietary TG are emulsified by bile salts in the duodenum where colipase activated pancreatic lipase hydrolyzes them. Free fatty acids (FFA) are taken up by enterocytes, esterified into to TG by DGAT1 and 2 within the ER membrane, and packaged into nascent chylomicrons with apolipoproteins and cholesterol by MTP (4). Nascent chylomicrons are secreted into lymph vessels and later enter blood circulation through the subclavian vein (3). B) Hepatocytes esterify FFA into TG and are packaged into VLDL particles with apolipoproteins and cholesterol by MTP. Nascent VLDL particles are secreted directly into circulation and mature as they bind additional apolipoproteins like apoC-II and apoE (125). C) The LPL-GPIHBP1 complex marginates lipoproteins within gaps of the HSPG-rich glycocalyx in the vascular lumen (86). VLDL-bound LPL is activated in the presence of apoC-II and apoA-V to hydrolyze TG cargo and release FFA to surrounding tissues. TG hydrolysis shrinks VLDL particles to form remnant lipoproteins, or IDL, which dissociate from LPL. D) Remnant lipoproteins are removed from circulation by the liver upon binding HSPGs and LDLR or LRP1. LPL circulates with remnant lipoproteins and facilitates their uptake by bridging the interaction between the lipoprotein and LDLR and LRP1 (10, 11).

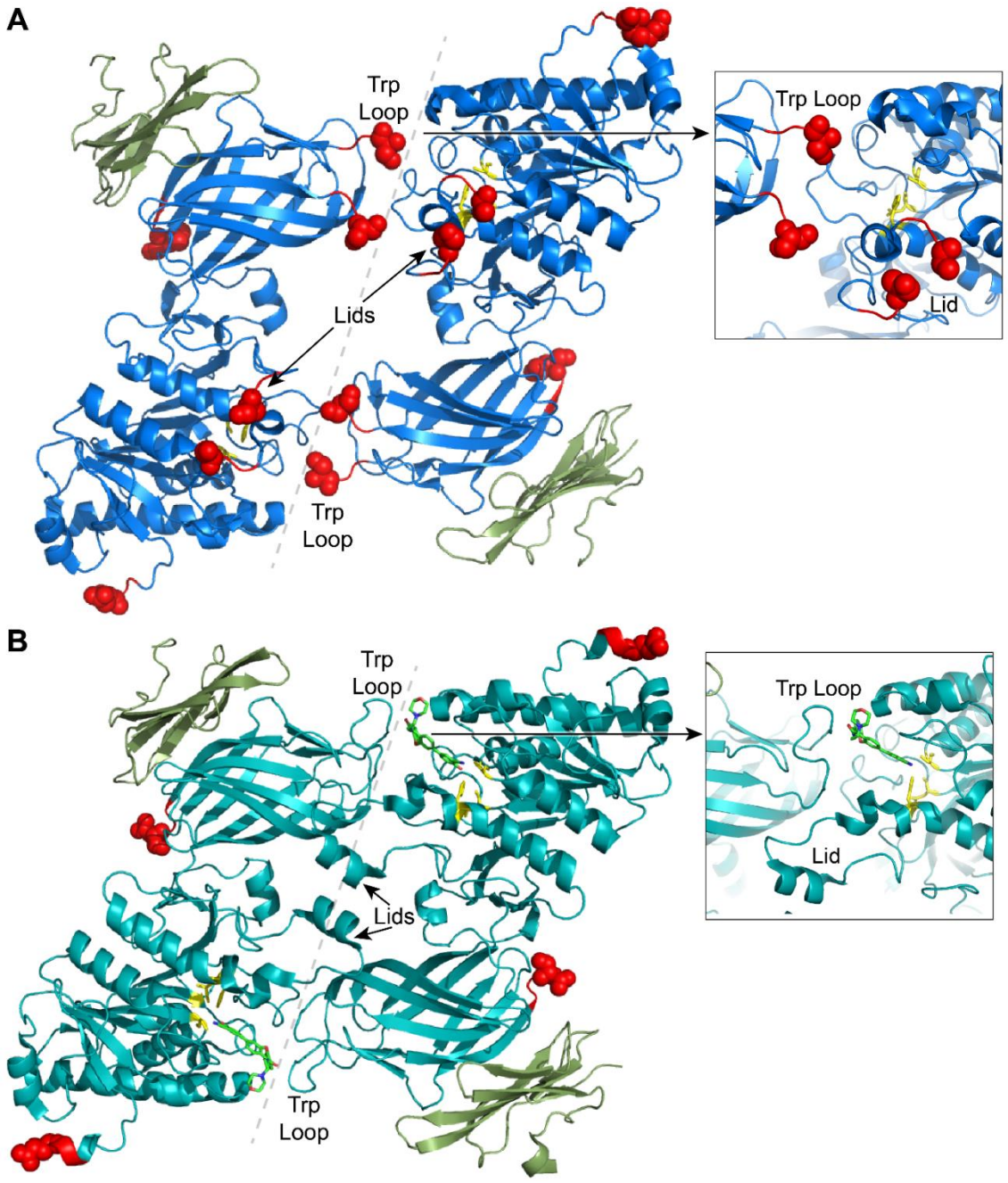

Figure 1.2 LPL-GPIHBP1 crystal structure comparison. A) Crystal structure of dimeric LPL (*blue*) in complex with GPIHBP1 (*green*) solved by Birrane and colleagues with the active site (*yellow*) and flanking residues of unresolved areas marked with spheres (*red*) (PBD: 6E7K) (19). Panel is zoomed in on the active site with the lid of one monomer and tryptophan-rich lipid-binding region of a second monomer labeled (19). The dimer interface is marked with a dashed line (*gray*). B) Arora and colleagues crystal structure of monomeric LPL (*teal*) in complex with GPIHBP1 (*green*) with the interface of a crystallographic dimer marked with dashed line (*gray*) (PDB: 6OB0) (20). Active site (*yellow*) and flanking residues of unresolved amino acids at the N- and C-terminus are marked with spheres (*red*). For reference, panel is zoomed in on the inhibitor-bound active site with the lid domain and tryptophan-rich lipid-binding loop labeled (20).

CHAPTER 2

Mapping the sites of the lipoprotein lipase (LPL)-angiopoietin-like protein 4 (ANGPTL4) interaction provides mechanistic insight into LPL inhibition[1]

2.1 Introduction

LPL is a key enzyme for regulating plasma TG levels (7). LPL hydrolyzes TG contained within lipoprotein particles in the capillary endothelium to facilitate the passage of free fatty acids into surrounding tissues (126, 127). Patients with loss-of-function mutations in LPL have extremely high levels of plasma TG, or HTG, that can cause complications such as pancreatitis, eruptive xanthomas, and lipemia retinalis (128). While LPL deficiency is rare, moderate HTG is common with more than three million cases diagnosed every year in the United States (129). Despite the frequency of HTG, treatment options are limited to diet and exercise, statins, or fibrates (17). Historically, the development of novel TG-lowering therapeutics was curbed due to inconclusive epidemiological associations between HTG and cardiovascular risk (130, 131). However, recent genetic studies have demonstrated that HTG is an independent risk factor for cardiovascular disease and should be addressed in the clinic (14, 132, 133). LPL is first synthesized in the parenchymal cells of heart, skeletal muscle, and adipose tissue. LPL is then secreted and transported to the vascular endothelium where it is anchored to the walls of the vessel lumen (6). Here, LPL is regulated by activators and inhibitors to precisely control the delivery of free fatty acids to either oxidative tissues for catabolism or adipose tissue for storage

[1] This chapter originally appeared in the Journal of Biological Chemistry. The original citation is as follows: Gutgsell, A.R., Ghodge, S.V., Bowers, A.A., Neher, S.B. Mapping the sites of the lipoprotein lipase (LPL)-angiopoietin-like protein 4 (ANGPTL4) interaction provides mechanistic insight into LPL inhibition. *Journal of Biological Chemistry* 294 (8):2678-2689.

(7, 73, 134, 135). One family of inhibitory proteins, known as angiopoietin-like proteins (ANGPTL3, 4 and 8), are upregulated in response to nutritional cues to inhibit LPL in a tissue-specific manner (136). More specifically, ANGPTL4 is upregulated in fasted conditions within adipocytes to inhibit LPL in white adipose tissue and, thereby, direct the release of free fatty acids to other tissues for catabolism (73).

Human genome-wide association studies have identified individuals with loss-of-function mutations in ANGPTL4 as having a unique lipid profile that significantly decreases their risk for developing cardiovascular disease (90, 94). Inactivating mutations in ANGPTL4 results in low levels of plasma TG, high levels of HDL cholesterol, and no apparent effect on LDL cholesterol (89, 90, 93). Previous studies using either antibodies to silence ANGPTL4 in monkeys or genetic loss of ANGPTL4 in mice recapitulate low levels of plasma TG seen in humans with loss-of-function ANGPTL4 mutations (89, 91). However, both ANGPTL4 knockdown monkeys and knockout mice inexplicably developed severe mesenteric lymphadenitis, or inflammation in the abdominal lymph nodes, when placed on a high-fat diet (89, 91, 137). Individuals with loss-of-function mutations in ANGPTL4 do not have increased rates of lymphadenopathy and the animals do not develop this phenotype on a standard chow or low-fat diet (89, 93).

ANGPTL4 was originally thought to be an adipokine given its robust expression in adipocytes and hepatocytes but has since been reclassified with roles in angiogenesis, wound repair, kidney function, tumorigenesis, redox regulation, and energy homeostasis (72). Structurally, ANGPTL4 is composed of a coiled-coil N-terminal domain and C-terminal fibrinogen-like domain that is selectively cleaved by proprotein convertases in certain tissues (138, 139). Adipocytes primarily secrete full-length ANGPTL4 and hepatocytes secrete the cleaved N- and C-terminal domains (72, 140). The N-terminal domain, herein referred to as nANGPTL4, is known to potently inhibit LPL, while the C-terminal domain is thought to be involved in other roles like angiogenesis or wound repair (141–143). Given the diverse roles for ANGPTL4, it is not surprising that complete silencing results in a severe diet-induced pathology

(72, 144). The disparity between an advantageous phenotype in human variants and a pathological phenotype in animals suggests additional research is needed to understand the precise function of each ANGPTL4 species.

We set out to characterize how nANGPTL4 binds LPL and use this information to block the interaction using a small peptide mimetic of an LPL binding site. Using both hydrogen-deuterium exchange mass spectrometry (HDX-MS) and site-specific mutagenesis, we determined that nANGPTL4 binds near the active site of LPL at the lid domain (residues 224-238) and a nearby α-helix (residues 89-102). Moreover, a peptide mimetic of the LPL lid domain is capable of binding nANGPTL4 and protects full-length LPL from inhibition. Our data suggest nANGPTL4 reversibly inhibits LPL by binding the lid domain to prevent substrate catalysis by the active site.

2.2 Results

Hydrogen-deuterium exchange mass spectrometry reveals four nANGPTL4 binding sites on bovine LPL. To inform the question of how nANGPTL4 mediates inhibition of LPL, we used HDX-MS to identify residues at the interface of this protein-protein interaction. The rate of deuterium exchange between amide hydrogens is used to probe protein secondary structure and allosteric conformational changes induced by binding interactions (145, 146). We performed HDX-MS on bovine LPL (bLPL) alone, nANGPTL4 alone, and a combination of bLPL and nANGPTL4. Samples were incubated in deuterated buffer for 0, 1, 5, and 10 minutes, quenched, and digested for immediate analysis by reverse-phase chromatography coupled to mass spectrometry. Between bLPL and nANGPTL4, we identified 710 unique peptides.

The difference in deuterium uptake for bLPL was measured in the -nANGPTL4 and +nANGPTL4 condition and represented using a heat map to highlight areas with decreased exchange (*dark blue)* and increased exchange (*red*) (Figure 2.1A). Peptide sequences that were statistically different (*p value < 0.05*) between the -nANGPTL4 and +nANGPTL4 condition were represented with percent deuterium uptake curves (Figure 2.1A) and colored based on

differential deuterium exchange on the LPL crystal structure (PDB: 6OB0, (20)) (Figure 2.1B). A decrease in deuterium exchange in the complex condition suggests that those peptide sequences are at the binding interface. We identified four potential nANGPTL4 binding sites on bLPL at residues 17-26, 89-102, 224-238, and 290-311 (residue 1 is the first amino acid after signal peptide cleavage, Figure 2.1A-B). Herein, these sites will be referred to as the N-terminal β-turn, lid-proximal helix, lid, and the furin cleavage region, respectively. Interestingly, there were several sites within bLPL that increased in exchange: residues 63-72, 75-83, 103-113, 133-146, 166-180 (after signal peptide cleavage) (Supplemental Figure S2.1). Regions of increased deuterium exchange correspond to more structurally dynamic regions (146). It is unclear at this time whether regions with increased deuterium exchange is a result of allosteric conformational change or due to bLPL unfolding as suggested by Mysling *et al*. (87, 146, 147).

To address the possibility of nANGPTL4-mediated irreversible unfolding of bLPL, we utilized a kinetic assay. Reversible, noncompetitive inhibition can be distinguished from irreversible inactivation by measuring bLPL activity at different concentrations under V_{max} conditions in the presence and absence of nANGPTL4. By plotting V_{max} versus the total concentration of bLPL, the data fits a linear equation with the slope equal to the forward reaction rate, or k_{cat} ($V_{max} = k_{cat}[E_{Total}]$ where E_{Total} is the total enzyme concentration) (148). For a reversible, noncompetitive inhibitor, both the uninhibited and inhibited conditions intersect the origin and the slope of the inhibited condition is less than the uninhibited control by the quantity $1 + \left(\frac{[I]}{K_i}\right)$, where [I] is the concentration of inhibitor and K_i is the inhibition constant (Supplemental Figure S2.2A). For an irreversible inhibitor, the slope of the inhibited condition is the same as the uninhibited control. However, the line does not intersect the x-axis at the origin, but rather, at a position on the x-axis that is equivalent to the amount of enzyme that is irreversibly inactivated (Supplemental Figure S2.2B). Plotting V_{max} versus the total concentration of active bLPL shows that both the inhibited and control conditions intersect the origin (Supplemental Figure S2.2C).

Additionally, the slope of the inhibited plot decreased from 1.097 to 0.541. These indicate a mode of reversible, noncompetitive inhibition (Supplemental Figure S2.2A).

We identified two sites with decreased deuterium exchange in nANGPTL4: residues 15-33 and 95-106 (after signal peptide cleavage) (Fig. 2.2). Residues 15-33 are in agreement with previous reports detailing a peptide sequence necessary for nANGPTL4 inhibition of LPL and site 95-106 has not been previously reported (142, 143). There were no sites on nANGPTL4 that increased in deuterium exchange in the presence of bLPL.

Human LPL_{HL} chimeric molecules are insensitive to inhibition by nANGPTL4. To validate potential nANGPTL4 binding sites on LPL, we mutagenized human LPL in regions with decreased deuterium exchange and screened for nANGPTL4 inhibition *in vitro* (Figure 2.3). LPL shares 44% sequence identity with hepatic lipase (HL), which has been putatively shown to be resistant to ANGPTL4 inhibition, although data surrounding this issue has been contradictory (88, 149, 150). Here, we show that HL is not inhibited by nANGPTL4, even at a 1:4000 molar excess (Figure 2.4B and Figure 2.5A). Therefore, we used the corresponding HL sequences to generate LPL_{HL} chimeras in two regions near the active site: the lid-proximal helix and the lid (Figure 2.3). Previous studies have shown that lipase lids alone dictate substrate specificity and chimeric lid mutants of LPL, HL, and endothelial lipase (EL) alters both substrate specificity and enzyme kinetics (71, 151, 152). If nANGPTL4 binds the lid of LPL, it could explain why ANGPTL4 specifically inhibits LPL rather than HL, as these lid sequences have only 32% identity (149).

Purified LPL and variants, $LPL_{HL\ lid}$ or $LPL_{HL\ helix}$, were assayed for nANGPTL4 inhibition by measuring the rate of substrate hydrolysis in the presence of increasing concentrations of nANGPTL4. While LPL was sensitive to nANGPTL4 inhibition with a K_i of $1.7^{+/-}0.74$ µM, both LPL_{HL} chimeric mutants appeared to be resistant to nANGPTL4 inhibition (Table 2.1). The $LPL_{HL\ helix}$ had a slight sensitivity to nANGPTL4 with an estimated K_i of $15^{+/-}7.0$ µM (Figure 2.4C). Unless 50% enzyme inhibition occurred, reported K_i values could only be estimated. $LPL_{HL\ lid}$

showed similar resistance to nANGPTL4 inhibition as HL, such that a K_i value could not be calculated (Figure 2.4B, D). These data suggest that both the lid and lid-proximal helix are necessary for nANGPTL4 binding LPL. While it is possible that the mutations altered the three-dimensional structure of the lipase, both LPL_{HL} chimeric molecules displayed no obvious catalytic defects (Table 2.1).

We next tested if the furin protease cleavage region was necessary for nANGPTL4 inhibition (residues 288-309) (Supplemental Figure S2.3A). Furin protease recognizes the consensus sequence "RXXK/R" present in LPL at residues 294-297, resulting in inactive N- and C-terminal cleavage fragments (18, 153). In HL, the furin consensus sequence is disrupted by a proline residue and, therefore, protected from proteolytic cleavage in this region (residues 314-334).

We first exchanged LPL residues 288-309 for the corresponding HL sequence (Supplemental Figure S2.3A). As expected, this mutation abolished furin cleavage in LPL but also abolished LPL enzymatic activity (Supplemental Figure S2.3B, C). It is important to note that the proline residue in the corresponding HL sequence at position 294 may compromise the three-dimensional structure of LPL, and possibly, result in catalytic inactivation. Therefore, we split the full sequence into two parts: 288-299 and 300-309 (Supplemental Figure S2.3A). Similar to $LPL_{HL288-309}$, $LPL_{HL288-299}$ was not enzymatically active. Although $LPL_{HL300-309}$ does not contain the R294P mutation, its enzymatic activity could not be detected either (Supplemental Figure S2.3B). Western blot analysis revealed that nearly the entire population of $LPL_{HL300-309}$ was cleaved by furin protease (Supplemental Figure S2.3C) (153, 154). Since we were unable to measure lipase activity for any of the LPL_{HL} furin cleavage chimeras, we cannot determine if residues 288-309 are directly involved in nANGPTL4 binding.

Human HL_{LPL} chimeric proteins are sensitive to inhibition by nANGPTL4. To further validate sequences needed for nANGPTL4 inhibition of LPL, we aimed to "sensitize" HL to nANGPTL4 inhibition by generating human HL chimeric mutants containing the corresponding

LPL sequences for the lid-proximal helix and the lid (Figure 2.3). Similar to LPL_{HL} chimeric mutants, all HL_{LPL} chimeric mutants were generated using overlap extension PCR whereby each sequence of interest was exchanged for the corresponding LPL sequence (Figure 2.3).

$HL_{LPL\ lid}$ and $HL_{LPL\ helix}$ were kinetically similar to HL with average V_{max} and K_M values of 2.0 µmol/sec and 0.6 µM, respectively, using DGGR lipase substrate (Table 2.1). However, unlike HL, $HL_{LPL\ helix}$ and $HL_{LPL\ lid}$ were sensitive to nANGPTL4 inhibition with an estimated K_i of $32.7^{+/-}5.6$ µM and $45.5^{+/-}2.4$ µM, respectively (Figure 2.5B, C). $HL_{LPL\ lid\ +\ helix}$ appeared to be the most sensitive to inhibition with an estimated K_i of $22^{+/-}8.7$ µM (Figure 2.5D). Taken together, these data show that the LPL lid and the lid-proximal helix provide binding sites for nANGPTL4.

LPL lid peptide blocks nANGPTL4 mediated inhibition of LPL. Given that mutating the LPL lid abolished nANGPTL4 inhibition, we wanted to know if the LPL lid domain alone could compete with full-length LPL for binding nANGPTL4. We, therefore, synthesized a peptide comprised of the LPL lid sequence (CNIGEAIRVIAERGLGDVDQLVKC). The native LPL lid is circularized via a disulfide bond between two cysteine residues at the termini of the lid motif. The synthetic lid peptide was tested in cyclic form (disulfide bonded) or linear form (NEM-capped). Correct synthesis and cyclization of the peptide were verified by mass spectrometry, as shown in Supplemental Figure S2.4A, B. We tested if the peptide could prevent LPL inhibition by nANGPTL4 by incubating the inhibition reaction with increasing concentrations of either cyclic and linear NEM-capped lid peptide. Interestingly, the cyclic peptide protected full-length LPL from nANGPTL4 inhibition in a dose-dependent manner, while the linear NEM-capped peptide did not (Figure 2.6A-B). Presumably, the cyclic peptide adopts a structure similar to the native lid domain. Isothermal calorimetry (ITC) was used to confirm that the cyclic lid peptide binds nANGPTL4 with micromolar affinity. These data suggest that two lid peptides bind each nANGPTL4 tetramer with a K_d of approximately 57 µM (Figure 2.6C). Although the ITC shows that the lid peptide binds nANGPTL4 with relatively low affinity, these data confirm that the LPL lid is an important site for nANGPTL4 binding.

2.3 Discussion

HTG is an independent risk factor for cardiovascular disease with relatively limited treatment options and, therefore, an unmet need for new therapies (14, 129). Given LPL has a direct influence on plasma TG levels, it is a promising target for novel TG-lowering therapeutics. One approach for targeting LPL is to prevent its inhibition by ANGPTL4. Previous reports describing ANGPTL4 knockout animals demonstrated significantly reduced TG levels with little negative side effects under standard chow diets (89, 91). However, the safety of ANGPTL4 knockdown has been called into question due to severe lymphadenopathy observed in animals placed on high-fat diets (91, 137). Intriguingly, humans with loss-of-function mutations in ANGPTL4 do not appear to be at an increased risk for lymphadenopathy (89, 93). Therefore, additional research is needed to assess if specifically blocking ANGPTL4 inhibition of LPL can be a viable treatment for HTG. Our goal was to study the interaction of nANGPTL4 with LPL to inform the development of specific inhibitors for this interaction.

The exact mechanism for LPL inhibition by ANGPTL4 has been controversial. nANGPTL4 was first shown to irreversibly inhibit LPL by converting active dimers into inactive monomers (78, 83). Our previous data support an alternative model, whereby nANGPTL4 inhibits LPL in a reversible, noncompetitive mechanism (11, 79). The difference in observed mechanisms of inhibition may depend on the initial stability of the LPL in the assay. Purified LPL is notoriously unstable in standard buffer conditions and is prone to thermal denaturation (79). Therefore, many *in vitro* LPL activity assays and purification protocols use a bile acid, deoxycholate, to stabilize LPL (11, 18, 45, 79, 81, 87, 155). In the presence of deoxycholate, nANGPTL4 inhibits LPL by a reversible, noncompetitive mechanism (79, 87). Since LPL is known to have enhanced thermal stability within biological fluids that contain bile acids, like serum and milk, we used them to better mimic physiological conditions in our kinetic assays (45, 156).

We have identified both the lid and lid-proximal helix as key nANGPTL4 binding sites. Removing these sites from LPL abolished nANGPTL4 binding and protected the enzyme from inhibition. Alternatively, cloning these sites into HL sensitized this resistant lipase to nANGPTL4 inhibition. Our data suggest nANGPTL4 binds the lid and lid-proximal region of LPL, which may prevent proper lid function and inhibit substrate catalysis. There are conflicting reports as to whether nANGPTL4 can inhibit LPL in the presence of natural chylomicron or VLDL substrates (45, 157). Here, the synthetic substrate DGGR was needed to enable precise measurements of LPL inhibition kinetics. Natural lipoprotein substrates have different properties than DGGR, so our work does not address this conflict.

Our HDX-MS data also identified a third, potential, binding site for nANGPTL4 on LPL at residues surrounding its furin cleavage site (residues 288-309). LPL is inactivated by furin protease cleavage into the N- and C-terminal domains at the consensus sequence 'RAKR' (residues 294-297). Although we were unable to generate enzymatically active chimeric mutants at this site, we have shown that furin resistant LPL point mutants, R297N and R297N/S298C, are sensitive to nANGPTL4 inhibition (18). These data suggest residues R297 and S298 may not be necessary for nANGPTL4 mediated inhibition of LPL. Recent reports have shown ANGPTL4 enhances furin cleavage of LPL in adipocytes (153). Given ANGPTL4 is also cleaved by the furin protease, it is possible ANGPTL4 binds LPL intracellularly to recruit the furin protease for cleavage of both ANGPTL4 and LPL.

Lastly, we demonstrate that a small peptide containing the LPL lid sequence can protect full-length LPL from nANGPTL4 inhibition. Although this interaction is not yet sufficiently strong, it serves as a starting point for the development of potent peptide inhibitors for nANGPTL4 that specifically abolish LPL inhibition and leave both full-length and cleaved forms of ANGPTL4 intact to perform their other functions.

2.4 Materials and Methods

Molecular cloning. Human LPL, HL, and chimeric mutants were cloned into pCDNA5/FRT/TO vectors (Thermo Fisher Scientific) containing lipase maturation factor 1 (LMF1) with an internal ribosome entry site (IRES) for co-expression. All constructs contain a 6x polyhistidine-tag on the C-terminus, except the wild type HL construct has no tag. All chimeric mutants were generated using overlap extension PCR. Cloning of pET16B nANGPTL4 was previously described (79). All plasmid sequences are available upon request.

Cell Culture and Protein Expression. LPL, HL, and chimeric mutant plasmids were stably integrated into FlpIn™ T-REx™ HEK293 cell lines (Thermo Fisher Scientific) using the manufacturer's instructions. Each stable cell line was maintained in Dulbecco's Modified Eagle Medium, 10% fetal bovine serum, 1% penicillin/streptomycin, and 1% L-glutamine (growth media). At 70% confluence, cells were given Dulbecco's Modified Eagle Medium, 1% fetal bovine serum, 1% penicillin/streptomycin, 1% L-glutamine, 10 units/mL heparin, and 2 µg/mL tetracycline (expression media) to induce the expression of lipase. Expression media for all LPL species and HL was collected and flash frozen in liquid nitrogen every 24 hours for 6 days. Expression media for all HL variants was collected every 48 hours, bound to Ni Sepharose Excel™ resin (GE Healthcare Life Sciences), washed, and flash frozen in liquid nitrogen for -80°C storage until further purification as described below.

Protein Purification:

bLPL - bLPL was purified from fresh bovine milk as previously described (158). Briefly, chilled bovine milk was centrifuged and filtered using glass wool to remove milk fat. Solid NaCl was added to the skim milk to 0.34mol/liter and bLPL was purified using Heparin Sepharose 6 Fast Flow resin (GE Healthcare).

LPL, $LPL_{HL\ lid}$, and $LPL_{HL\ helix}$ – Filtered expression media was loaded onto two tandem 1mL HiTrap Heparin Sepharose High Performance columns (GE Healthcare Life Sciences) then washed with 75 mL of 20 mM bis-tris pH 6.5, 850 mM NaCl, 10% glycerol and eluted in 20 mM

bis-tris pH 6.5, 1500 mM NaCl, 10% glycerol over a linear gradient. All LPL containing fractions were concentrated using Amicon Ultra Centrifugal Units (Millipore), aliquoted, and flash frozen for -80°C storage until use.

HL – Filtered expression media loaded onto two tandem 1 mL HiTrap Heparin Sepharose High Performance columns (GE Healthcare Life Sciences) was washed with 20 mL of HL heparin buffer (20 mM Na_2HPO_4 pH 7.2, 500 mM NaCl, 10% glycerol) and eluted along a linear salt gradient from 500 mM to 2000 mM NaCl in HL heparin buffer. Fractions containing HL were pooled, concentrated using Amicon Ultra Centrifugal Units (Millipore), aliquoted, and flash frozen for -80°C storage until use.

$HL_{LPL\ lid}$, $HL_{LPL\ helix}$, and $HL_{LPL\ lid\ +\ helix}$ chimeras- Fresh expression media (150 mL) bound to Ni Sepharose Excel™ resin (0.15 mL) (GE Healthcare Life Sciences) was washed with 2.5 mL using 20 mM Na_2HPO_4 pH 7.2, 360 mM NaCl, 10 mM imidazole, 10% glycerol. The resin was suspended in a high salt storage buffer (1X phosphate buffered saline, 800 mM NaCl, 40% glycerol) and flash frozen for storage at -80°C until final purification. Frozen resin (1 mL total) was thawed on ice, washed with 10 mL of 20 mM Na_2HPO_4 pH 7.2, 500 mM NaCl, 50 mM imidazole, 10% glycerol, and eluted over 10 mL using 20 mM Na_2HPO_4 pH 7.2, 500 mM NaCl, 280 mM imidazole, 10% glycerol. Fractions containing HL chimeras were pooled and concentrated using dialysis against 400 g/L high molecular weight polyethylene glycol (PEG) in 20 mM bis-tris pH 6.5. Concentrated samples were aliquoted and flash frozen for storage at -80°C until use.

nANGPTL4- His-GST tagged nANGPTL4 was expressed in BL21 (DE3) cells, grown at 37°C until reaching an A_{600} of 0.4 and induced with 0.1 mM isopropyl 1-thio-β-$_D$-galactopyranoside for 16 hours at 18°C. Cells were pelleted at 6000 x *g*, resuspended in 20 mM tris pH 8.3, 360 mM NaCl, 20 mM imidazole, 1 mM betaine, 1 mM fresh phenylmethylsulfonyl fluoride (Sigma), and lysed using Emulisflex C5 (Avestin) at 15,000 p.s.i. Lysate was cleared by centrifugation at 34,000 x *g* for 60 minutes. Cleared lysate was added to equilibrated nickel-

nitrilo-triacetic acid resin (Qiagen). Resin was washed with 10 column volumes using 20 mM tris pH 8.3, 360 mM NaCl, 80 mM imidazole, 1 mM betaine, followed by a second wash using 20 mM tris pH 8.3, 150 mM NaCl, 80 mM imidazole, 1 mM betaine. His-GST-nANGPTL4 was eluted over 10 column volumes using 20 mM tris pH 8.3, 150 mM NaCl, 500 mM imidazole, 1 mM betaine. Elution fractions containing His-GST-nANGPTL4 were combined with 32 µg/mL tobacco etch virus, 3 mM reduced glutathione (GSH), and 0.3 mM oxidized glutathione (GSSG) for cleavage of the N-terminal His-GST tag. Protein fractions were dialyzed into Mono S start buffer (20 mM tris pH 8.3, 100 mM NaCl), injected onto a 1mL Mono S 5/50 GL column (GE Healthcare Life Science), and eluted over a linear gradient from 100 mM to 2000 mM NaCl in Mono S buffer. Fractions containing nANGPTL4 were furthered purified using HiLoad™ 16/600 Superdex™ 200 PG (GE Healthcare Life Sciences) in nANGPTL4 storage buffer (20 mM tris pH 8.3, 150 mM NaCl, 5% glycerol). Fractions containing nANGPTL4 were concentrated using Amicon Ultra Centrifugal Units (Millipore), aliquoted, and flash frozen for -80°C storage until use.

Quantification of active lipase. Quantification was performed as previously described(11). Briefly, ActivX™ TAMRA-FP Serine Hydrolase Probe (Thermo Fischer Scientific) was used to label active LPL and HL variants where bovine LPL of known concentration was used as a protein standard. The relative purity of all purified protein can be seen by both Coomassie stain and TAMRA-FP labeling in Supplemental Figure S2.5A-D.

Hydrogen-deuterium exchange mass spectrometry (HDX-MS):

HDX labeling. bLPL and nANGPTL4 alone were diluted in 50 mM sodium phosphate buffer (pH 7.2) to 8 µM and 16 µM, respectively, and a condition with 8 µM bLPL and 16 µM nANGPTL4 was created prior to deuterium labeling. An automated HDX labeling LEAP robot was used for deuterium labeling. Briefly, 5 µL of each protein sample were diluted with 45 µL of 50 mM sodium phosphate in H_2O for time 0 injections or 45 µL 50 mM sodium phosphate in D_2O (99.9% Sigma) for deuterium uptake injections at 1, 5, and 10 minutes. Deuterium exchange was quenched with 45 µL of pre-chilled 0.3% formic acid in water with 1 mM TCEP at the

corresponding times. Quenched samples were subjected to online pepsin digestion using Waters Enzymate BEH pepsin column (2.1 x 30 mm x 5 µm) at 200 µL/min at 20°C for 2 minutes (pH 2.5, 0.05% formic acid in water). Sample processing was managed within Waters HDX Acquity Module (Waters Corp.).

LC-MS-MS. Downstream LC-MS-MS was acquired in duplicate using nanoAcquity UPLC system (Waters Corp.) coupled to a Waters Synapt G2 high resolution accurate mass tandem mass spectrometer via an electrospray ionization source. The sample was first trapped on a VanGuard 2.1 x 5 mm BEH C18 1.7 µm trapping column (40 µl/min at 5% v/v water/acetonitrile 0.1% formic acid). Analytical separation was performed using a 1.7 µm Acquity BEH130 C18 1 mm Å~ 100 mm column (Waters Corp.) using a linear gradient from 5% acetonitrile, 0.1% formic acid to 35% acetonitrile, 0.1% formic acid over 7 min at 40 µL/min. Trapping and analytical separation were all performed at 1.0°C with the HDX manager. Data collection on the Synapt G2 mass spectrometer was performed in an ion-mobility enabled data-independent acquisition (IM-DIA) mode of acquisition alternating between a 1.0 second low energy scan from m/z 50-2000 followed by a 1.0 second high energy scan from m/z 50-2000. Every 30 seconds a low energy lock-mass scan of 400 fmol/µL Glu-Fibronectin peptide was performed.

Data analysis. All non-deuterated, time 0, data files were imported and searched within ProteinLynx Global Server (v2.5.2) against a SwissProt_Human database containing bLPL and ANGPTL4 sequences. Nonspecifc enzyme rules were selected with +/- 10 ppm mass accuracy tolerances and 5% retention time RSDs criteria. ProteinLynx Global Server peptide score of at least 6.5 were included in the final analysis for a final peptide false discovery rate of < 2.0%. DynamX HDX Data Analysis Software (v2.0, Waters Corp.) was used to calculate deuterium uptake for all identified peptide sequences. To identify residues of differential uptake on bLPL as a function of nANGPTL4, or vice versa, the calculated uptake values were subjected to an unpaired two-tailed students t-test calculation at each time point for every condition. Only sites with significant differential uptake with a p value < 0.05 were selected for manual interrogation

to ensure correct identification of peaks with no interference from neighboring peaks and to assess the global uptake distribution across all time points. Deuterium uptake was represented in a heat map using percent deuterium uptake values for all peptides with a standard deviation of less than 0.2 Da at each time point. Heat maps for bLPL alone and bLPL + nANGPTL4 were generated using 393 and 350 unique peptides, respectively. Heat maps for nANGPTL4 alone and nANGPTL4 + bLPL were generated using 520 and 505 unique peptides, respectively.

Peptide production. Peptide synthesis was carried out using solid-phase peptide synthesis on a Biotage Initiator+ Alstra microwave peptide synthesizer using Rinkamide Chemmatrix resin (Biotage). Peptidic scaffolds were synthesized from the C-terminus to the N-terminus with a C-terminal amide functional group using standard fluorenylmethoxycarbonyl (Fmoc) chemistry. The building blocks are comprised of commercially available N-α-Fmoc-L-amino acids. Briefly, the resin was initially wetted and swollen with 1:1 mixture of dichloromethane and DMF. Fmoc deprotection was achieved using incubation of the resin with 20% (v/v) piperidine/DMF for 3 min and 10 min each, with DMF wash at the end of each incubation step. The N-α-Fmoc-L-amino acids (5 equivalents) were coupled using HATU (5 equivalents) as the coupling agent and DIEA (10 equivalents) as the base. Coupling steps were carried out at 75°C for 5 min each using microwave irradiation. After the final deprotection to obtain a primary amine at the N-terminus of the synthesized peptide, the resin was washed with dichloromethane and dried. The synthesized peptide was cleaved from the resin using 94-95% (v/v) TFA, 2.5% (v/v) water, and 2.5% (v/v) triisopropylsilane (TIPS) while incubating at 37°C for one hour followed by room temperature incubation for 30 minutes. Resin-cleaved peptide was precipitated by the dropwise addition of the cleavage reaction mixture into cold diethyl ether. The precipitate was separated by centrifugation, and the supernatant was decanted. Dried peptide was dissolved in DMSO and diluted with a mixture of 50% (v/v) acetonitrile-water. The crude peptide was then purified using semi-preparative HPLC. Each fraction was analyzed using the UV trace at 220 nm, 280 nm, and LC-MS. Fractions containing pure peptide were

collected and lyophilized. The solid peptide was dissolved in DMSO, and then diluted to a peptide concentration of 200 µM using 0.1 M ammonium bicarbonate (pH 8.0). This step allowed it to circularize via intramolecular disulfide bond formation. Completion of circularization was verified by LC-MS, and the peptide was lyophilized and stored at -20°C until use.

NEM capping of lid peptide. LPL lid peptide purified as described above was dissolved in DMSO, and diluted to a final concentration of 0.4% DMSO and 0.1 M TCEP using 1X phosphate buffered saline pH 7.8. The solution was incubated at 37°C for 15 minutes to reduce disulfide bonds. Following TCEP reduction, 0.1 M NEM was added to the reaction and incubated at 37°C for 60 minutes. The capped peptide was recovered by HPLC, verified by LC-MS, and lyophilized for storage at -20°C.

Inhibition of LPL, HL, and chimeric mutants by nANGPTL4. Inhibition assays using purified lipase and lipase variants by nANGPTL4 were carried out essentially as described (79). LPL and bLPL are equivalently inhibited by nANGPTL4. Briefly, nANGPTL4 was added to dilute LPL, HL, or chimeric mutants at a final volume of 70 µL/reaction. The reaction was initiated by the addition of 30 µL of varying concentrations of fluorescent substrate 1,2-di-O-lauryl-*rac*-glycero-3-(glutaric acid 6-methlyresofurin ester) (DGGR) (Sigma) in anzergent 3-16 (Affymetrix), to a final volume of 100 µL. Samples were shaken in a Spectramax M5 plate reader at 37°C for 5 seconds and substrate hydrolysis was measured by fluorescence excitation at 529 nM, emission at 600 nM, and a filter of 590 nM. Final assay buffer concentrations were 215 mM NaCl, 1 mM deoxycholate, 20 mM tris pH 8.0, 0.2 % fatty-acid free BSA, and 0.01 % anzergent 3-16. Final ANGPTL4 concentrations were 0, 0.2, 0.4, 0.8, 1.5 and 3.7 µM or 0, 0.4, 0.8, 2, 6, 10 µM. The rate of initial lipase substrate hydrolysis was plotted as a function of substrate concentration. Next, data were fit to the equation for noncompetitive inhibition: $v = V_{max}*[S]/\{(K_M*(1+[I]/K_i))+([S]*(1+[I]/K_i))\}$ where V_{max} is the uninhibited maximum rate of substrate hydrolysis, K_M is the Michaelis-Menten constant, [S] is substrate concentration, [I] is

inhibitor concentration, and K_i is the inhibition constant. Data were fit using simultaneous nonlinear regression with the program Mathematica (Wolfram Research).

Inhibition of LPL by nANGPTL4 in the presence of an LPL lid peptide. LPL inhibition by nANGPTL4 was measured using the DGGR fluorescent assay described above in the presence of the LPL lid peptide. nANGPTL4 (0 or 0.4 µM) was incubated with increasing concentrations of cyclic lid peptide (0, 20, 50, or 100 µM) or linear NEM-capped peptide (0, 30, 90, or 160 µM) for 10 minutes at room temperature. After incubation, the mixture was added to dilute LPL in a final volume of 70 µL/reaction and incubated for an additional 5 minutes at room temperature. LPL activity was measured upon the addition of 30 µL DGGR for a final reaction volume of 100 µL. Final assay buffer concentrations were 20 mM tris, pH 8.0, 150 mM NaCl, 1 mM deoxycholate, 0.2% fatty-acid free BSA, 0.01% anzergent 3-16, 10 µM DGGR, 0.8% DMSO, 2.5 nM LPL, 0 or 0.4 µM nANGPTL4, and 0, 20, 50, or 100 µM cyclic lid peptide or 0, 30, 90, 160 µM linear NEM-capped peptide.

Isothermal Titration Calorimetry. Lyophilized lid peptide was resuspended in DMSO and diluted in nANGPTL4 dialysis buffer (1X phosphate buffered saline pH 7.8) to a final concentration of 3087 µM and 4% DMSO. Purified nANGPTL4 was at a concentration of 338 µM and brought to 4% DMSO to exactly match the peptide buffer. Isothermal titrations were performed using the MicroCal Auto-iTC200 (Malvern Panalytical). Injections of 1.5 µL of peptide were added in 180 second intervals at 10°C. Heat of dilution was measured by titrating the peptide into a blank solution and subtracted from our data before a one-site curve fitting was preformed using MicroCal Auto-iTC200 software. Stoichiometry (*N*), association and dissociation constants (K_a, K_d), and enthalpy change (ΔH) were obtained directly from the data.

2.5 Tables

Lipase	V_{max} (RFU/sec)	K_M (μM)	K_i (μM)
LPL	1.19 $^{+/-}$ 0.26	0.39 $^{+/-}$ 0.04	1.71 $^{+/-}$ 0.74
$LPL_{HL\ Lid}$	1.78 $^{+/-}$ 0.30	0.93 $^{+/-}$ 0.28	-
$LPL_{HL\ Helix}$	1.80 $^{+/-}$ 0.39	0.48 $^{+/-}$ 0.07	15.11 $^{+/-}$ 7.00
HL	1.91 $^{+/-}$ 0.57	0.91 $^{+/-}$ 0.37	-
$HL_{LPL\ Lid}$	2.10 $^{+/-}$ 0.39	0.57 $^{+/-}$ 0.08	45.52 $^{+/-}$ 2.37
$HL_{LPL\ Helix}$	1.45 $^{+/-}$ 0.17	0.61 $^{+/-}$ 0.05	32.70 $^{+/-}$ 5.61
$HL_{LPL\ Lid\ +\ Helix}$	0.64 $^{+/-}$ 0.03	0.43 $^{+/-}$ 0.10	22.00 $^{+/-}$ 8.72

Table 2.1. Enzyme kinetics for each LPL and HL chimeric variant. Michaelis-Menten curves were generated for each lipase in the presence of increasing concentrations of nANGPTL4 over multiple fluorescent substrate concentrations. LPL and LPL_{HL} chimeric mutants have similar V_{max} and K_M values. $LPL_{HL\ lid}$ and $LPL_{HL\ helix}$ have an increased resistance to nANGPTL4 inhibition, relative to LPL. HL and HL_{LPL} chimeric mutants have similar V_{max} and K_M values, except $HL_{LPL\ lid\ +\ helix}$ has a significantly lower V_{max} than HL. HL_{LPL} chimeric mutants have increased sensitivity to nANGPTL4, relative to HL. Average values of at least three biological replicates ± standard deviation. *RFU,* relative fluorescent units.

2.6 Figures

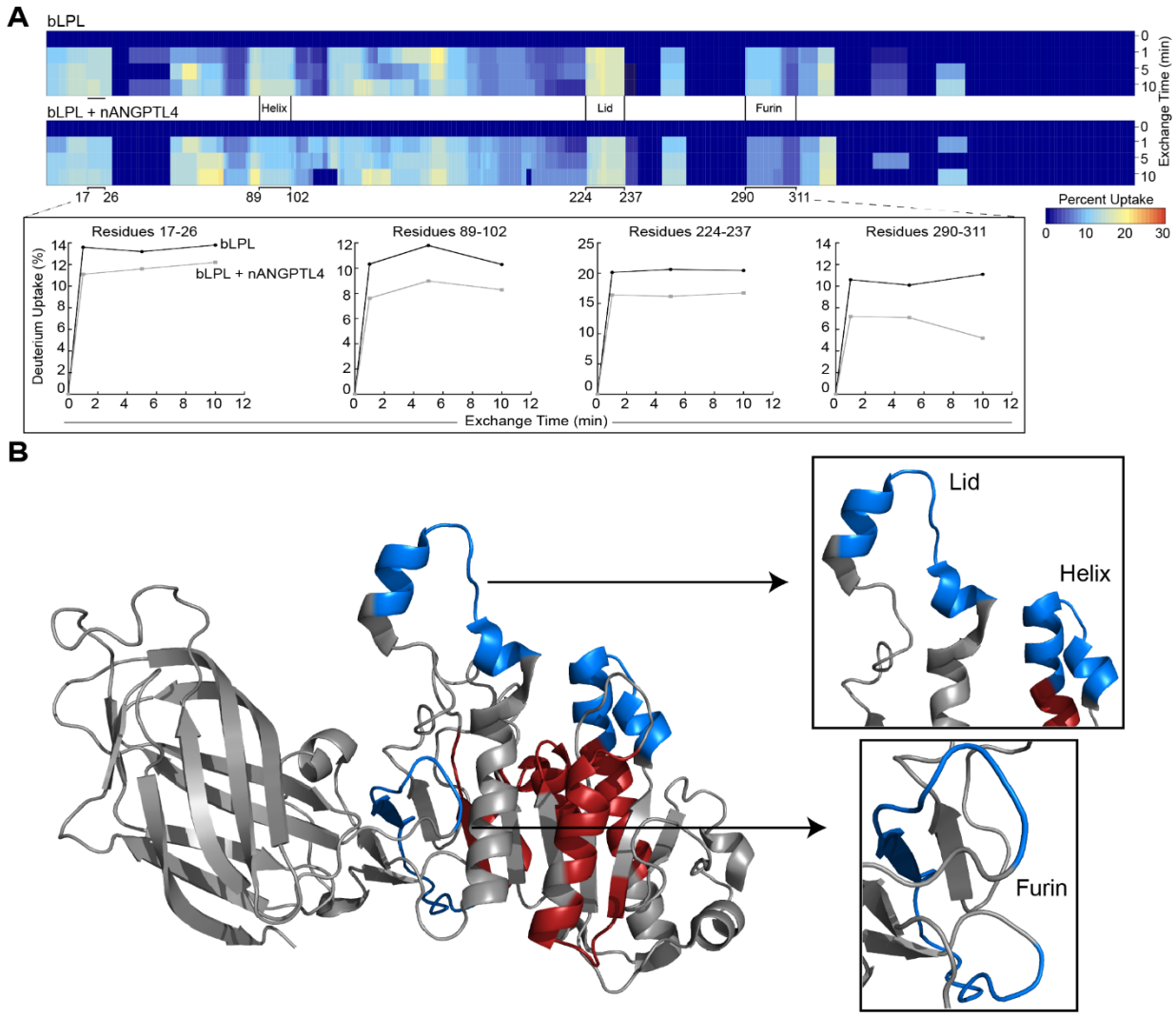

Figure 2.1. Decreased deuterium exchange suggest four potential binding sites on LPL. Sites of deuterium exchange were identified using LC-MS-MS after incubation of bLPL, nANGPTL4, or a combination of bLPL and nANGPTL4 in 99.9% deuterated solution for 0, 1, 5, and 10 minutes. (A) Heat maps were generated using percent deuterium uptake values for all peptides with a standard deviation of less than 0.2 Da. Deuterium uptake curves are shown for peptides that were statistically different between the bLPL apo (*black*) and complex state (*grey*) at each time point. Sites of differential deuterium exchange were determined using unpaired two-tailed students t-test with cutoff of $p < 0.05$. (B) LPL crystal structure (PDB: 6OB0, (20)) where peptide sequences with differential deuterium exchange in the complex state at every time point are colored blue for decreased exchange and red for increased exchange. For simplicity, one monomer unit is represented as a cartoon model (*grey)*. Panels are zoomed in on the lid-proximal helix, lid, and furin cleavage sites (*blue*).

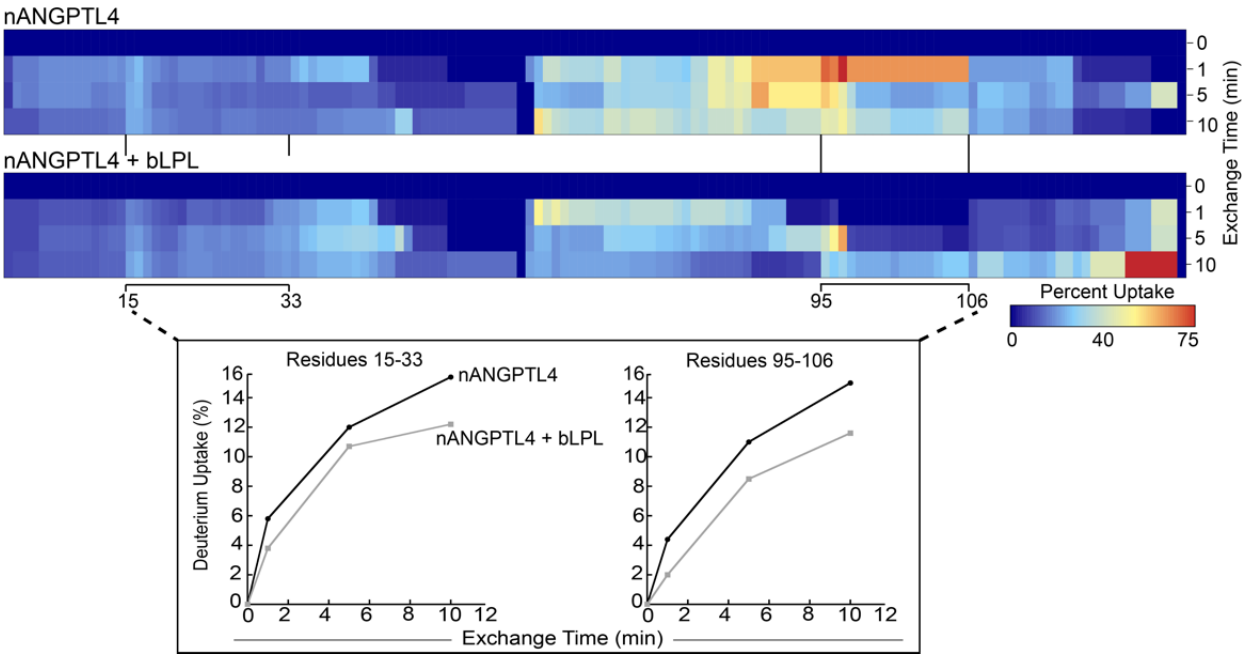

Figure 2.2 Decreased deuterium exchange suggest two potential binding sites on nANGPTL4. Heat maps of nANGPTL4 and nANGPTL4 + bLPL were generated using percent deuterium uptake values for peptide sequences with a standard deviation of less than 0.2 Da. Percent uptake curves were generated for sites that were statistically different between the nANGPTL4 apo and complex state. Sites of differential deuterium exchange were determined using unpaired two-tailed students t-test with cutoff of $p < 0.05$.

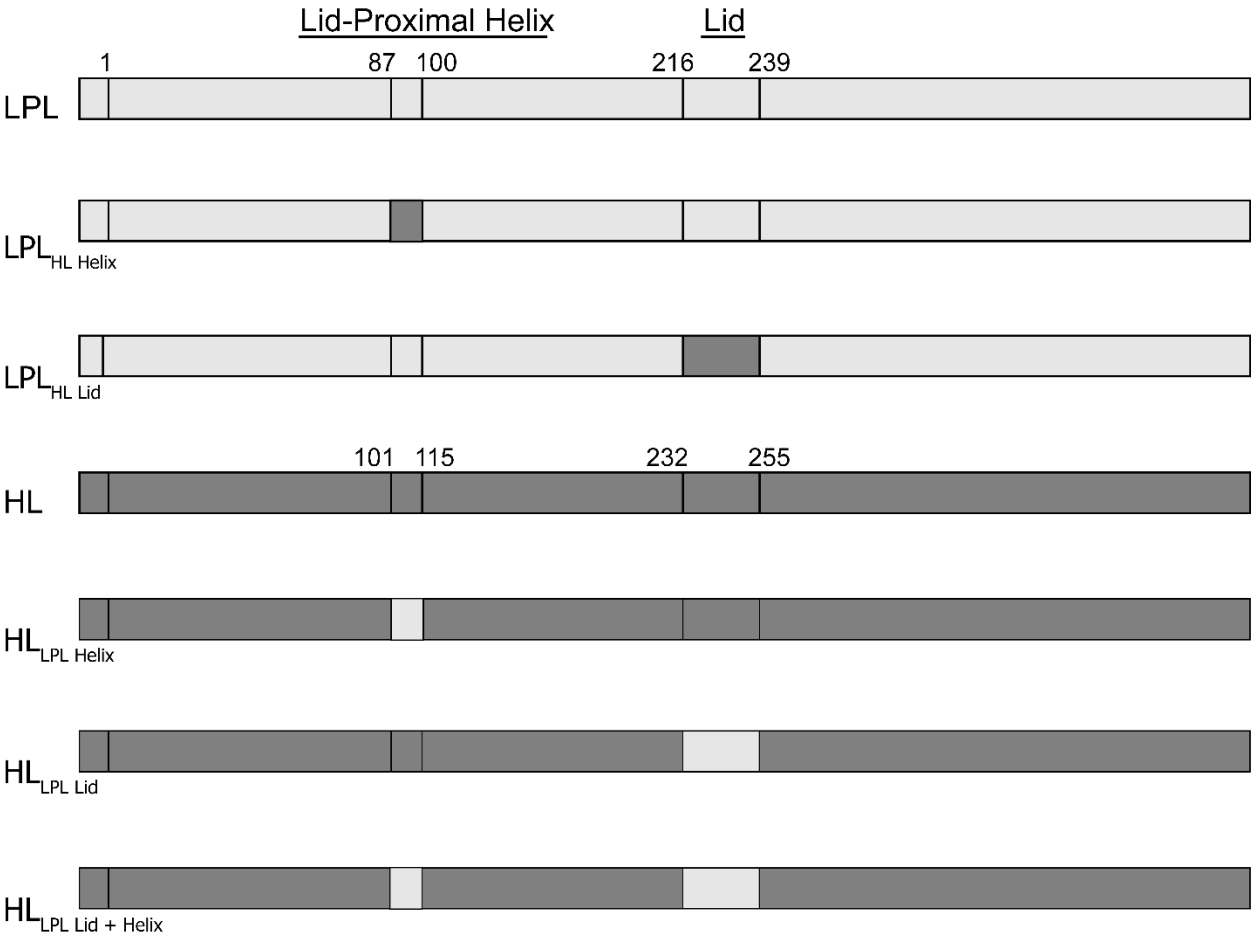

	Lid-Proximal Helix	Lid
LPL	L S R A Q E H Y P V S A G Y	C N I G E A I R V I A E R G L G D V D Q L V K C
HL	I T L A H D H Y T I A V R N	C H F L E L Y R H I A Q H G F N A I T Q T I K C

Figure 2.3. Human LPL and HL construct schematic. LPL (*light grey*) and HL (*dark grey*) sequences were aligned and defined according to potential nANGPTL4 binding sites identified by our HDX-MS experiments using bLPL. The corresponding sequences in human LPL and HL are defined as the lid-proximal helix (residues 87-100 or 101-115) or the lid (residues 216-239 or 232-255). Chimeric mutants were generated using overlap extension PCR.

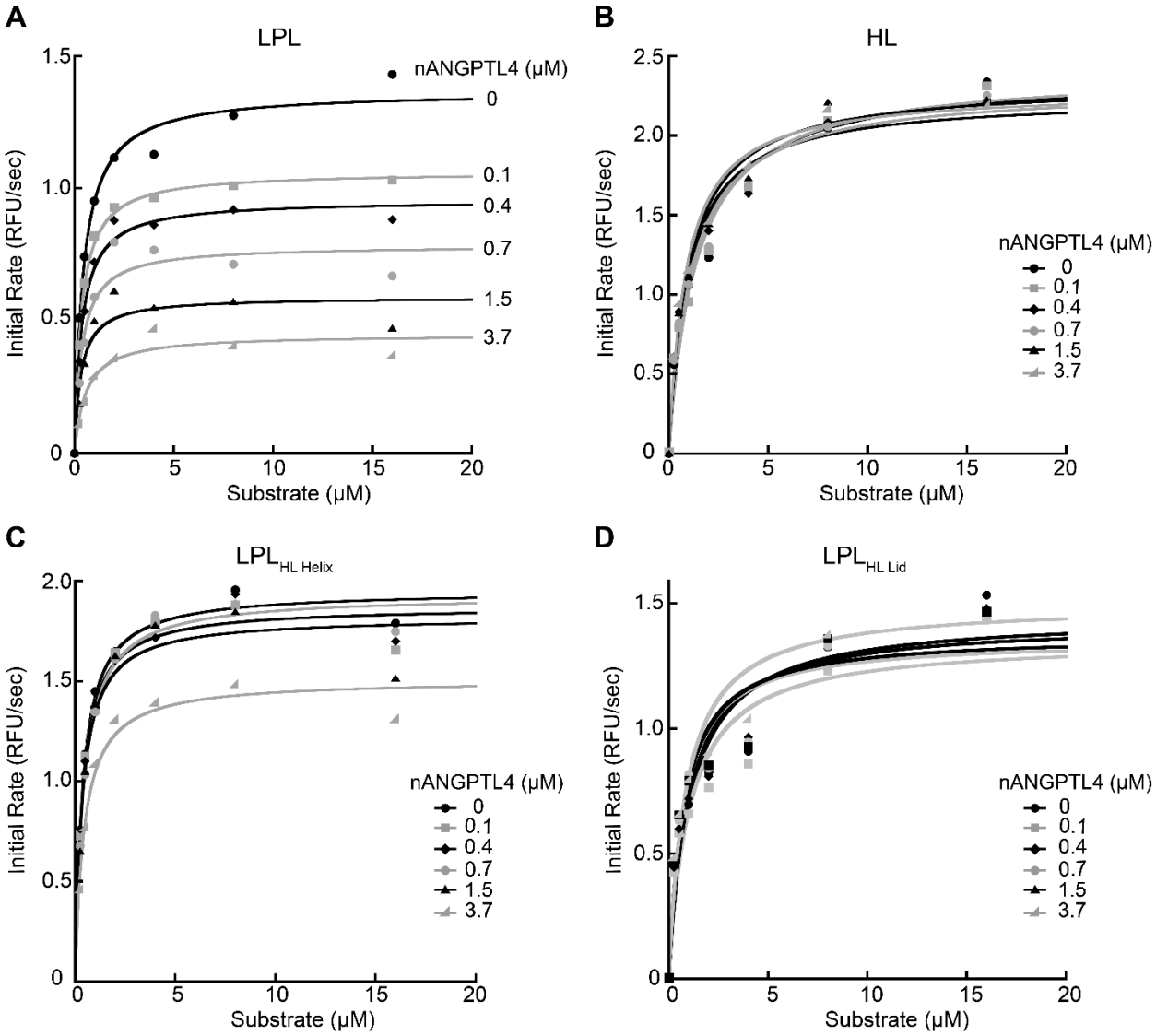

Figure 2.4. LPLHL chimeric mutants are resistant to nANGPTL4 inhibition. Michaelis-Menten curves were generated in the presence of increasing concentrations of nANGPTL4 over multiple concentrations of fluorescent substrate to obtain K_i values. (A) LPL is inhibited by nANGPTL4 with a K_i value of approximately $1.4^{+/-}0.13$ μM. (B) HL is resistant to nANGPTL4 inhibition. (C) $LPL_{HL\ helix}$ is resistant to nANGPTL4 with an estimated K_i of $14.0^{+/-}1.4$ μM. (D) $LPL_{HL\ lid}$ is resistant to nANGPTL4, similar to HL, a K_i could not be calculated. Representative data of four biological replicates ± standard error. *RFU,* relative fluorescent units.

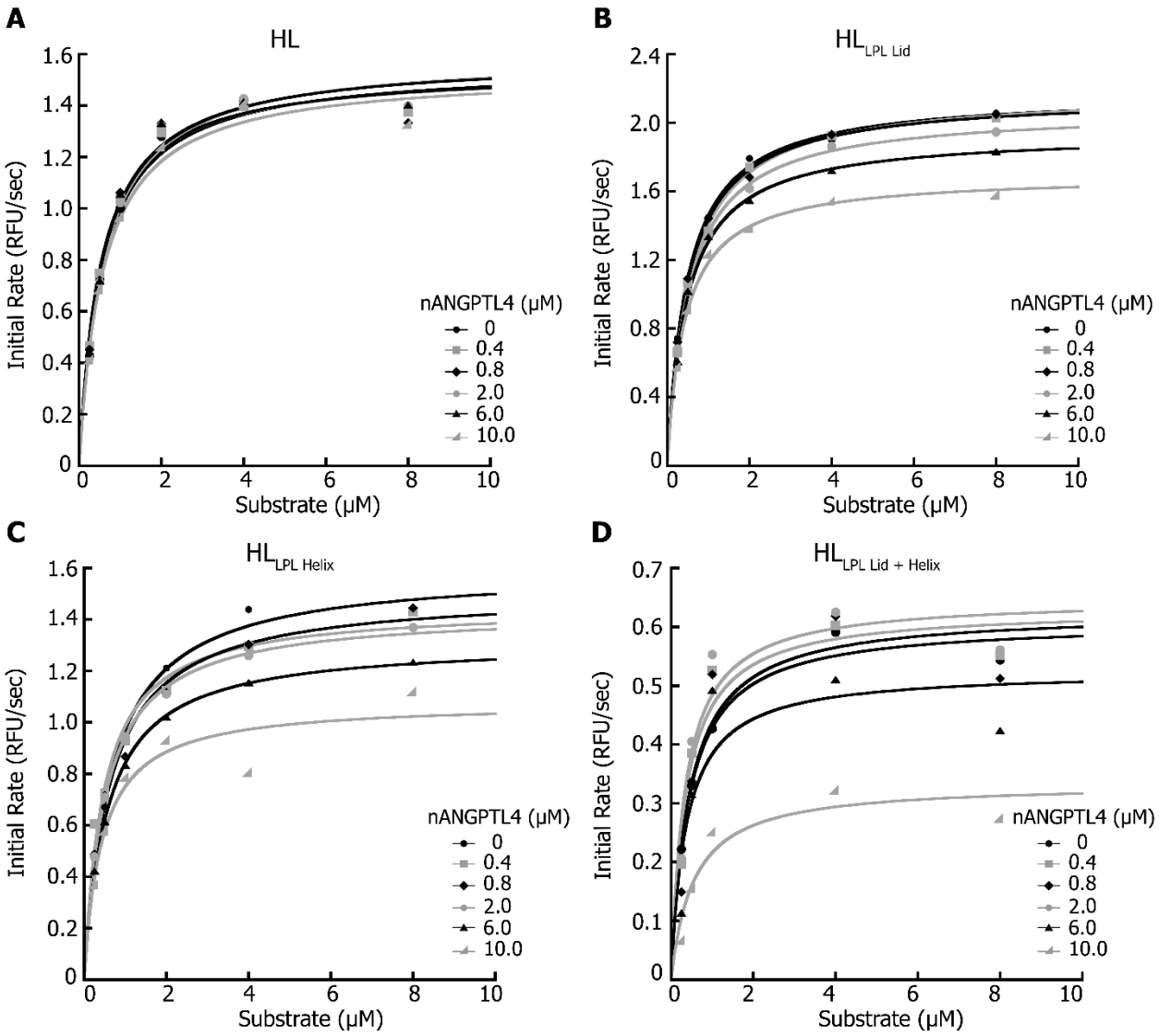

Figure 2.5. HLLPL chimeric mutants are sensitive to nANGPTL4 inhibition. (A) HL is resistant to nANGPTL4. (B) $HL_{LPL\ lid}$ is slightly sensitive to nANGPTL4 inhibition with an estimated K_i of $42.9^{+/-}2.8$ μM. (C) $HL_{LPL\ helix}$ is moderately sensitized to inhibition with an estimated K_i of $30.3^{+/-}3.5$ μM. (D) $HL_{LPL\ lid\ +\ helix}$ is the most sensitive to inhibition an estimated K_i of $22.9^{+/-}5.3$ μM. Representative data of four biological replicates ± standard error. *RFU,* relative fluorescent units.

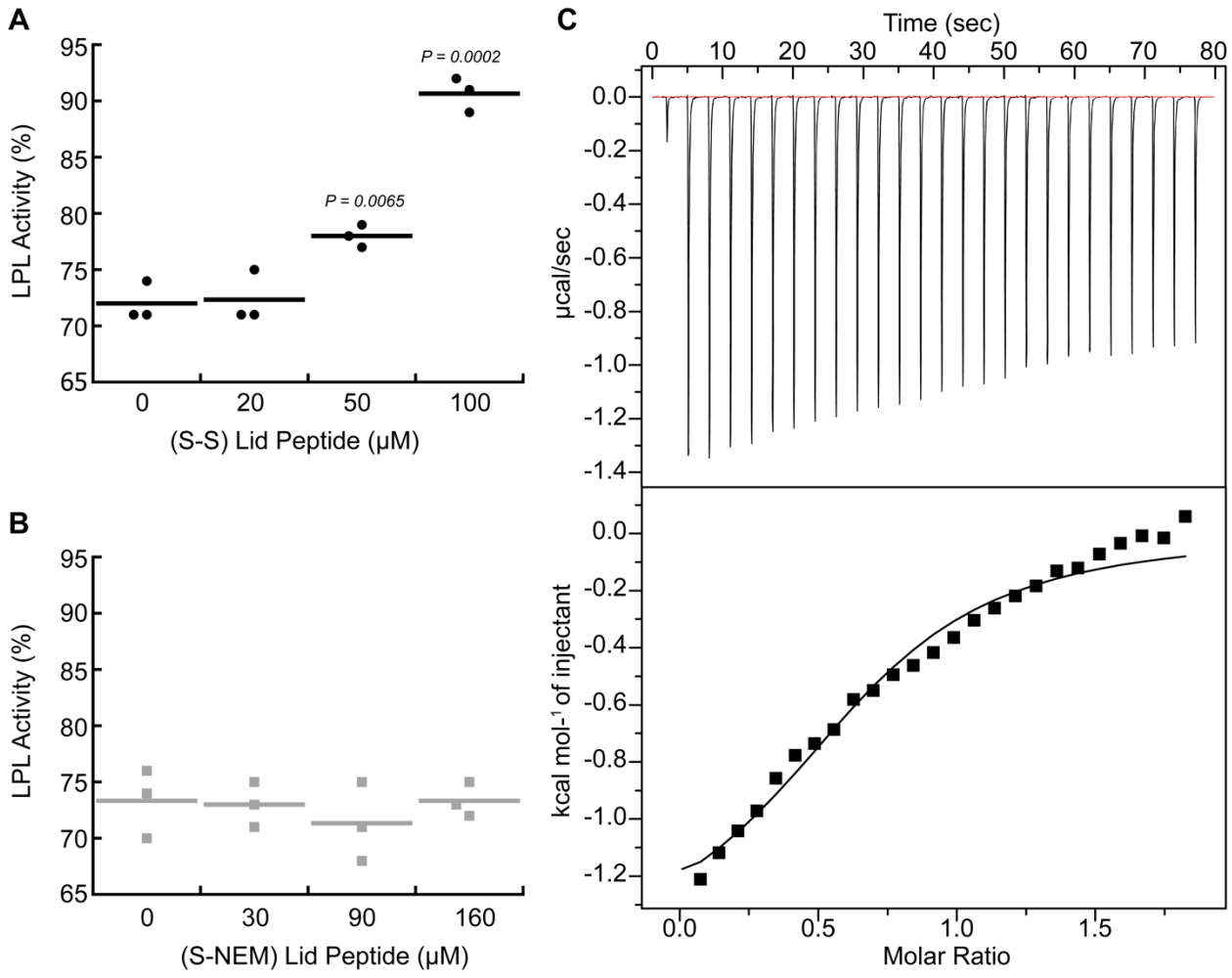

Figure 2.6. LPL lid mimetic binds nANGPTL4 and prevents inhibition of full-length LPL. (A) Cyclic lid peptide (S-S) blocks nANGPTL4 inhibition of full-length LPL in a dose-dependent manner. (B) Linear lid peptide with terminal cysteine residues capped with NEM does not block nANGPTL4 inhibition. (C) Isothermal titration calorimetry reveals the cyclic lid peptide binds nANGPTL4 with an approximate K_d = 57 μM. Representative data of at least three biological replicates.

2.7 Supplemental Information

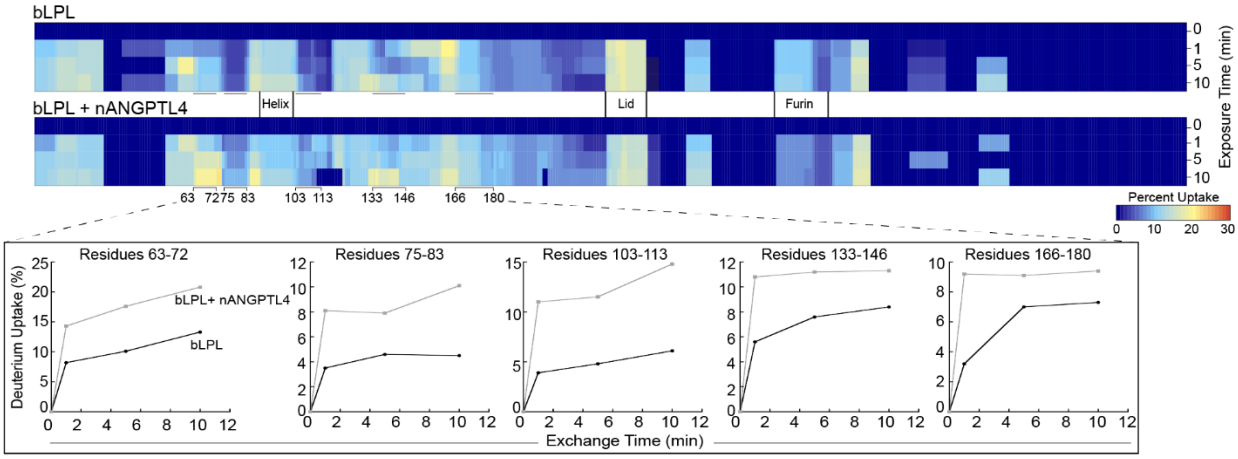

Supplemental Figure S2.1. Sites of increased deuterium exchange within bLPL upon nANGPTL4 inhibition. Heat map from Figure 2.1 is shown, except deuterium uptake curves depict peptides with increased uptake in the complex state. Deuterium uptake curves were generated for sites that were statistically different between bLPL apo (*black*) and complexed state (*grey*) at every time point. Sites of differential deuterium exchange were determined using unpaired two-tailed students t-test with cutoff of $p < 0.05$.

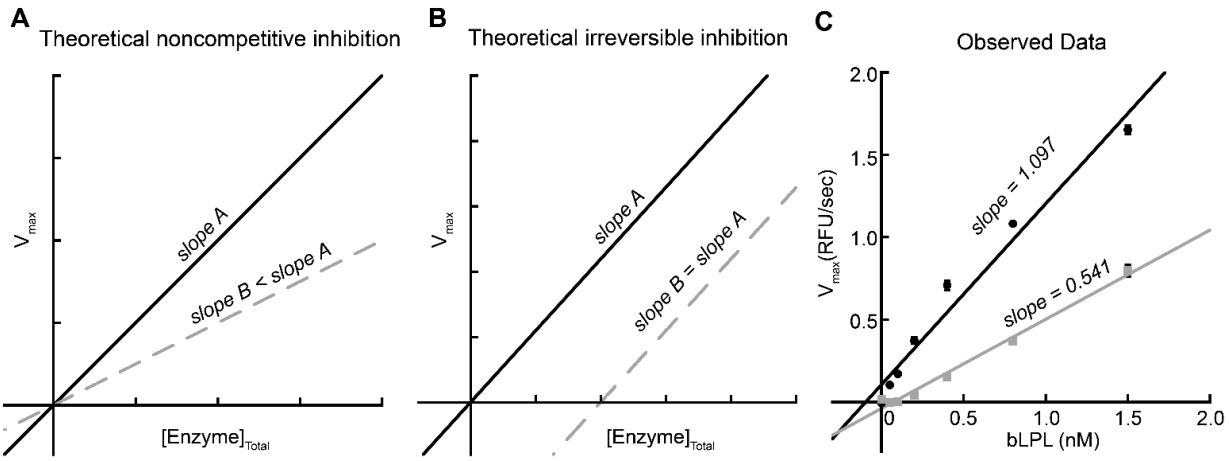

Supplemental Figure S2.2. nANGPTL4 is a reversible, noncompetitive inhibitor of bLPL using DGGR substrate. Irreversible enzyme inhibition can be distinguished from reversible, noncompetitive inhibition by plotting V_{max} versus the total concentration of enzyme in the assay (148). (A) Theoretical plot for reversible, noncompetitive inhibition demonstrates that in the presence of an inhibitor (*dashed grey*) the slope is less than the non-inhibited control (*solid black*) and both conditions pass through the origin. (B) Theoretical plot for irreversible inhibition demonstrates the control (*solid black*) and + inhibitor condition (*dashed grey*) have the same slope but cross the x-axis at two different enzyme concentrations. (C) Observed data where bLPL activity was measured at multiple concentrations in the presence of 0 μM (*solid black*) or 2 μM nANGPTL4 (*dashed grey*) under V_{max} conditions using 10 μM DGGR substrate. In the presence of nANGPTL4, the slope of the line decreases from 1.097 to 0.541 and both conditions converge near the origin. (A) and (B) adapted from (148). Error bars represent standard deviation. Representative data of three biological replicates. *RFU*, relative fluorescent units.

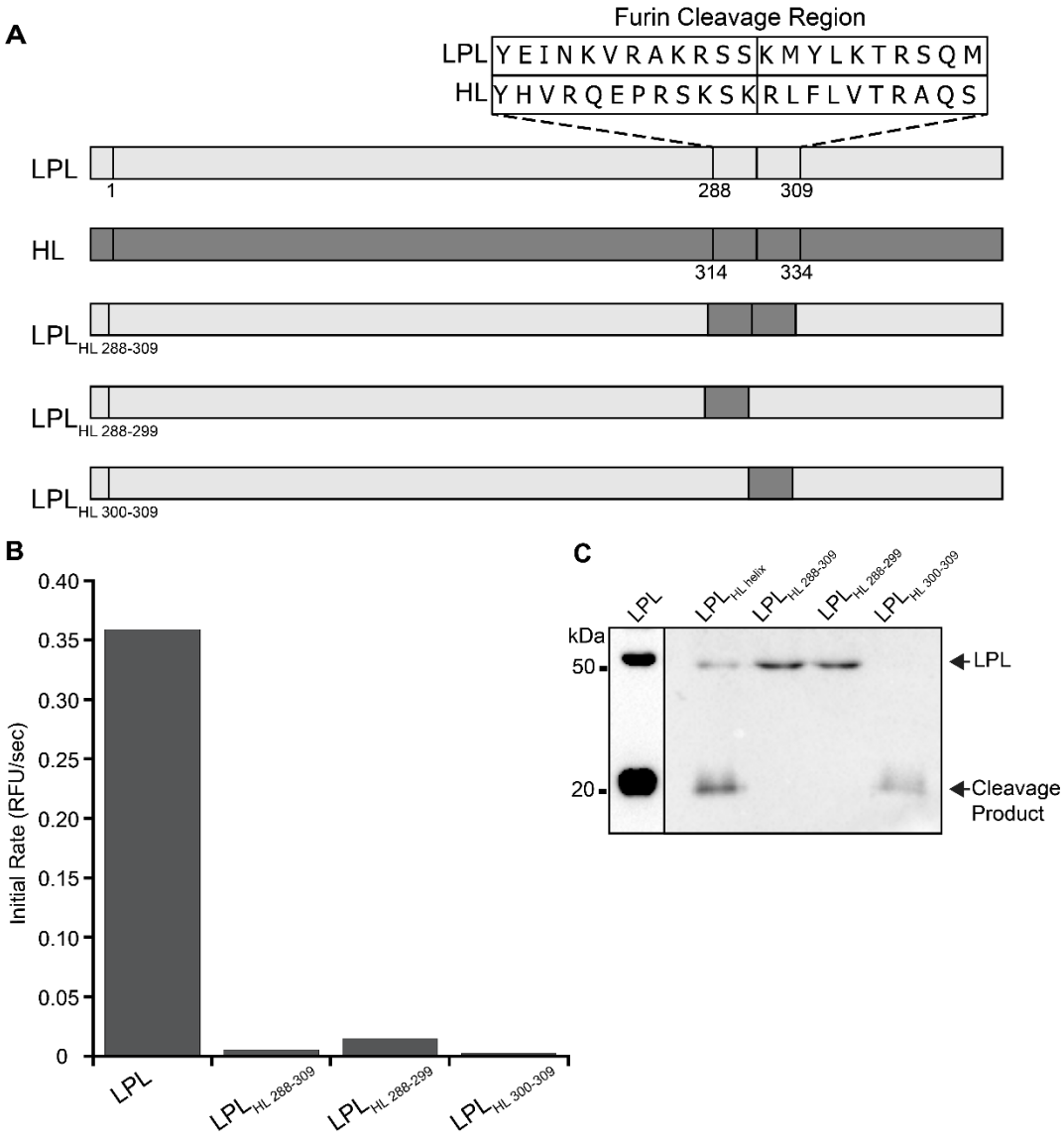

Supplemental Figure S2.3. HL chimeric mutations in the LPL furin cleavage region are not tolerated. (A) LPL (*light grey*) and HL (*dark grey*) sequences were aligned with residues 288-309 or 314-334 defined as the furin cleavage region. Overlap extension PCR was used to generate $LPL_{HL\ 288\text{-}309}$, $LPL_{HL\ 288\text{-}299}$, $LPL_{HL300\text{-}309}$. (B) Lipase activity was measured using DGGR substrate in cell culture media from transfected HEK 293 cells. LPL_{HL} chimeric mutants were not enzymatically active. (C) Western blot against C-terminal His tag detects both full length LPL (MW 55 kDa) and C-terminal cleavage product (MW~25 kDa) in cell culture media. Box indicates LPL was developed on a separate blot from the other LPL variants.

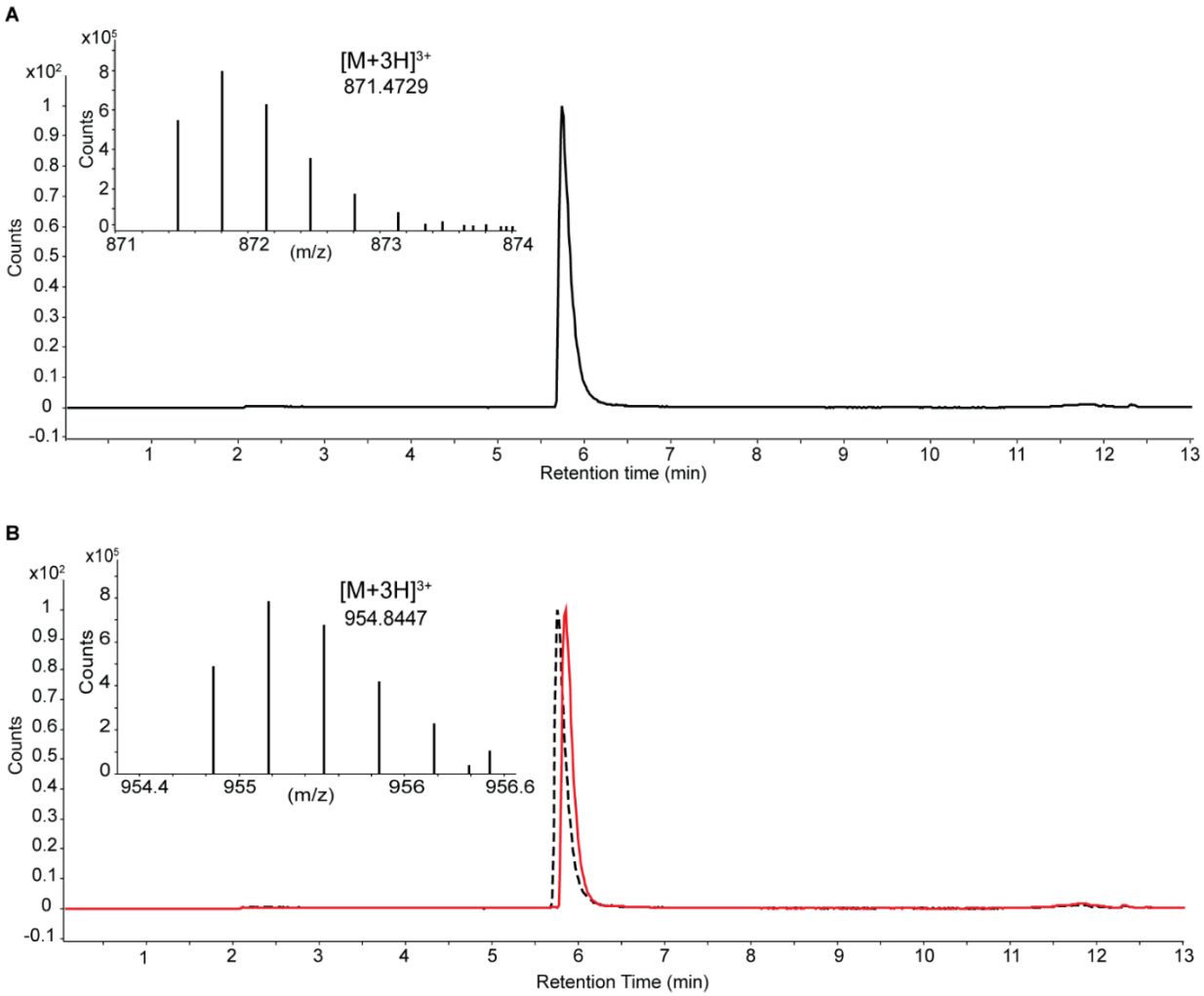

Supplemental Figure S2.4. Extracted ion chromatogram for cyclic (S-S) and linear (S-NEM) lid peptide. (A) Cyclic (S-S) lid peptide (*solid black*) has an m/z = 871.4729 corresponding to a MW of 2571 Da. (B) Lid peptide was linearized by capping terminal cysteine residues with NEM, whereby the capped species were isolated by HPLC. Ion chromatogram shows the elution of the (S-NEM) lid peptide (*solid red*) is slightly shifted from cyclic (S-S) lid peptide (*dashed black*). (S-NEM) lid peptide has an m/z = 954.8447 corresponding to a MW of 2821 Da, indicating both cysteine residues are bound to an NEM molecule.

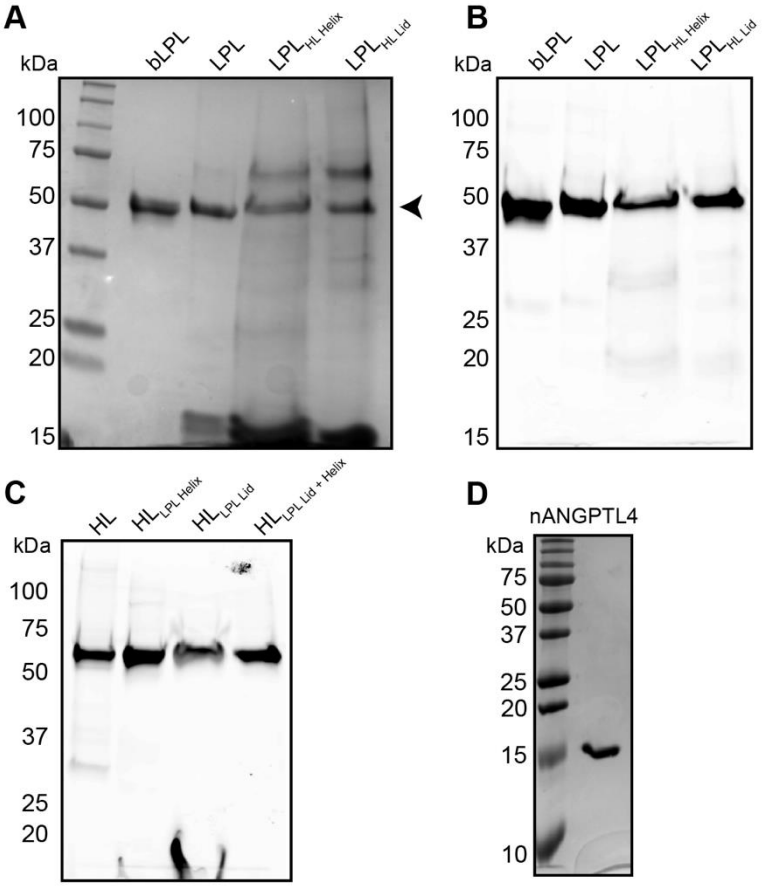

Supplemental Figure S2.5. Relative purity of each lipase variant and nANGPTL4. (A) Coomassie stained gel with all purified LPL variants used in this study (arrow). LPL purified from tissue culture contain two common contaminants from fetal bovine serum. (B-C) An activity-based probe was used to both quantify the amount of active lipase using bLPL as a standard and verify the purity for each lipase. A Coomassie stained gel for HL variants was not included because their concentration was below the limit of detection. (D) Coomassie stained gel of nANGPTL4 (15.4 kDa)

CHAPTER 3

Discovery of biologic inhibitors of angiopoietin-like protein 4 using display technologies.

3.1 Introduction

Protein-protein interactions (PPIs) are difficult to disrupt with small molecule modalities (159). Small molecule drugs have been widely successful at targeting proteins with well-defined cavities like enzymes, ligand-activated transcription factors, or receptors (160). Despite the widespread success of small molecule drugs, there are still many diseases with no effective treatment options. Protein-protein interfaces have largely been considered “undruggable” due to their large, flat surfaces that lack distinct binding pockets (161). However, with an expanding toolbox of biological drug libraries and high throughput screening tools, PPIs are within a druggable space and are at the forefront of important drug discovery efforts.

Angiopoietin-like protein 4 (ANGPTL4) is a potent inhibitor of lipoprotein lipase (LPL) that binds across a relatively large surface area (85). A point mutation at residue 40 of ANGPTL4, E40K, abolishes the ability of ANGPTL4 to inhibit LPL by disrupting this PPI. Therefore, humans with E40K mutations have lower average triglyceride levels (TG), higher HDL cholesterol levels, and a lower risk of developing cardiovascular disease and type II diabetes (89, 93, 94). E40 is located in the LPL binding site within the N-terminal domain of ANGPTL4, herein referred to as nANGPTL4 (85). To date, no humans with complete loss of ANGPTL4 expression have been reported. All predicted loss-of-function variants are either heterozygous or homozygous for missense variants, like E40K, that do not abolish ANGPTL4 expression (93)

The cardioprotective phenotype observed in human ANGPTL4 variants provided strong rationale to develop anti-ANGPTL4 monoclonal antibodies for the potential treatment of hypertriglyceridemia (HTG) (89, 91). However, anti-ANGPTL4 treatment was not tolerated in animals maintained on a diet high in saturated fat. The treated animals developed severe mesenteric lymphadenitis, or inflammation of the lymph nodes, chylous ascites, fibrinopurulent peritonitis, cachexia, and died after 15-25 weeks (89, 91, 137, 162). Additional studies have shown that this disease phenotype is specific for diets high in saturated fat, as animals fed high polyunsaturated fat diets do not develop systemic inflammation or chylous ascites (162). The animal pathophysiology is a curious discovery because human E40K ANGPTL4 variants have not been reported to have a higher incidence of lymphadenopathy than noncarriers (89, 93).

Research efforts to target ANGPTL4 for potential TG-lowering therapeutics have largely been abandoned due to the severe pathophysiology observed in anti-ANGPTL4 treated animals. It is important to consider that ANGPTL4 is a multifaceted secreted protein involved in metabolic and nonmetabolic pathways like angiogenesis, vascular permeability, wound repair, and kidney function (72). These preclinical studies highlight an important, but often overlooked, downside concerning the universality of conventional antibody therapeutics. Conventional antibodies often result in complete loss of soluble target proteins since antibody-target complexes are eliminated from the body by phagocytic cells (163). This mechanism of action is widely successful for nonessential target proteins where complete loss is well tolerated (164). However, ANGPTL4 has several mechanisms of action and knock out studies suggest that complete loss of ANGPTL4 expression is not tolerated due weakened endothelial junctions, diminished vascular integrity, and impaired lymphatic and blood vessel partitioning (144, 165). As discussed previously, all humans with predicted loss-of-function mutations are heterozygous or homozygous for missense variants that do not abolish ANGPTL4 expression. Therefore, anti-ANGPTL4 antibodies are not a safe method for lowering TG and clearly do not replicate the cardioprotective phenotype observed in human population studies (90, 93).

Our goal is to better mimic the cardioprotective phenotype observed in human carriers of E40K by developing a PPI inhibitor of LPL-ANGPTL4. Given that the nANGPTL4 binding site on LPL is on a flexible lid domain near its active site and LPL has several partner proteins, we opted to target nANGPTL4 (85). In this way, we avoid interfering with the enzymatic activity of LPL. However, nANGPTL4 is a notoriously difficult protein to work with as it contains a predicted intrinsically disordered domain and is prone to aggregation (139). With this in mind, we opted to screen nANGPTL4 against two types of biologic-based libraries using two different display technologies: 1) mRNA display for macrocyclic peptides and 2) yeast surface display for heavy chain only single domain antibodies.

Peptides are a unique class of biologics that are well equipped to modulate PPIs and are amenable to high-throughput screening methods, like mRNA display, for drug discovery (160). In mRNA display, large peptide libraries are coupled to their progenitor mRNA sequence, screened against an immobilized target protein, and amplified for additional rounds of selection to enrich for a population of peptides that bind the target protein (166). Suga and co-workers have developed a robust and efficient method for generating cyclic peptide libraries for mRNA display screening, known as the Random nonstandard Peptides Integrated Discovery (RaPID) system (167). RaPID incorporates nonproteinogenic amino acids into peptide libraries for spontaneous cyclization using an engineered ribozyme to acylate tRNA molecules with nonstandard amino acids, like N-chloroacetyl-tyrosine (ClAc-Y), and removes the cognate tRNA from *in vitro* translation mixtures. This system has been used to successfully identify cyclic peptides that bind and inhibit a wide range of PPIs for a variety of potential therapeutic applications (167). Therefore, we employed the RaPID system to identify cyclic peptides that bind nANGPTL4 and inhibit its ability to interact with LPL.

Heavy chain only single domain antibody fragments, or nanobodies, are naturally found in camelid species. They are composed of a small (15 kDa) antibodies with a single antigen-binding V-domain. A key difference between nanobodies and conventional antibodies is that

nanobodies lack an Fc domain. The Fc domain of the antibody-bound target protein binds Fc receptors on the surface of dendritic cells and macrophages and phagocytose the complex for degradation. In contrast, nanobodies bind their target protein with similar affinities and specificities as antibodies but do not promote the degradation of their target proteins. In a similar way to a smaller peptide inhibitor, we can develop a nanobody specifically against the N-terminal domain of ANGPLT4 that will inhibit its ability to interact with LPL without affecting its C-terminal domain or degrading the entire protein. Therefore, we screened nANGPTL4 against a synthetic library of nanobodies using yeast surface display (168).

3.2 Results

mRNA display for nANGPTL4 targeted cyclic peptides. We utilized an mRNA-encoding library containing up to a trillion non-standard, cyclic peptides to pan for high affinity binders to nANGPTL4. To generate a peptide library barcoded with progenitor mRNA sequences, we used a randomized DNA library containing seven to twelve NNK codons, a TGC codon for cysteine dependent cyclization, three repeating (GGC AGC) codons for a peptide glycine-serine linker, a stop codon, and a complementary sequence for puromycin linker base pairing (Figure 3.1) (169). The DNA library was transcribed into RNA and ligated to puromycin. Puromycin is an antibiotic that enables the formation of a stable amide bond between the progenitor mRNA sequence and peptide during the subsequent *in vitro* translation step (166). We incorporated the non-natural amino acid, *N*-chloroacetyl tyrosine (ClAc-Y), into our library by doping an initiator tRNA precharged with ClAc-Y into a methionine deficient translation mixture. The N-terminal chloroacetyl group spontaneously reacts with the closest cysteine side chain to cyclize via a thioether linkage (167). The final step of library preparation, was a reverse transcription reaction on the RNA linked peptide to remove potential secondary RNA structure and protect the library from RNA degradation (Figure 3.1) (166).

Selections were performed against biotinylated nANGPTL4 immobilized on streptavidin-coated magnetic beads. cDNA from nANGPTL4 bound RNA-peptides was eluted and PCR

amplified for iterative rounds of selection to enrich for a population of peptides that bind nANGPTL4 with high affinity. Enrichment was monitored after each round by quantitative PCR (qPCR) and submitted for next-generation sequencing (NGS). Unfortunately, our efforts to enrich populations of cyclic peptides that bind nANGPTL4 were unsuccessful (Figure 3.2A, B). We performed several independent selection campaigns against nANGPTL4 biotinylated on either the N- or C-terminus and were unsuccessful with both constructs. We did, however, find that biotinylated nANGPTL4 with an N-terminal 6X His and AviTag is not as active against LPL as biotinylated nANGPTL4 with a C-terminal AviTag and N-terminal 6X His tag (Figure 3.2C). These data suggest either biotinylation or the additional 34 amino acids on the N-terminus occlude or interfere with the LPL binding site on nANGPTL4.

Yeast display for anti-nANGPTL4 nanobodies. Yeast display is a platform whereby recombinant protein libraries are fused to a cell surface anchor protein for display on the surface of the cell. Each individual cell expresses a single protein variant and, together, make a library with an average diversity of 10^8-10^9 yeast cells. We screened nANGPTL4 against a synthetic nanobody library developed by Dr Andrew Kruse and colleagues (168). Briefly, they designed the library using the entire set of unique nanobody structures available in the Protein Data Bank (PDB) to identify residues suitable for either partial or complete randomization within the complementarity determining loops (CDRs) (Figure 3.3A) (168). Upon galactose induction, HA-tagged nanobodies are produced and tethered to the surface of yeast via a covalent C-terminal linkage to an engineered glycosylphosphatidylinositol anchor sequence (Figure 3.3A) (168). The library is composed of ~5 x 10^8 transformants with ~26% of yeast showing high expression of nanobodies when measured by flow cytometry.

To identify novel nANGPTL4-binding nanobody, we incubated the yeast library with either C-terminal biotinylated or c-Myc tagged nANGPTL4, stained nANGPLT4 bound yeast with either streptavidin microbeads or an anti-c-Myc-FITC conjugated antibody and anti-FITC microbeads, and then isolated magnetically labeled yeast using magnetic activated cell sorting

(MACS) (Figure 3.3B). For each round of selection, we alternated between c-Myc tagged nANGPTL4 and biotinylated nANGPTL4 to decrease the probability of enriching tag binders. To select for high affinity binders, we started round 1 with 8 µM nANGPTL4 and decreased the selection concentration by 10-fold for each subsequent round. After each round of selection, we used flow cytometry to evaluate enrichment of nanobody binders. After four rounds of selection, we successfully enriched for high affinity nanobody binders to nANGPTL4 whereby 23% of the isolated population were positive for binding just 8 nM nANGPTL4 (Figure 3.4).

3.3 Discussion

LPL is a master regulator of plasma TG levels and, therefore, an ideal target for novel TG-lowering therapeutics. LPL has a multitude of activators and inhibitors and modulation of any of these partner proteins directly affects TG levels. For example, researchers have developed a peptide mimetic of an activator of LPL, apolipoproteinC-II (apoC-II), that enhances LPL activity and rapidly lowers TGs in hypertriglyceridemic mice and zebrafish (124). Another example comes from Regeneron's anti-ANGPTL3 antibody, evinacumab, which has successfully completed phase III trials for the treatment of familial hypercholesterolemia and is currently in phase II trials for the treatment of severe HTG (103). In spite of the clinical success of anti-ANGPTL3 antibodies, anti-ANGPTL4 therapeutics have largely been abandoned due to the severe intestinal pathology of animals maintained on a high-fat diet. However, it is not entirely clear if the intestinal pathology is a direct consequence enhanced LPL activity within the mesenteric lymph nodes or weakened endothelial cell junctions resulting from loss of cANGPTL4. Therefore, our goal is to develop a therapeutic that inhibits the PPI between LPL and nANGPTL4 in order to preserve functionality in cANGPTL4. To do so, we screened nANGPTL4 against a panel of cyclic peptides and nanobodies and are currently tested their ability to inhibit its LPL binding interface.

Our efforts to identify a high affinity cyclic peptide against nANGPTL4 were unsuccessful. We do not know the exact reason for this, but we have three potential

explanations. In previous studies, we performed biophysical experiments to generate low-resolution structural information on nANGPTL4 in the absence of a known crystal structure. Our SEC-MALS and SEC-SAXS experiments suggest that nANGPTL4 is an elongated, highly flexible, trimer in solution. Perhaps, nANGPTL4 lacks distinct binding pockets for a rigid, cyclic peptide to bind. A second possibility stems from the fact that, in our hands, nANGPTL4 appears to be sensitive to shear stress. nANGPTL4 loses its ability to inhibit LPL and forms aggregated clumps by negative stain electron microscopy after rigorous pipetting. Lastly, we found nANGPTL4 aggregates in isothermal titration calorimetry experiments when placed in the sample cell. Stir speeds had to be decreased significantly to avoid nANGPTL4 aggregation. Although these lines of evidence are anecdotal, we hypothesize that immobilized nANGPTL4 aggregated after several wash steps before and after incubation with the peptide library. A final potential explanation could be that the selection concentration of 200 nM nANGPTL4 was too stringent, perhaps, using a higher concentration of nANGPTL4 would have selected a lower affinity binder. Overall, our efforts support the notion that nANGPTL4 is a difficult protein to work with and has interesting biophysical characteristics.

Nanobodies and yeast display offered several advantages over mRNA display from both a therapeutic and technical standpoint. Nanobodies are highly stable and often stabilize their binding partner such that co-crystal structures can be solved. Most importantly, nanobodies have similar binding specificities and affinities as conventional antibodies but lack Fc domains. The absence of an Fc domain will prevent complete loss of ANGPTL4 through Fc receptor-mediated uptake and allow us to specifically neutralize nANGPTL4. From a technical standpoint, yeast display may be more amenable to nANGPTL4 than mRNA display. Since the nanobody library is immobilized on the surface of the yeast, nANGPTL4 can be screened against the library without the need for immobilization and extensive wash steps. Overall, we isolated several high affinity nanobody binders of nANGPTL4 and are currently screening full length ANGPTL4 for cANGPTL4 functionality in the presence of anti-nANGPTL4 nanobodies.

Our ultimate goal is to determine if neutralizing nANGPTL4 can recapitulate the cardioprotective phenotype observed in the E40K variant population safely and effectively. Therefore, after completing functional studies on our nanobody hits, we will test our lead nanobody candidate in mice fed a diet high in saturated fat to determine if they develop severe intestinal pathologies like mesenteric lymphadenitis, chylous ascites, and fibrinopurulent peritonitis. These studies will determine if diet-induced intestinal pathology is a result of enhanced LPL activity in mesenteric lymph nodes or loss of cANGPTL4.

3.4 Materials and Methods

Molecular cloning- nANGPTL4 (residues 26-164) was cloned into the pNIC-Bio3 plasmid, which incorporates a TEV cleavable N-terminal 6X His tag and a C-terminal AviTag and nANGPTL4 (residues 26-161) was cloned in the pMCSG51 plasmid with a TEV cleavable N-terminal 6X His tag and AviTag and a C-terminal c-Myc tag separated with a glycine-serine linker $(G_4S)_2$. Both cloning methods utilized ligation-independent cloning (LIC). Briefly, nANGPLT4 was amplified using Phusion® High-Fidelity DNA Polymerase (New England BioLabs Inc) to create LIC-overhangs. The pNIC-Bio3 vector was linearized with BsaI, dephosphorylated with Antarctic Phosphatase, and treated with T4 DNA polymerase to create LIC-overhangs. The treated vector and nANGPTL4 PCR product were incubated for 15 minutes at room temperature and transformed into DH5α competent cells.

Protein expression and purification

nANGPTL4 - pNIC-Bio3-nANGPTL4 was co-transformed with pET21a-BirA into BL21 (DE3) cells for expression and *in vivo* biotinylation on the C-terminus. pMCSG51-nANGPTL4 was transformed into BL21 (DE3) cells for expression and *in vivo* biotinylation on the N-terminus. The culture was grown at 37°C until reaching an OD_{600} of 0.4-0.6, supplemented with 0.1 mM biotin, and induced with 0.1 mM IPTG (Thermo Fisher Scientific) overnight at 18°C. Cells were pelleted at 6,000 X *g*, resuspended in 50 mM tricine pH 7.9, 300 mM NaCl, 10 mM imidazole, 5 mM betaine, 10% glycerol, 1 mM fresh phenylmethylsulfonyl fluoride (Sigma), and

lysed using Emulsiflex C5 (Avestin) at 15,000 p.s.i. Lysate was cleared by centrifugation at 34,000 X *g* for 60 min. Cleared lysate was added to equilibrated Ni-NTA resin (Qiagen). Resin was washed with 10 column volumes using 20 mM HEPES pH 7.8, 360 mM NaCl, 32 mM imidazole, 5 mM betaine, 10% glycerol, followed by a second wash with 10 column volumes using 20 mM HEPES pH 7.8, 360 mM NaCl, 60 mM imidazole, 5 mM betaine, 10% glycerol. nANGPTL4 was eluted over 6 column volumes using 20 mM HEPES pH 7.8, 360 mM NaCl, 250 mM imidazole, 5 mM betaine, 10% glycerol. Fractions containing nANGPTL4 were dialyzed to into 50 mM tricine pH 7.9, 360 mM NaCl, 2 mM EDTA, 10% glycerol, aliquoted, and flash frozen for -80°C storage until use. Untagged nANGPTL4 was purified as described previously (85).

bLPL – bLPL was purified from fresh bovine milk as described previously (158).

mRNA display using a panel of cyclic peptides:

RNA library and flexizyme preparation – DNA libraries containing 7-12 NNK codons and flexizyme (eFx) oligos were purchased from IDT Technologies and prepared by extension of extension primers, amplified using PCR reaction, and purified using phenol/chloroform extraction and ethanol precipitation. DNA was transcribed according to the manufacturer's instructions using T7 RNA polymerase (New England Biolabs) overnight at 37°C to maximize RNA yields and ensure complete library coverage. Residual template DNA was removed with DNase (Promega) at 37°C for 1 hour. Magnesium pyrophosphate precipitate was cleared by adding 0.5 M EDTA and recovered RNA by isopropanol precipitation. RNA libraries were further purified from an 8% urea PAGE gel, extracted using 0.3 M NaCl, and ethanol precipitated. RNA pellets were resolubilized in water and diluted to a working concentration of 20 µM and stored at -80°C until use.

Ligation of puromycin linker – The puromycin linker (P-linker) was purchased as a DNA oligo with special modifications from IDT Technologies. Ligation reactions were performed using 1 µM library, 1.5 µM P-linker, 1X T4 RNA ligase buffer, 1 mM ATP, 20% DMSO, and T4 RNA ligase (New England Biolabs) at 25°C for 30 min. Reactions were quenched by adding 1X

volume of 0.6 M NaCl and 10 mM EDTA. P-linked RNA was ethanol precipitated and resolubilized in 1/10 volume of water as the original P-linking reaction.

Flexizyme acylation of N-chloroacetyl-tyrosine – Flexizyme (eFx) was mixed in a 1:1 molar ratio with $tRNA^{fMet}$ in 83 mM HEPES-KOH pH 7.5 and heated at 95°C for 2 min. RNA was allowed to refold upon incubation at 25°C for 5 min. 3 M $MgCl_2$ was added to the reaction to a final concentration of 750 mM and incubated at 25°C for 5 min. The reaction was chilled on ice, mixed with 25 mM ClAc-Y for a final concentration of 5 mM, and incubated at 4°C for 2 hours. RNA was pelleted and washed to remove residual $MgCl_2$ with 0.3 M sodium acetate and 70% ethanol three times. $tRNA^{ClAc\text{-}Y}$ was ethanol precipitated and stored as a pellet at -80°C until use.

Peptide translation, fusion, and reverse transcription – Cell free translation was performed using a customized NEB PURExpress® Δrf123, Δaa, ΔtRNA kit. Briefly, we mixed 1X translation solutions A and B with 25 µM initiator tRNA precharged with *N*-chloro-acetyl tyrosine (ClAc-Y), 0.5 mM methionine deficient amino acid mix, 1.2 µM P-linked RNA library and incubated the reaction at 37°C for 30 min. To promote mRNA-peptide fusion, the translated reaction was left at room temperature for 15 min. The library was dissociated from the ribosome upon the addition of 100 mM EDTA pH 8.0 and incubated at 37°C for 30 min. To protect RNA by complimenting with cDNA via reverse transcription, we added 0.25 mM dNTPs, 2 µM reverse primer, 25 mM Tris-HCl pH 8.3, 15 mM $Mg(OAc)_2$, 10 mM KOH, and 1X MMLV reverse transcriptase H (-) point mutant (Promega) to the prepared library. The reaction incubated at 42°C for 1 hour. Lastly, the library was passed through Sephadex G-25 resin prepacked in a small, 1 mL, column to exchange into selection buffer (20 mM tris-HCl pH 8.0, 360 mM NaCl, 5 mM betaine, 10% glycerol) prior to incubation with nANGPTL4.

nANGPTL4 selection – Biotinylated nANGPTL4 was immobilized on Dynabeads™ M-280 Streptavidin magnetic beads (ThermoFisher Scientific), beads were washed three times with selection buffer, blocked with 25 µM biotin, and washed three more times with selection

buffer. For the initial round, nANGPTL4 coated beads were incubated with library for 30 min at a final concentration of 200 nM. cDNA/mRNA-peptide bound beads were washed three times with selection buffer and cDNA was eluted in 1X PCR buffer by heating at 95°C for 5 min. For subsequent rounds, the library was precleared of potential biotin-streptavidin bead binders by incubating the library with a 50:50 mixture of biotin-coated beads at 4°C for 30 min prior to incubation with nANGPTL4-coated beads. Beads used to preclear the library (negative selection) were washed and eluted in the same way as nANGPTL4-coated beads (positive selection) to later assess for library enrichment by quantitative PCR (qPCR). Eluted cDNA was amplified by PCR using Taq polymerase, purified by phenol/chloroform extraction and ethanol precipitation, and stored at -20°C until use in RNA transcription reactions for the following round of selection.

Next generation sequencing – Next generation sequencing adapters were added to cDNA samples eluted from rounds 3-5 using PCR amplification and Taq polymerase. DNA samples were quantified using Nanodrop™ 1000 and sent for sequencing using Genewiz's Amplicon Ez service. Sequencing analysis was performed using a python script to translate DNA sequences into amino acid sequences and list the top 1000 sequences that were enriched across each round of selection. Sequences were visualized using CLC Sequence Viewer (Qiagen).

Yeast display using magnetic activated cell sorting (MACS)- The nanobody library was developed by Dr. Andrew Kruse and colleagues (168). Briefly, nanobodies are expressed as an N-terminal fusion of the mating factor alpha pro-peptide for secretion and a C-terminal fusion of hemagglutinin (HA) tag and 649 amino acid glycosylphosphatidylinositol anchor sequence for covalent tethering of the nanobody to the yeast cell wall. We performed four rounds of selection against nANGPTL4 where the first round was done using magnetic sorting and MACS® Cell Separation (Miltenyi Biotec) for all subsequent rounds. The first round of selection was performed using 5×10^9 induced yeast (roughly 10-fold over the estimated library diversity) and

1-2 x 10^7 cells for subsequent rounds. Yeast were washed, resuspended in selection buffer (1X PBS pH 7.4, 1 mM EDTA, 5% glycerol, 0.1% BSA) containing Pierce™ anti-c-Myc magnetic beads (ThermoFisher Scientific) for the first round of selection and streptavidin microbeads (Miltenyi Biotec) or anti-c-Myc-FITC antibody and anti-FITC microbeads (Miltenyi Biotec) for subsequent rounds. The yeast-bead mixture was incubated for 40 min at 4°C. Yeast nonspecifically bound to magnetic beads were removed from the first round using a DynaMag™-5 Magnet (ThermoFisher Scientific) and, for subsequent rounds, were by passed through an equilibrated LD column (Miltenyi Biotec). After pre-clearing, nANGPTL4 binding nanobodies were isolated after incubating the yeast with biotinylated or c-Myc tagged nANGPTL4 at 4°C for 1 hour. Throughout these four selection rounds, yeast were stained with successively lower concentrations of nANGPTL4: 8 µM, 800 nM, 80 nM, and 8 nM to enrich for binders with higher affinities. nANGPTL4 bound yeast were pelleted and resuspended in Pierce™ anti-c-Myc magnetic beads for the initial round or streptavidin microbeads (Miltenyi Biotec) or anti-c-Myc-FITC antibody and anti-FITC microbeads (Miltenyi Biotec) for subsequent rounds and incubated at 4°C for 20 min. For the initial round, bead bound yeast were isolated and washed twice using a DynaMag™-5 Magnet (ThermoFisher Scientific). For subsequent rounds, bead bound yeast were passed over an LS column and washed prior to elution. After every round, isolated yeast were recovered in 3 mL of Trp dropout media containing glucose shaking at 230 rpm for 24 hours at 30°C. After selection, nanobody plasmids were extracted from yeast isolated from round 3 and 4 using 25 mM tris pH 7.5, 5 mM 2-mercaptoethanol (Sigma), Zymolase, and a QIAprep Spin Miniprep Kit (Qiagen). Isolated nanobody plasmids were transformed into DH5α competent cells and sent for bacterial colony sequencing (Functional Biosciences).

Flow cytometry and cell sorting- Yeast isolated from each round of selection were was washed with selection buffer (1X PBS pH 7.4, 1 mM EDTA, 5% glycerol, 0.1% BSA) and incubated with 800 nM, 80 nM, or 8 nM biotinylated nANGPTL4 for 1 hour at 4°C. nANGPTL4

bound cells were pelleted and washed once with selection buffer. Pelleted yeast were resuspended in 3 µg/mL Streptavidin Alexa Fluor™ 633 conjugate (ThermoFisher Scientific) or anti-HA-tag (6E2) Alexa Fluor™ 488 conjugate (Cell Signaling Technology) and incubated at 4C for 30 min. Labeled cells were washed three times and passed through a 40 µm filter prior to sample loading onto a BD FACSCanto™ flow cytometer (BD Biosciences) for analysis. Yeast isolated following MACS selection in round 3 were further isolated using a BD FACSAria™ III (BD Biosciences) flow cytometer for cell sorting. Gating for stained yeast was determined manually based on the cell profile of unstained yeast. All data was analyzed using the FlowJo™ v10.6.1 software.

3.6 Figures

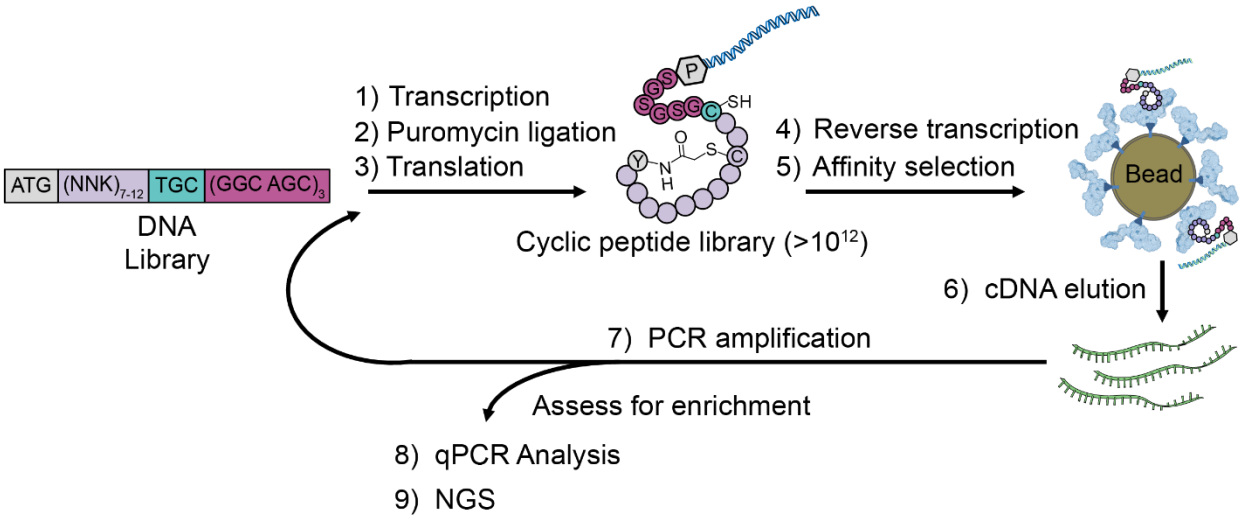

Figure 3.1 Overview of the RaPID system utilized for a campaign against nANGPTL4. A DNA library containing codons for an initiator methionine, 7-12 random amino acids, a C-terminus cysteine residue, followed by a glycine serine linker was transcribed into mRNA. Puromycin was ligated to the mRNA to enable peptide fusion in the subsequent *in vitro* translation step. The non-natural amino acid, *N*-chloroacetyl tyrosine, was precharged onto the initiator tRNA by flexizyme and doped into a translation mixture deficient in methionine. *N*-chloroacetyl tyrosine spontaneously forms a thioether linkage with a downstream cysteine residue to form a macrocyclic peptide. The peptide-linked mRNA was reverse transcribed to protect from RNase degradation and abolish interfering RNA secondary structure. The library was then incubated with immobilized nANGPTL4 to facilitate peptide binding and washed extensively to remove nonspecifically bound peptides. The cDNA of nANGPTL4-bound peptides was eluted and amplified by PCR for subsequent rounds of selection. After each round of selection, enrichment was monitored by qPCR and then sequenced by NGS after 4-6 rounds of selection. Figure adapted from Huang et al. 2018 (166)

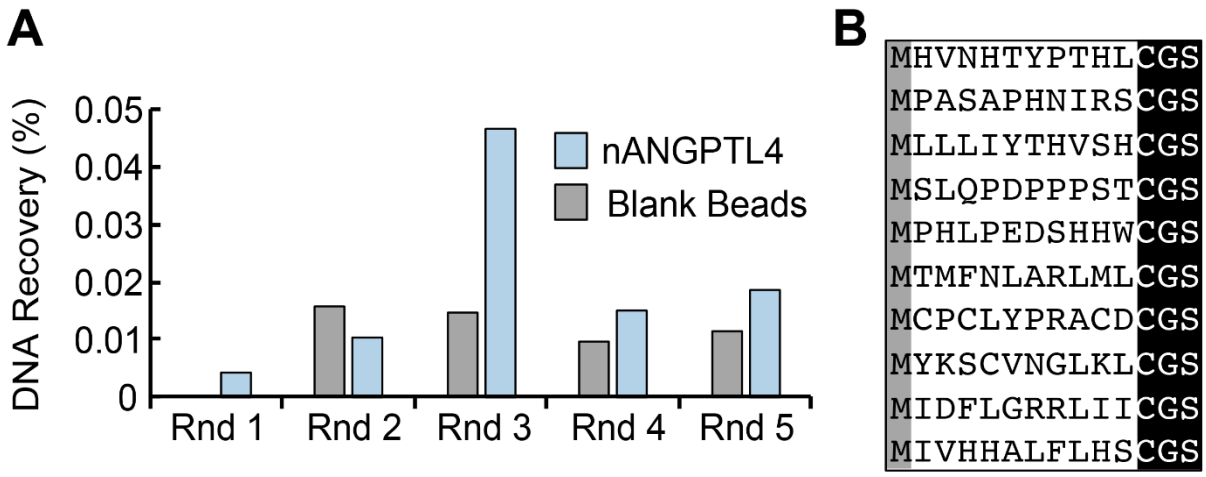

Figure 3.2 No enrichment observed after several campaigns against nANGPTL4. A) Representative qPCR result where we could not see significant signs of enrichment, indicated by percent DNA recovery (*blue*) in comparison to the negative control (*gray*). B) Representative NGS sequencing result where no obvious consensus sequence emerged. Note the initiator methionine is actually *N*-chloroacetyl tyrosine (*gray*) and C-terminus cysteine and glycine-serine linker are highlighted (*black*).

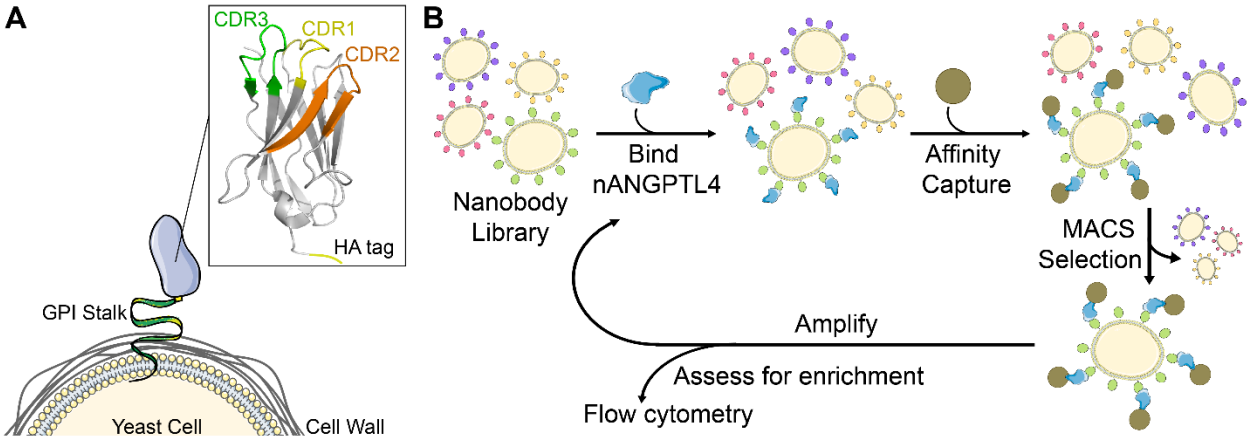

Figure 3.3 Overview of yeast display campaign against nANGPTL4. A) Kruse and colleagues generated a synthetic nanobody library with variation in each CDR loop was fused with an HA tag and GPI stalk on the C-terminus for display on the surface of yeast (168). B) The naïve nanobody library was incubated with soluble nANGPTL4, washed, and affinity captured using magnetic beads. nANGPTL4 bound yeast were isolated using magnetic activated cell sorting (MACS) and grown for additional rounds of selection. We assessed for nanobody enrichment after each round of selection using flow cytometry. Figure adapted from McMahon *et al*. 2018 (168).

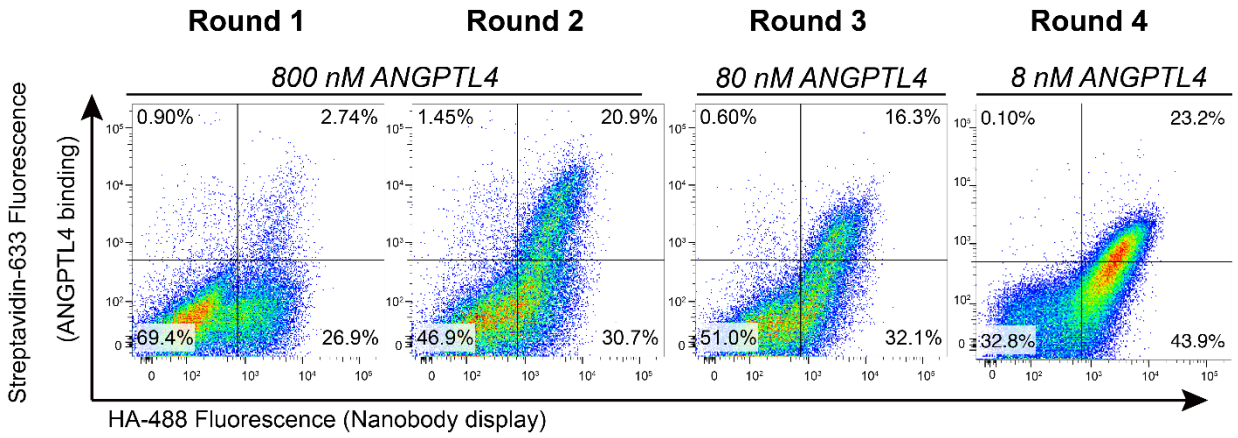

Figure 3.4 Enrichment of anti-nANGPTL4 nanobodies after four rounds of selection. Flow cytometry analysis where each dot is an individual yeast cell fluorescently labeled to monitor nanobody display and nANGPTL4 binding. Nanobody surface display is indicated on the x-axis where HA-tagged nanobodies were stained with an anti-HA-488 antibody. nANGPTL4 binding is indicated on the y-axis where biotinylated nANGPTL4 is labelled with streptavidin-633. Yeast cells displaying nANGPTL4 specific nanobodies are in the upper right quadrant with significant enrichment observed from 2.7% in round 1 to 23.2% in round 4 at the lowest nANGPTL4 concentration (8 nM).

CHAPTER 4

Comparison of ANGPTL3 and 4 reveals heparin binding to ANGPTL3 blocks LPL inhibition

4.1 Introduction

Lipoprotein lipase (LPL) plays a central role in the regulation of whole-body energy balance by hydrolyzing triglycerides (TG) within circulating lipoproteins to provide free fatty acids to tissues. LPL activity is differentially regulated in adipose vs. muscle tissue depending on nutritional state, in order to ensure appropriate distribution of available energy throughout the body (57). Specifically, LPL activity is downregulated in adipose tissue during fasting to direct TG-rich lipoproteins to muscle tissue for fatty acid oxidation (95). Conversely, in the postprandial state LPL activity increases in adipose tissue, but decreases in oxidative tissues, allowing utilization of glucose by oxidative tissue and TG storage in adipose tissue (170). This tissue specific regulation is facilitated by three members of the angiopoietin-like protein (ANGPTL) family of proteins: ANGPTL3, ANGPTL4, and ANGPTL8. Each protein is an inhibitor of LPL, and each has a different pattern of expression (171). ANGPTL3 is highly expressed in the liver and is largely insensitive to nutritional state (77). In fasted conditions, ANGPTL4 is upregulated in adipocytes to inhibit LPL locally in adipose tissue. ANGPTL8 is upregulated in postprandial conditions and expressed in the liver and adipose. Unlike ANGPTL4, the effect of ANGPTL3 inhibition on LPL is only observed when ANGPTL8 is present after feeding (60). ANGPTL3 and ANGPTL8 circulate in complex to inhibit LPL in oxidative tissues, however, the mechanistic details for how they form an inhibitory complex are not well understood (60–62).

As members of the ANGPTL family, ANGPTL3 and ANGPTL4 share similar structural characteristics and have 29% sequence identity. Both have an N-terminal coiled-coil domain and a C-terminal fibrinogen-like domain separated by a furin cleavage site (138, 172). The N-terminal coiled-coil domain of both proteins inhibit LPL *in vitro* through a conserved inhibition motif. However, biochemical studies suggest ANGPTL4 is a notably better inhibitor of LPL than ANGPTL3 on its own (143). With so many biochemical similarities, some puzzling differences emerge between the physiological role of ANGPTL3 and ANGPTL4. Specifically, why can ANGPTL3 inhibit LPL *in vitro*, but is codependent on ANGPTL8 for inhibition *in vivo*?

In previous work, comparisons of *in vitro* LPL inhibition by ANGPTL3 and ANGPTL4 showed that ANGPTL4 inhibition of LPL was up to 100x more potent than ANGPTL3 (45, 82, 83). Differences have also been observed in the abilities of ANGPTL3 and ANGPTL4 to inhibit LPL in the presence of other proteins and additives. For example, heparin was found to protect LPL from inhibition by ANGPTL3 (82, 83). In contrast, heparin enhanced the rate of ANGPTL4-mediated inactivation of LPL (82). It was proposed that this protection was due to competitive binding of heparin to LPL, resulting in occlusion of the ANGPTL3 binding site on LPL (83). The mechanism of ANGPTL3 has remained unclear, partially due to its poor *in vitro* inhibition of LPL. Different studies have arrived at conflicting conclusions about whether ANGPTL3 is an irreversible or reversible LPL inhibitor, indicating more data is needed to elucidate how ANGPTL3 inhibits LPL (83, 87).

Here, we set out to better understand ANGPTL3 inhibition of LPL. First, we performed biophysical experiments to compare the structures and oligomeric states of the N-terminal coiled-coil domains of ANGPTL3 and ANGPTL4, herein referred to as nANGPTL3 and nANGPTL4. As predicted, both proteins were found to share structural similarities in that they form elongated, flexible oligomers in solution. nANGPTL3 and nANGPTL4 both predominated as trimers, but nANGPTL3 also formed a hexamer that does not interconvert into a trimer. In preparing for our biophysical studies, we discovered that nANGPTL3 co-purifies with a DNA

contaminant. Removal of this DNA contaminant significantly enhanced nANGPTL3 inhibition of LPL. Heparin mimics the inactivating effect of the DNA contaminant on nANGPTL3. In contrast, heparin did not affect the ability of nANGPTL4 to inhibit LPL. These data reveal that despite having structural similarities, nANGPTL3 and nANGPTL4 have different mechanisms of action on LPL.

4.2 Results

DNA-bound nANGPTL3 is an ineffective inhibitor of LPL. In previous *in vitro* studies, ANGPTL3 was shown to be a less potent inhibitor of LPL than ANGPTL4 (45, 82, 83). Most of these studies used nANGPTL3 recombinantly produced in *E. coli* and purified using nickel chromatography (82, 83). We repeated this protocol and included a size-exclusion chromatography (SEC) step for additional purification. Unexpectedly, we found that nANGPTL3 co-purified with significant nucleic acid contamination, as observed by absorbance at 254 nm (Figure 4.1A). The contaminating nucleic acid was sensitive to DNase treatment, but resistant to RNase treatment, indicating that nANGPTL3 was bound to DNA (data not shown). We also observed two peaks in the included volume of the SEC that contained nANGPTL3. We pooled and concentrated the nANGPTL3 from each peak and assessed *in vitro* LPL inhibition using the fluorescent substrate, DGGR. These experiments showed that neither nANGPTL3 peak 1, nor peak 2, significantly inhibited LPL activity (Figure 4.1B, C). In order to remove the contaminating DNA from the nANGPTL3 preparation, we added an additional purification step, anion exchange chromatography (MonoQ), which led to a significant reduction in DNA and cleaner nANGPTL3 as observed from the 254 nm trace from subsequent SEC (Figure 4.1D). Interestingly, nANGPTL3 still eluted in two distinct peaks from the SEC after this additional anion exchange step. Both peak 1 and peak 2 contained >95% pure nANGPTL3 and had enhanced potency against LPL (Figure 4.1E, F).

nANGPTL3 and nANGPTL4 size determination. We next set out to determine the oligomeric state of the clean nANGPTL3 in SEC peaks 1 and 2. Although a previous study

showed that nANGPTL3 elutes from SEC across a broad peak as high-molecular weight oligomers, the precise composition of these oligomers has not been determined (77). Thus, both peak 1 and 2 were collected, concentrated, and separately analyzed by SEC in line with multi-angle light scattering (SEC-MALS). These experiments revealed that peak 1 had a molecular weight of 151 kDa, which corresponds to a hexamer of nANGPTL3 (monomer 26.8 kDa) (Figure 4.2A). The second peak had a molecular weight of 76 kDa, which corresponds to an nANGPTL3 trimer (Figure 4.2B). Intriguingly, we also found that the nANGPTL3 hexamers and trimers do not interconvert. When we re-injected each peak onto SEC, we observed only a single peak on the second SEC run (Figure 4.2A, B), indicating that nANGPTL3 hexamers do not break down into trimers and trimers do not assemble into hexamers. Similar to nANGPTL3, nANGPTL4 has been reported to form higher order oligomers by SEC and ultracentrifugation (77, 84). However, the exact composition of these oligomers has not been determined. To accurately compare the oligomeric state of nANGPTL3 and nANGPTL4, we performed SEC-MALS on nANGPTL4. We found nANGPTL4 elutes in a single peak with a molecular weight of 46 kDa, which corresponds to a trimer of nANGPTL4 (monomer 15.4 kDa, Figure 4.2C).

Structural comparison of nANGPTL3 and nANGPTL4. To further analyze the structural differences between nANGPTL3 and nANGPTL4, we carried out SEC-small angle X-ray scattering studies (SEC-SAXS). Analysis of nANGPTL3 hexamers and trimers also suggest elongated structural envelopes, with the trimer being about half the length of the hexamer (Figure 4.3A-D, Supplemental Figure 4.2B-C, Supplemental Table 4.1). Because there is currently no structure of the N-terminal region of ANGPTL3, we did not attempt to model in the predicted coiled-coil domains. However, the length of molecules seen here would be consistent with other coiled-coil proteins of similar size. nANGPTL4 was found to have an elongated and highly flexible structure (Figure 4.3E-F, Supplemental Figure 4.2A, Supplemental Table 4.1). Although these SAXS envelopes are low resolution, they reveal that both nANGPTL3 and

nANGPTL4 adopt elongated structures in solution and confirm that the SEC-MALS data accurately describes the oligomeric state of the proteins.

Low molecular weight heparin binds to and inhibits nANGPTL3 but not nANGPTL4. Previous work demonstrated that nANGPTL3 inhibition of LPL is blocked by the presence of heparin (82, 83). Given that DNA-contaminated nANGPTL3 does not inhibit LPL, we hypothesized that both heparin and DNA can occupy the heparin binding motif in nANGPTL3 (V61-G66), which is adjacent to the LPL inhibitory motif (I46-L57), and consequently prevent LPL inhibition (59, 142, 143). We tested this hypothesis by measuring the effects of three different heparin oligosaccharides: disaccharide (2-mer), hexasaccharide (6-mer), and dodecasaccharide (12-mer) on LPL activity and inhibition (Supplemental Figure 4.1A). First, we tested the ability of the heparin to stabilize LPL activity (Figure 4.4A). The 2-mer did not stabilize LPL, and therefore no increase in LPL activity was observed, however, both 6-mer and 12-mer did stabilize LPL. At low concentrations, heparin stabilizes LPL; this stabilization has been attributed to heparin bridging two monomers to stabilize active LPL dimers. We found that 6-mer significantly stabilizes LPL activity, although to a lesser extent than 12-mer, for which we observed an even larger increase in LPL activity and, therefore, stabilization. These data agree with a previous study that showed that shorter heparin saccharides (tetra- and hexasaccharides) do not stabilize LPL activity to the same extent as longer ones (octa- and decasaccharides) (173).

We next tested LPL inhibition by nANGPTL3 and nANGPTL4 in the presence of the three heparin species. Briefly, nANGPTL3 and nANGPTL4 were preincubated with heparin, added to LPL, and assessed for their ability to inhibit LPL activity using a synthetic substrate, DGGR. The data were normalized to LPL conditions without inhibitor present for each heparin size. nANGPTL3 effectively inhibited LPL in the presence of 2-mer and 6-mer. However, nANGPTL3 did not inhibit LPL in the presence of 12-mer (Figure 4.4B). By contrast, nANGPTL4 showed no impairment of inhibition at any heparin size (Figure 4.4C). Interestingly, the 6-mer

stabilized LPL activity but did not block nANGPTL3 inhibition of LPL. These data reveal that heparin-mediated inactivation of nANGPTL3 is dependent on the length of heparin. Although nANGPTL3 was preincubated with heparin, we do not know for sure if heparin-mediated inactivation is due to heparin binding LPL or heparin binding to ANGPTL3. The 6-mer data suggests that nANGPTL3 can inhibit heparin-bound LPL and, perhaps, longer heparins inactivate nANGPTL3 by blocking its LPL inhibitory motif.

To test the idea that nANGPTL3 is inactivated by longer heparins, we synthesized biotinylated 6-mer and 12-mer. We analyzed LPL, nANGPTL3, and nANGPTL4 binding to both biotinylated heparin variants. Each protein was incubated with one of the biotinylated heparin variants and then pulled down using streptavidin coated beads. The beads were washed and the protein bound to the biotinylated heparin was analyzed by western blot. We found that nANGPTL3 significantly bound to 12-mer, but had little binding to 6-mer (Figure 4D, Supplemental Figure 1B). This supports the notion that nANGPTL3 binding to longer heparins (12-mer) abolishes its ability to inhibit LPL, since LPL binds to both 6-mer and 12-mer (Figure 4.4D, Supplemental Figure 4.1C). nANGPTL4 has previously been shown to bind unfractionated heparin and, here, we see it also binds to low molecular weight heparins (78, 174). In spite of binding to nANGPTL4, the low molecular weight heparins do not affect nANGPTL4 inhibition of LPL (Figure 4.4D, Supplemental Figure 4.1D).

nANGPTL3 and nANGPTL4 interact with LPL differently. We hypothesized that one explanation for the differences in LPL inhibition may be due to nANGPTL3 having different LPL-binding sites than nANGPTL4. Previously, we determined that nANGPTL4 binds LPL on the lid domain that covers its active site and at an α-helix proximal to the LPL lid (85). Because hepatic lipase (HL) is resistant to nANGPTL4, we were able to make nANGPTL4-resistant LPL variants by creating LPL-HL chimeras. Specifically, we generated a chimera of LPL in which the LPL lid domain (C216-C239) was replaced with the HL lid ($LPL_{HL\ Lid}$) and a chimera in which the lid-proximal helix of LPL (L87-Y100) was swapped for the corresponding HL helix sequence (LPL_{HL}

$_{Helix}$). We investigated the nANGPTL3 inhibition of these LPL-HL chimeras, because a previous report indicated that nANGPTL3, like nANGPTL4, is not an effective inhibitor of HL (170). To determine if nANGPTL3 recognizes the same binding sites on LPL, we compared nANGPTL3 and nANGPTL4 inhibition of HL, LPL, $LPL_{HL\ Lid}$, and $LPL_{HL\ Helix}$ (Figure 4.5A, B). As expected, both nANGPTL3 and nANGPTL4 inhibited LPL, but neither inhibited HL. nANGPTL3 partially inhibited the $LPL_{HL\ Lid}$ chimera, which contrasts with a more substantial loss of nANGPTL4 inhibition. nANGPTL3 inhibited the $LPL_{HL\ Helix}$ chimera equivalently to native LPL, but nANGPTL4 was not able to inhibit the $LPL_{HL\ Helix}$. These results indicate that nANGPTL3 and nANGPTL4 likely have different binding sites on LPL. Both nANGPTL3 and nANGPTL4 interact with the LPL lid domain, but nANGPTL3 inhibition is less sensitive to mutations in the LPL lid than nANGPTL4. In the case of the lid-proximal LPL helix, nANGPTL3 robustly inhibits $LPL_{HL\ Helix}$, indicating the helix does not play a role in nANGPTL3 binding, unlike nANGPTL4.

4.3 Discussion

Our comparison of nANGPTL3 to nANGPTL4 has revealed many new aspects of nANGPTL3 inhibition of LPL. First, our discovery that nANGPTL3 co-purifies with DNA contamination likely explains reports of poor *in vitro* potency against LPL (82, 83). Because nANGPTL3 is sensitive to both DNA and heparin inhibition, the presence of either contaminant in nANGPTL3 preparations could lead to inactive nANGPTL3. After nANGPTL3 was purified without contaminating DNA, we found that it had enhanced potency against LPL, even in the absence of ANGPTL8. This discovery has implications for the debate surrounding whether ANGPTL8 activates ANGPTL3 or vice versa. Because ANGPTL3 can inhibit LPL without ANGPTL8, but the reverse has not been seen, we predict that ANGPTL8 activates ANGPTL3. The activation mechanism could involve a structural rearrangement or potentially the removal of inactivating agents, like heparin or DNA, from the ANGPTL3 active site.

This work presents the first structural characterization of the N-terminal domains of ANGPTL3 and ANGPTL4 using both SEC-MALS and SEC-SAXS experiments. Interestingly, we

found that nANGPTL3 purifies as two separate oligomeric forms, hexamers and trimers, that do not interconvert. nANGPTL4 was also observed to form trimers. The formation of an nANGPTL4 trimer is consistent with the oligomeric state observed for one of the nANGPTL3 oligomers, which is appealing because they share a predicted coiled-coil structure in addition to their LPL inhibitory activity. It remains to be seen if these oligomeric states are a result of recombinant purification of the N-terminal domains of ANGPTL3 and ANGPTL4. The SEC-SAXS structures of nANGPTL3 and nANGPTL4 revealed that both oligomers form elongated rod-like structures and likely have a high degree of flexibility.

We were able to observe differences in the LPL-binding sites of nANGPTL3 and nANGPTL4. In contrast to nANGPTL4, nANGPTL3 inhibition of LPL was only modestly affected by the $LPL_{HL\ Lid}$ chimera and not affected by the $LPL_{HL\ Helix}$ chimera. Given that the lid-proximal helix is only next to the lid when the lid is closed, it follows that, as a noncompetitive inhibitor, nANGPTL4 binds both of those sites on LPL. Overall, these experiments suggest nANGPTL3 has different binding sites on LPL than nANGPTL4 and may interact, weakly, with the lid domain.

Another difference between nANGPTL3 and nANGPTL4 is their interaction with low molecular weight heparin. N-terminal ANGPTL3 possesses a heparin binding site adjacent to its LPL inhibitory domain, whereas N-terminal ANGPTL4 binds heparin at an unidentified site (78, 143). It was initially hypothesized that ANGPTL3 inhibition of LPL could be blocked by heparin binding LPL (83). However, our data shows that nANGPTL3 itself binds to heparin, which leads to the loss of activity. We found that 6-mer was able to bind LPL and increase its activity, but did not bind to or inactivate nANGPTL3. If heparin binding to LPL blocked the ability of nANGPTL3 to bind LPL, we would have expected that 6-mer-bound LPL would be resistant to nANGPTL3 inhibition.

This work presents many new insights into nANGPTL3 and how it inhibits LPL. It opens more areas of exploration, including the exact binding site of nANGPTL3 on LPL and how

ANGPTL8 is able to activate ANGPTL3 *in vivo*. It is clear that nANGPTL3 and nANGPTL4, in spite of their global similarities, are two very different inhibitors of LPL. This knowledge helps advance our understanding of the regulation of LPL activity.

4.4 Materials and Methods

nANGPTL3 cloning. The N-terminal domain of human ANGPTL3 (UniProt accession ID Q9Y5C1), encompassing residues S17-R245, was cloned C-terminal to a hexa-histidine tag and a TEV cleavage site. The resulting molecular weight of the purified protein was 26.8 kDa. The sequence was placed into a pETDuET vector (Novagen) at the multiple cloning site 1 (MCS1) (pETDuET-ANGPTL3).

Purification of nANGPTL3 (both with and without DNA). pETDuET-ANGPTL3 was transformed into Bl21 (DE3) RIPL cells and grown in LB at 37°C to an optical density of 0.6 at 600 nm. Protein expression was induced using 1mM isopropyl β-D-1-thiogalactopyranoside (IPTG) and the cells were grown for 3 hours at 37°C before harvesting by centrifugation at 6700 x *g* for 30 minutes at 4°C. Cells were resuspended in binding buffer (20 mM tris-HCl pH 8, 500 mM NaCl, 5 mM imidazole pH 8, 10% glycerol) on ice and flash frozen. Cells were thawed, and all subsequent steps were performed at 4°C. Cells were lysed using an Emulsiflex C3 high-pressure homogenizer, then lysate was clarified by centrifugation at 27000 x *g* for 70 min. Supernatant was filtered with a 0.2 µm filter and applied to a Ni-NTA resin column equilibrated in binding buffer. Following binding, the column was washed in binding buffer followed by wash buffer 1 (20 mM tris-HCl pH 8, 500 mM NaCl, 25 mM imidazole pH 8, 10% glycerol), and wash buffer 2 (20 mM tris-HCl pH 8, 300 mM NaCl, 60 mM imidazole pH 8, 5% glycerol). Protein was eluted using 20 mM tris-HCl pH 8, 300 mM NaCl, 300 mM imidazole pH 8, 5% glycerol. Fractions containing nANGPTL3 were pooled and dialyzed overnight into either MonoQ Buffer A (20 mM tris-HCl pH 8, 100 mM NaCl, 5% glycerol) or SEC Buffer (20 mM tris-HCl pH 8, 500 mM NaCl, 5% glycerol). For purifications using anion-exchange MonoQ chromatography, samples

were loaded onto a 1 mL MonoQ column using an ÄKTA explorer system at 0.5 mL/min. The column was washed with MonoQ buffer A for 10 CV, then eluted via a linear gradient from MonoQ buffer A to MonoQ buffer B (20 mM tris-HCl pH 8, 1 M NaCl, 5% glycerol) over 10 CV. Fractions containing nANGPTL3 were pooled and dialyzed overnight into SEC Buffer. SEC was performed using either a Superdex S-200 or Sephacryl S-300 column equilibrated in SEC Buffer. The S-300 column provided more separation between the excluded volume and the first peak of nANGPTL3, although nANGPTL3 peak 1 and peak 2 were in the included volume of both columns. nANGPTL3 peak 1 and peak 2 were pooled separately and concentrated using 10 kDa cut-off Millipore filters. The final protein concentrations were determined by BCA assay and DNA contamination was assessed by reading the 260:280 nm ratio with a Thermo Nanodrop. Finally, the proteins were aliquoted and flash frozen.

Purification of other proteins. N-terminal ANGPTL4 (UniProt accession ID Q9BY76) was cloned and purified as previously reported (79). Bovine LPL (UniProt accession ID P11151) was purified from raw bovine milk using heparin chromatography as previously reported (158). Human LPL (UniProt accession ID P06858), HL (UniProt accession ID P11150), and LPL-HL chimeras ($LPL_{HL\ Lid}$ and $LPL_{HL\ Helix}$) were purified as previously reported (85). Furin-resistant human LPL was purified as previously reported (18).

LPL activity assays. Activity assays were performed using a final concentration of 2.5 nM bovine LPL (bLPL) or human LPL (hLPL) or LPL-HL chimeras, diluted in LPL assay buffer, which has a final concentration of 20 mM tris-HCl pH 8.0, 150 mM NaCl, 0.2% fatty-acid free bovine serum albumin (BSA), and 1 mM sodium deoxycholate. nANGPTL3 or nANGPTL4 were diluted to the necessary concentrations using SEC Buffer (20 mM tris-HCl pH 8, 500 mM NaCl, 5% glycerol). 30 μL of diluted LPL was mixed with 40 μL of diluted nANGPTL3 and incubated in a black-walled, 96 well plate at 22°C for 10 min. 30 μL of fluorescent substrate 1,2-di-O-lauryl-rac-glycero-3-glutaric acid-(6'-methylresofurin) ester (DGGR) (Sigma) in 0.01% Anzergent 3-16

(Anatrace) was added immediately before assaying activity at 37°C as previously described (79). Data was background corrected using samples without LPL. Curves for each nANGPTL3 concentration were individually fit with Michaelis-Menten kinetics.

SEC-MALS. SEC-MALS was performed using a 24 mL Sephadex S-200 column connected to a Wyatt DAWN HELEOS II light scattering instrument interfaced to an Agilent 1260 Infinity FPLC System, Wyatt T-rEX refractometer, and Wyatt dynamic light scattering module. For both nANGPTL3 and nANGPTL4 the S-200 column was equilibrated with 3 CV of SEC-MALS Buffer (20 mM tris-HCl pH 8, 150 mM NaCl, 5% glycerol) prior to injecting 90 μL of sample on to the column at 0.5 mL/min. Data was analyzed using the Wyatt ASTRA software package.

SEC-SAXS nANGPTL3. SEC-SAXS of both nANGPTL3 oligomers was performed using the SIBYLS beamline 12.3.1 at the Advanced Light Source in Berkeley, CA. SEC was performed using an Agilent 1260 series HPLC with a Shodex Protein KW-804 analytical column at a flow rate of 0.5 ml/min in 20 mM tris-HCl pH 7.5, 400 mM NaCl, 2% glycerol. Samples were shipped on ice and stored at 4°C. Protein flowing off of the SEC was examined using SAXS at a sample-to-detector distance of 1.5 m, with λ=1.03 Å incident light. This resulted in a q-range of 0.013 $Å^{-1}$ to 0.5 $Å^{-1}$. Each exposure frame was 3 s. SEC-SAXS curves were initially analyzed by the SIBYLS beamline staff using ScÅtter.

SEC-SAXS nANGPTL4. SAXS of nANGPTL4 was performed at the BioCAT beamline 18ID at the Advanced Photon Source in Chicago, IL with in-line SEC to separate samples from aggregates and other contaminants (175). Sample was loaded onto a WTC-015S8 column (Wyatt Technology) run by an Infinity II HPLC (Agilent Technologies) and run at 0.8 ml/min. After the SEC eluate passed through the UV monitor, it passed through the SAXS flow cell which consists of a 1.5 mm ID quartz capillary with 10 µm walls. Scattering intensity was recorded using a Pilatus3 1M (Dectris) detector which was placed 3.5 m from the sample, giving

us access to a q-range of 0.004 $Å^{-1}$ – 0.4 $Å^{-1}$. 0.5 second exposures were acquired every 2 seconds during elution and data was reduced using BioXTAS RAW 1.4.0 (176). Buffer blanks were created by averaging regions flanking the elution peak and subtracted from exposures selected from the elution peak to create the I(q) vs q curves used for subsequent analyses.

SAXS Data Analysis. We utilized the ATSAS software package for SAXS data analysis (177). PRIMUS was used to analyze the averaged and background subtracted SAXS data for guinier range with Autorg. P(r) was determined empirically with the help of GNOM. With these input parameters (Supplemental Table 4.1), DAMMIF was run using the slow setting for 20 runs, assuming P1 symmetry and unknown shape (178). The results of DAMMIF runs were fed into the DAMAVER package and assessed for NSD to determine how similar the 20 models were. The resulting damstart.pdb envelope from DAMAVER was used as the initial model for a final slow DAMMIN refinement with P1 symmetry, unknown shape, and all atoms unfixed. The fit of final structural envelopes were validated using CorMap (179).

Synthesis of Heparin and Biotinylated Heparin Oligosaccharides. Heparin disaccharide (2-mer) 1-H sodium salt was purchased from Sigma (H8892-1MG) and used without further purification. Both 6-mer and 12-mer were synthesized according to a chemoenzymatic method published previously (180). The structures of 2-mer, 6-mer, and 12-mer are illustrated in Supplemental Figure 4.1A. The products were purified by anion-exchange chromatography using a Q-Sepharose column. Nuclear magnetic resonance (NMR) and electrospray ionization mass spectrometry (ESI-MS) matched published data for 6-mer and 12-mer. Biotinylation of heparin oligosaccharides was performed using previously published methods (181). The final product was purified by DEAE-HPLC to generate biotinylated 6-mer and 12-mer. HPLC and MS results match the published report for these compounds.

Heparin LPL Activity Assays. Assays with heparin were performed using the same general parameters as the LPL activity assays. The final concentrations of each component were 2.5 nM bLPL, 6 μM nANGPTL3 trimer, 10 μg/mL heparin, and 10 μM of DGGR with the

buffers described in the LPL activity assay method. For assays with nANGPTL4, a final concentration of 2 μM nANGPTL4 was used rather than nANGPTL3. Diluted nANGPTL3 or nANGPTL4 and heparin were mixed together and incubated at 22°C for 10 min. Heparin controls without nANGPTL3 or nANGPTL4 were also diluted in SEC Buffer. 40 μL of heparin with or without nANGPTL3 or nANGPTL4 was added to 30 μL of bLPL immediately prior to adding 30 μL of DGGR. The plate was immediately read at 37°C as previously described (79). Each condition was performed as a technical triplicate. Data was background corrected using samples without LPL. Data for LPL with heparin and without nANGPTL3 or nANGPTL4 was normalized to LPL without heparin. Data for LPL with both nANGPTL3 or nANGPTL4 and heparin was normalized to the LPL with heparin (without nANGPTL3 or nANGPTL4). Significance was determined by students t-test.

Biotinylated Heparin Pull-Down and Western Blots. First, 5 pmol of each protein (furin-resistant hLPL or nANGPTL3 hexamer or nANGPTL4) was incubated with 275 pmol of each heparin (6-mer or 12-mer) in pull-down buffer (phosphate buffered saline (PBS) (137 mM NaCl, 2.7 mM KCl, 10 mM Na_2HPO_4, 1.8 mM KH_2PO_4), 0.1% fatty acid free BSA, 0.01% triton X-100) in a final volume of 8.5 μL. As a negative control, each protein was mixed with an equal volume of pull-down buffer instead of heparin. The samples were rotated at 4°C for 30 min. Each sample was then mixed with 0.5 μL of cleaned Streptavidin M-280 Dynabeads (Invitrogen) that had been diluted in pull-down buffer to a final volume of 2.5 μL. The samples with beads were rotated at 4°C for 30 min. The beads were pulled-down using a magnet and the supernatant was removed by pipetting. The beads were then washed with 200 μL of pull-down buffer three times. After removing the final supernatant, the beads were resuspended in 10 μL of SDS to denature the proteins and heated to 95°C. The reactions were analyzed using western blot. Proteins were separated by 14% SDS-PAGE, transferred to 0.22 μm PVDF membrane, and blocked with 5% non-fat milk in TBS-T (20 mM tris-HCl pH 7.6, 150 mM NaCl, and 0.01% tween

20). LPL and nANGPTL3 were probed with a mouse anti-histidine tag antibody (Bio-Rad) using a 1:5000 dilution and protein was detected with an HRP-conjugated goat anti-mouse antibody (Southern Biotech) using a 1:5000 dilution. nANGPTL4 was probed with a polyclonal rabbit anti-ANGPTL4 antibody (BioVendor) using a 1:5000 dilution and detected with an HRP-conjugated donkey anti-rabbit antibody (Southern Biotech) using a 1:5000 dilution. Western blots were developed as previously described (18).

4.6 Figures

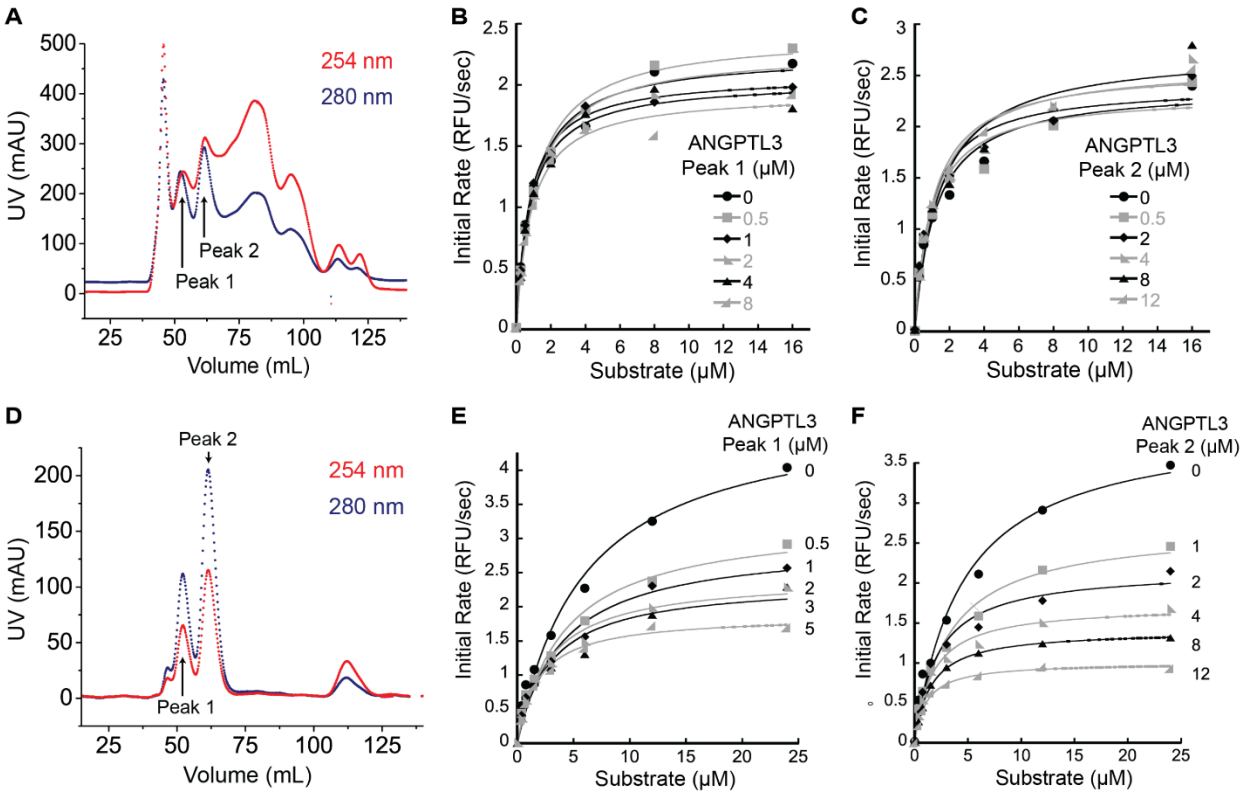

Figure 4.1: DNA contamination reduces nANGPTL3 inhibition potency. A) Representative nANGPTL3 SEC elution profile following nickel affinity purification. nANGPTL3 protein (280 nm, blue) eluted as 2 peaks, labeled peak 1 and peak 2. The nANGPTL3 was contaminated with nucleic acid (254 nm, red). Representative LPL activity assay using DGGR substrate with DNA contaminated nANGPTL3 peak 1 (B) and peak 2 (C) do not inhibit LPL. D) An additional MonoQ anion exchange purification step was performed between the nickel affinity column and SEC. A representative SEC trace shows that the nANGPTL3 DNA contamination was substantially reduced (254 nm, red), allowing better resolution of the nANGPTL3 peak 1 and peak 2 proteins (280 nm, blue). Representative LPL activity assay using DGGR substrate with pure nANGPTL3 peak 1 (E) and peak 2 (F) showing enhanced potency against LPL.

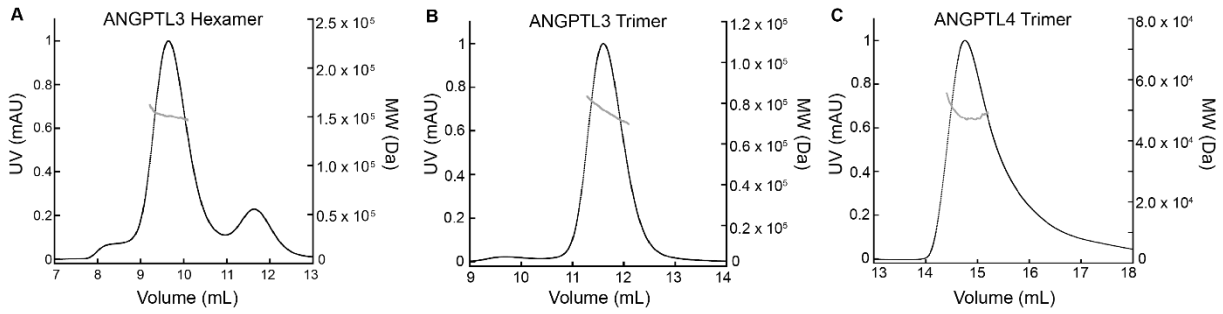

Figure 4.2: nANGPTL3 forms non-interconvertible hexamers and trimers. nANGPTL4 forms a trimer. Purified nANGPTL3 peak 1 (A) and peak 2 (B) were concentrated and re-injected for analysis with SEC-MALS. Peak 1 had a molecular weight of 151 kDa, which corresponds to a hexamer of nANGPTL3 (monomer 26.8 kDa). Peak 2 had a molecular weight of 76 kDa, which corresponds to a trimer of nANGPTL3. The nANGPTL3 trimers and hexamers did not interconvert when re-injected on SEC. C) Purified nANGPTL4 was concentrated and injected for SEC-MALS analysis. nANGPTL4 resolved as a single peak with a molecular weight of 46 kDa, which corresponds to a trimer of nANGPTL4 (monomer 15.4 kDa). The UV trace representing protein absorbance at 280 nm is in black and molecular weight (MW) is represented in gray.

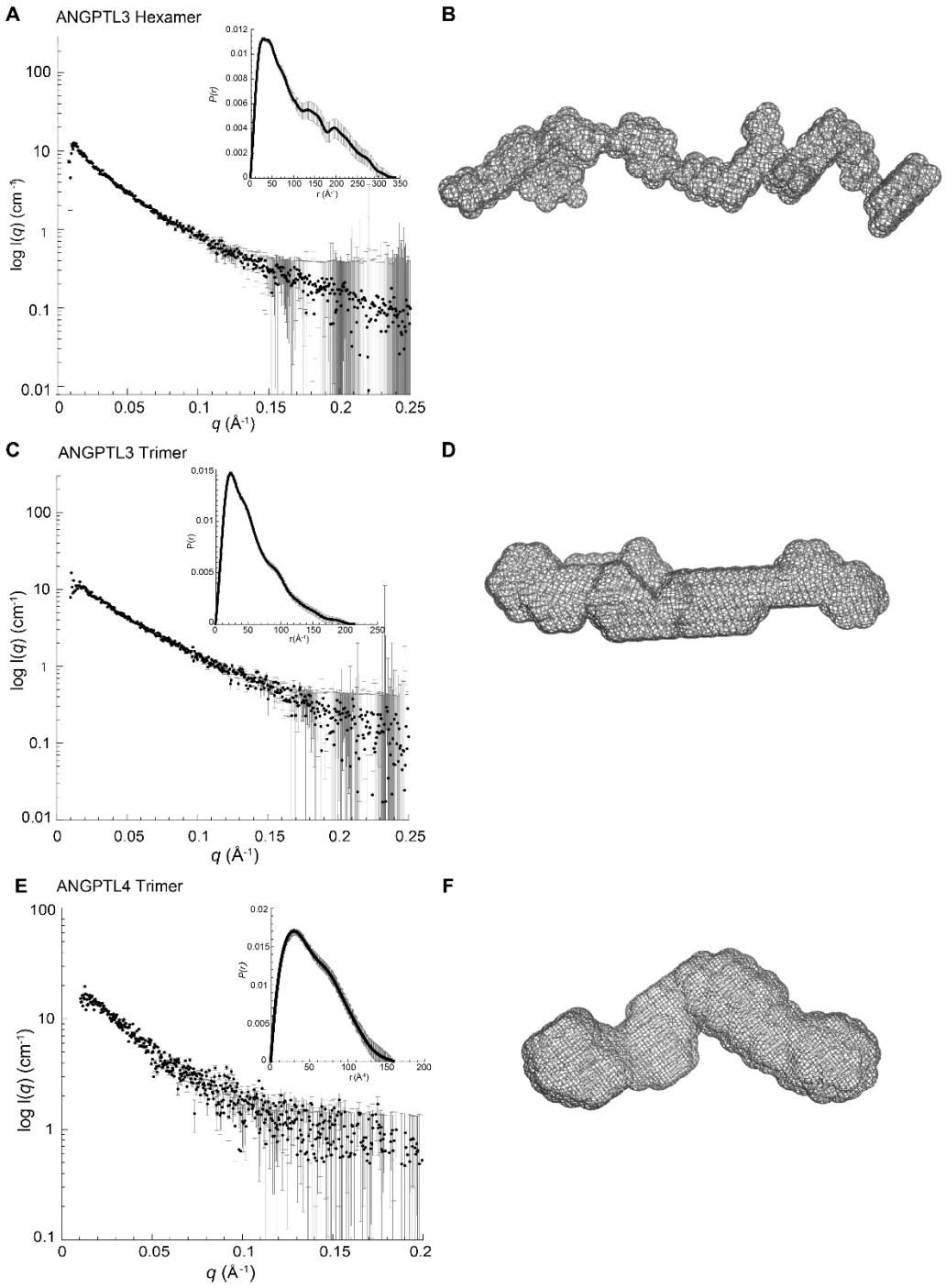

Figure 4.3: nANGPTL3 has an elongated structure. A) SEC-SAXS scattering data for nANGPTL3 hexamers as log-linear plot with inset showing the real-space distance distribution. B) Filtered average *ab initio* model of an nANGPTL3 hexamer determined using DAMMIN. C) nANGPTL3 trimer SEC-SAXS log-linear plot with inset showing the real-space distance distribution. D) Filtered average *ab initio* model of an nANGPTL3 trimer determined using DAMMIN. E) SEC-SAXS scattering data for nANGPTL4 as log-linear plot with inset showing the real-space distance distribution. F) Filtered average *ab initio* model of nANGPTL4 determined using DAMMIN.

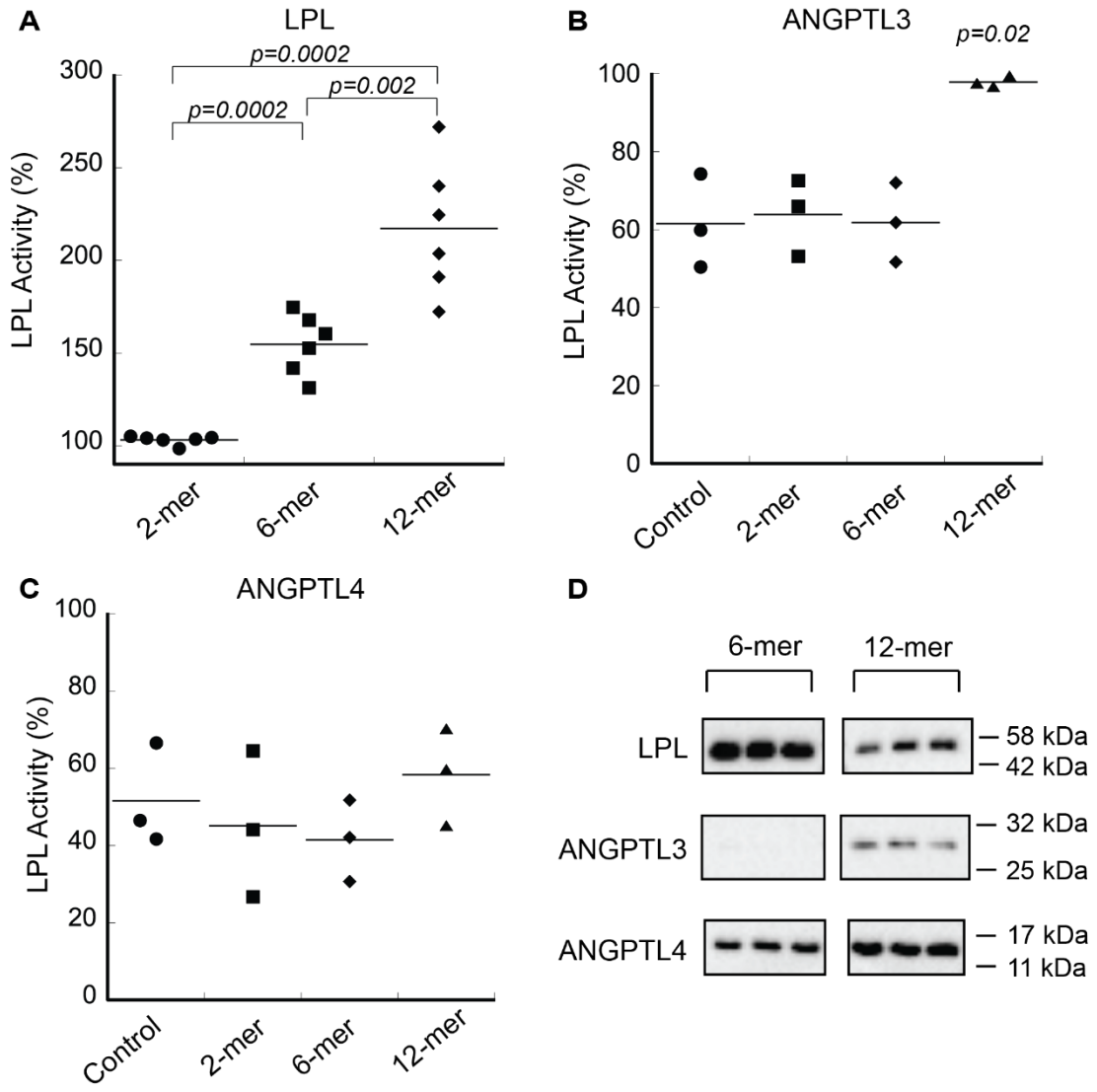

Figure 4.4: Heparin negatively affects nANGPTL3 inhibition, but not nANGPTL4. A) Activity assays of LPL were performed in the presence of heparin 2-mer, 6-mer, or 12-mer. A control of LPL without heparin was used to set 100% activity. Heparin 2-mer does not significantly increase LPL activity above the control, while both 6-mer and 12-mer led to a significant increase in LPL activity. 12-mer also resulted in significantly more LPL activity than 6-mer. B) nANGPTL3 was incubated with heparin and then assessed for inhibition of LPL. Samples were normalized by comparing to LPL and heparin without nANGPTL3 present. The control sample is nANGPTL3 inhibition of LPL without heparin. Both 2-mer and 6-mer did not affect nANGPTL3 inhibition. However, 12-mer led to an almost complete loss of inhibition. C) nANGPTL4 was incubated with heparin and assessed for LPL inhibition. Heparin had no significant effect on nANGPTL4 inhibition. Each point represents an independent biological replicate. The horizontal lines represent the average of the biological replicates. Significance was calculated with student's t-test. D) Pull-downs were conducted using biotinylated 6-mer or 12-mer and analyzed by western blot. LPL and nANGPTL4 bound to both 6-mer and 12-mer, whereas nANGPTL3 bound primarily to 12-mer.

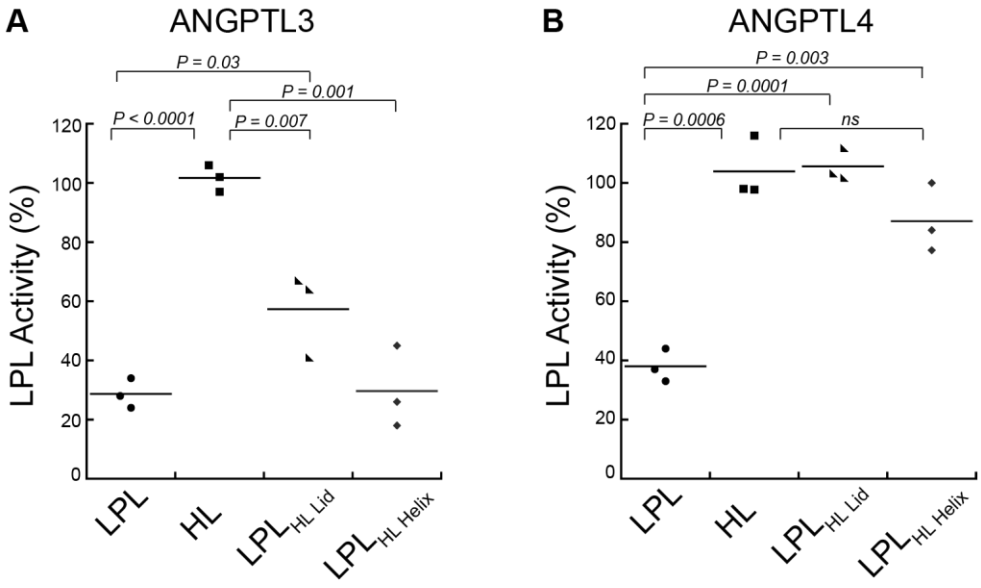

Figure 4.5: nANGPTL3 and nANGPTL4 inhibition of LPL/HL mutants indicates differing interactions with LPL. A) nANGPTL3 or B) nANGPTL4 was incubated with LPL, HL, $LPL_{HL\ Lid}$, or $LPL_{HL\ Helix}$ and assessed for lipase activity. Results were normalized by setting lipase without nANGPTL3 or nANGPTL4 activity to 100%. Each point represents an independent biological replicate. Both nANGPTL3 and nANGPTL4 inhibit LPL and do not inhibit HL. nANGPTL4 inhibition is lost with both the $LPL_{HL\ Lid}$ and $LPL_{HL\ Helix}$. However, nANGPTL3 is partially able to inhibit $LPL_{HL\ Lid}$ and is impervious to the $LPL_{HL\ Helix}$ chimera. Significance was calculated with a student's t-test.

4.6 Supplemental Information

Sample details		
	nANGPTL3	nANGPTL4
Organism	*H. sapiens*	*H. sapiens*
Source (Catalogue No. or reference)	*E. coli*	*E. coli*
Description: sequence (including Uniprot ID + uncleaved tags), bound ligands/modifications, *etc.*	N-term hexahistidine tag + TEV cleavage site + Q9Y5C1 (17-245)	Q9BY74 (26-161)
Extinction coefficient ε (A_{280}, 0.1% w/v)	0.277	0.357
Partial specific volume $\bar{\nu}$ ($cm^3\,g^{-1}$)	0.731	0.733
Particle contrast from sequence and solvent constituents, $\Delta\bar{\rho}$ (cm^{-2})	2.842 (12.414-9.571)	1.902 (12.382-10.479)
Molecular mass *M* from chemical composition (Da)	26847.07	15397.35
SEC-SAXS column Loading volume/concentration (mg ml^{-1}) Injection volume (µl) Flow rate (ml min^{-1})	Shodex Protein KW-804 5.6 mg ml^{-1} (Hexamer) 6.15 mg ml^{-1} (Trimer) 80 µL 0.5 ml min^{-1}	Wyatt WTC-030S5 5 mg ml^{-1} 300 µL 0.8 ml min^{-1}
Solvent composition and source	20 mM Tris-HCl pH 7.5, 400mM NaCl, 2% Glycerol	50mM Tris-HCl pH 7.4, 300mM NaCl, 100mM Betaine, 500mM Arginine
SAXS data collection parameters		
Instrument/data processing	Advanced Light Source SIBYLS Beamline 12.3.1 (182)	Argonne National Laboratory Advanced Photon Source Undulator 18-ID (BioCAT) Beamline (175)
Wavelength (Å)	0.73 – 2.5	1.03
Beam size (µm)	5000 x 500	35 x 135
q-measurement range ($Å^{-1}$)	0.013 – 0.5	0.010 – 0.4
Exposure time	Continuous 3 s data-frame measurement of SEC elution	Continuous 0.5 s data-frame measurements of SEC elution
Sample configuration	SEC-SAXS	SEC-SAXS
Sample temperature (ºC)	25	25
Software employed for SAS data reduction, analysis and interpretation		
SAXS data reduction	Solvent subtraction *ScÅtter*	Solvent subtraction *PRIMUSqt*

Calculation of ε from sequence	*ProtParam*		*ProtParam*
Calculation of $\Delta\bar{\rho}$ and $\bar{\nu}$ values from chemical composition	*MULCh 1.1*		*MULCh 1.1*
Basic analyses: Guinier, *P*(*r*), scattering particle volume (*e.g.* Porod volume V_P or volume of correlation V_c)	*PRIMUSqt*		*PRIMUSqt*
Shape/bead modelling	*DAMMIF* and *DAMMIN*		*DAMMIF* and *DAMMIN*
Molecular graphics	*Pymol v1.8.2.2* Mac		*Pymol v1.8.2.2* Mac
Structural parameters			
Guinier Analysis	nANGPTL3 Hexamer	nANGPTL3 Trimer	nANGPTL4
I(0) (cm^{-1})	13.89	13.34	18.28
R_g (Å)	56.41	46.58	46.45
q-range ($Å^{-1}$)	0.013 - 0.026	0.013 - 0.025	0.015 - 0.027
Coefficient of correlation, R^2	0.93	0.78	0.79
P(*r*) analysis			
I(0) (cm^{-1})	19.88	13.25	17.50
R_g (Å)	92.74	49.0	45.31
d_{max} (Å)	340	215	160
q-range ($Å^{-1}$)	0.012 - 0.22	0.013 – 0.25	0.013 – 0.17
Shape modelling results			
	nANGPTL3 Hexamer	nANGPTL3 Trimer	nANGPTL4
q-range for fitting ($Å^{-1}$)	0.012 - 0.22	0.013 - 0.25	0.013 - 0.17
Symmetry/anisotropy assumptions	P1, none	P1, none	P1, none
χ^2 value	1.19	2.3	0.8
P value	0.16	0.33	0.89

Supplemental Table 4.1 Detailed information for nANGTPL3 hexamer, nANGPTL3 trimer, and nANGPTL4 SEC-SAXS analysis. Table includes: sample details, data acquisition, data analysis, modelling fitting and software utilized. Table adapted from Trewhella et al. (183).

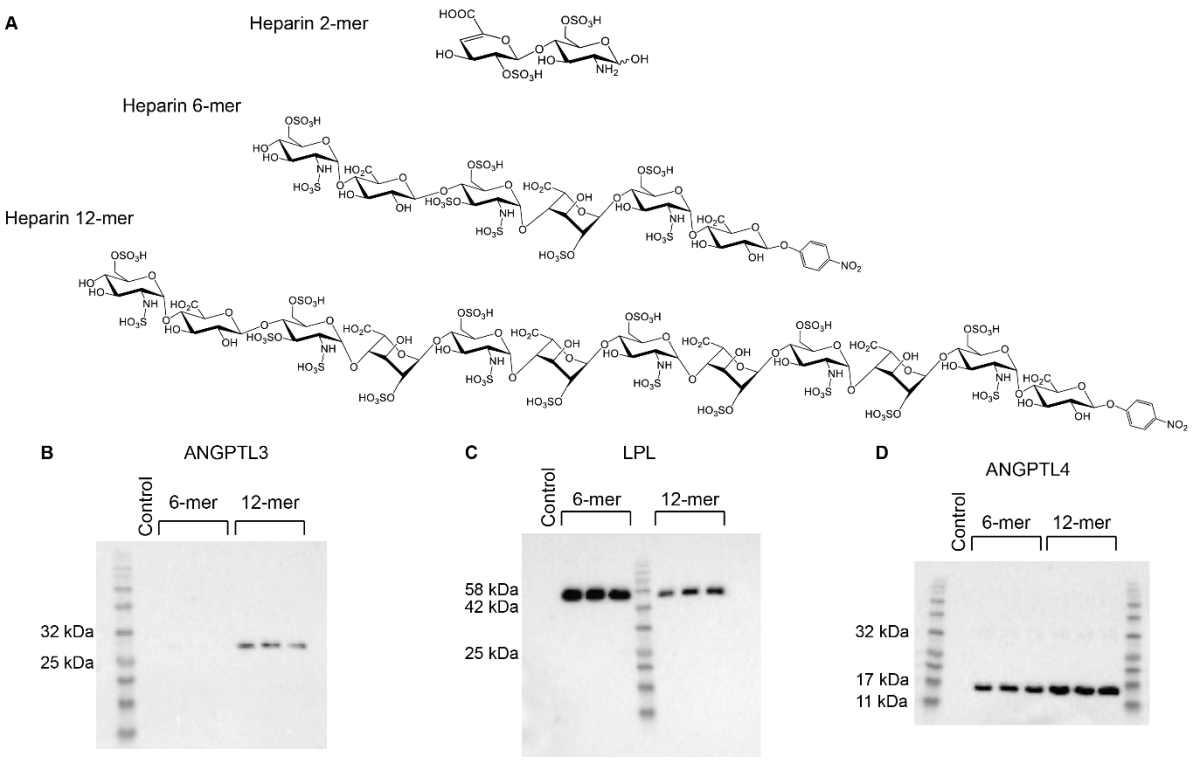

Supplemental Figure S4.1 A) Structures of heparin 2-mer, 6-mer, and 12-mer used in activity assays. Full blots of biotinylated heparin pull-down of A) LPL, B) nANGPTL3, or C) nANGPTL4 seen in Figure 4.4D. The protein molecular weight ladder is labeled to the left of the gel.

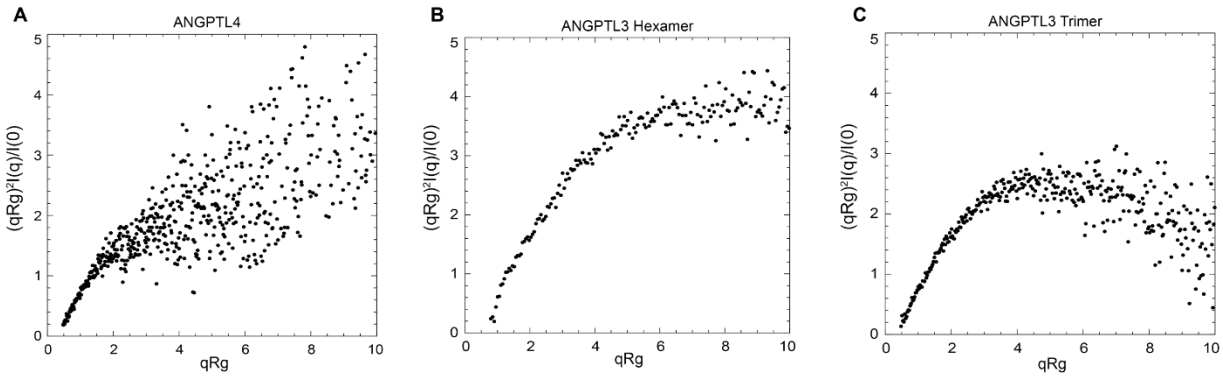

Supplemental Figure S4.2 nANGPTL3 and nANGPTL4 form highly flexible and elongated structures. Dimensionless Kratky plots reveal a high degree of flexibility in nANGPTL4 (A) nANGPTL3 hexamers (B) nANGPTL3 trimers (C) characteristic of unfolded or intrinsically disordered flexible proteins.

CHAPTER 5

Final Thoughts and Discussion

5.1 Molecular mechanisms of ANGPTL-mediated inhibition of LPL

LPL is a notoriously difficult protein to work with *in vitro*. It is highly prone to thermal unfolding where more than 50% of its enzymatic activity is lost within 5-10 minutes at 37°C in standard buffer conditions (79, 184). *In vivo*, LPL interacts with an array of stabilizing, activating, and inhibitory elements that include partner proteins, HSPGs, bile salts, and fatty acids (5, 81, 82, 173, 185, 186). The stability issues observed *in vitro* are not likely representative of LPL stability *in vivo,* as it has been shown to maintain enzymatic activity under zero-order reaction conditions for at least one hour in human plasma (45). In the absence of biological fluids, stabilizing factors are supplemented in *in vitro* kinetic assays to better replicate LPL stability observed in *in vivo* conditions. Heparin was the first factor reported to stabilize LPL and is, therefore, often included in LPL activity assays (80). Alternatively, bile salts like deoxycholate have been used in place of heparin (79, 81, 85). Recent studies have utilized GPIHBP1 as, perhaps, the most physiologically relevant stabilizing factor of LPL (34). Interestingly, different assay conditions seem to give different results surrounding the molecular mechanism of ANGPTL-mediated inhibition of LPL and have contributed to a lack of consensus within the field of lipid metabolism.

Several publications report that ANGPTL3 alone is a weak inhibitor of LPL and ANGPTL4 is an irreversible inhibitor in the presence of heparin (78, 82, 87). Our work in chapter 4 reveals that ANGPTL3 was largely inactivated by heparin and its potency is enhanced in the absence of heparin. These data suggest that the addition of standard heparin additives in LPL

activity assays will affect the potency of ANGPTL3-mediated inhibition observed. In terms of irreversible inhibition, heparin has a well characterized role in enhancing the rate of irreversible enzyme inhibition in the blood coagulation cascade (187, 188). Heparin forms a ternary complex with antithrombin and thrombin that enhances the rate of irreversible inhibition by 2000-4000-fold (189). This mechanism of inhibition is highly dependent on heparin chain length such that the chain must contain at least 18 saccharides (187, 189). In chapter 4, we observed that ANGPTL4 avidly bound short chain heparins (3, 6, and 12-mers) and this did not significantly affect its ability to inhibit LPL. However, others have reported that standard heparin, which contains longer chain heparins, enhanced the rate of ANGPTL4-mediated inhibition of LPL (82). To date, we do not know if heparin is mediating a similar template mechanism for LPL and ANGPTL4, but the chain length dependence and enhanced rate of inhibition draw interesting parallels to heparin-mediated antithrombin inhibition.

As discussed in chapter 1 and 2, ANGPTL4 is a reversible, noncompetitive inhibitor of LPL in the presence of deoxycholate. Deoxycholate is a bile salt that binds and stabilizes LPL (79, 81). Interestingly, in the presence of deoxycholate, the potency of ANGPTL4 is greatly diminished with an inhibition constant of 0.9 – 1.7 μM in comparison with low nanomolar quantities in the presence of heparin (79, 85). As discussed previously, the mode of inhibition observed is entirely dependent on which LPL stabilizer is present. This raises important questions concerning which assay better mimics physiological conditions. Bile salts are naturally found in biological fluids, like serum, where LPL is known to have enhanced stability. Heparin and heparan sulfate are glycosaminoglycans where heparin is secreted by mast cells and heparan sulfate is covalently bound to cell surface proteins and is in the extracellular matrix (173). Within the vasculature, we do not know if LPL interacts with heparin but it is well documented to interact with heparan sulfate proteoglycans (HSPGs) within the interstitium (8). Neither assay quite replicates the LPL-stabilizing conditions within human serum as both assays supplement heparin and deoxycholate at super-physiological concentrations.

More recently, the mechanism of ANGPTL4-mediated inhibition of LPL was investigated in the presence of its natural binding partner and stabilizer, GPIHBP1 (34). Nimonkar and colleagues demonstrated that full-length ANGPTL4 binds LPL at residues 157-189 and dissociates it from GPIHBP1 (34). In agreement with the work described in chapter 2, the authors showed evidence for ANGPTL4-LPL complex formation using HDX-MS. This conflicts with HDX-MS experiments performed by Ploug and colleagues where they report ANGPTL4 catalyzes the unfolding of LPL and could not identify residues at the LPL-ANGPTL4 interface (87, 190). The ANGPTL4 binding site reported by Nimonkar et al is different than the sites that we observed in chapter 2, but it is possible that full-length ANGPTL4 binds LPL differently in the presence of GPIHBP1 than the N-terminal domain of ANGPTL4. Overall, I think the data surrounding this mechanism of ANGPTL4-mediated inhibition is very compelling and opens several interesting questions surrounding the fate of GPIHBP1-dissociated LPL and ANGPTL4. For example, how long does ANGPTL4 remain bound to LPL? Where does the LPL-ANGPTL4 complex go? Is this process reversible? The question of reversibility is difficult to answer using standard *in vitro* activity assays for the reasons discussed above. However, it is an important question.

A lack of consensus within the scientific community regarding the mechanism of ANGPTL4-mediated inhibition of LPL could be a cause for alarm, but I think it could provide a glimpse of a complex system where LPL is inhibited by different mechanisms in different cellular environments. In support of this notion, Reimund and colleagues demonstrated that ANGPTL4 inhibited LPL both reversibly and irreversibly in a concentration-dependent manner when measured in human plasma using isothermal titration calorimetry (ITC) (45). The authors observed that low concentrations of ANGPTL4 (10 nM) reversibly inhibited LPL and higher, super-physiological concentrations of ANGPTL4 (100-1000 nM) irreversibly inhibited LPL. Figure 5.1 illustrates a proposed model where the mechanism of ANGPTL4-mediated LPL inhibition depends on the tissue environment. HSPG-bound LPL in the interstitial space could

be potently inhibited by ANGPTL4 via an HSPG-mediated template mechanism (Figure 5.1A). Alternatively, bile salt stabilized-LPL could be weakly inhibited by a reversible, noncompetitive mechanism within tissues like the small intestine (Figure 5.1B). In the vasculature, ANGPTL4 could dissociate LPL from its GPIHBP1-anchor and associate with distal partners like HSPGs, heparin, or remnant lipoprotein particles (Figure 5.1C). As mentioned previously, the fate of the GPIHBP1 dissociated LPL-ANGPTL4 complex is entirely unknown but is of great interest.

5.2 Biologic therapeutics for treating hypertriglyceridemia

Statin therapy has been the cornerstone of lipid-lowering regimes for more than three decades (110). Pfizer's blockbuster statin, Lipitor, was the best-selling drug by revenue in the United States from 1992-2017 having generated 94.67 billion USD (191). Despite the widespread success of statin therapy, cardiovascular disease has been the leading cause of death worldwide for two decades (192). The frequency of cardiovascular events demonstrates that statin therapy alone is not a universal treatment for every dyslipidemia. Biologics are a fast-growing class of therapeutics that can address some of the shortcomings of small molecule drugs and offer new treatment options for a variety of dyslipidemias. One of the major advantages of biologics is their ability to target protein-protein interactions (PPI), which is an area largely considered to be undruggable with small molecule modalities (193). The vast network of PPIs involved in lipid metabolism is a rich landscape for the development of novel biologics for the treatment of dyslipidemia.

To date, all biologics on the market for dyslipidemia are antisense oligonucleotides (ASO), monoclonal antibodies, and enzyme replacement therapies (103). Although the primary mechanism of action is different for ASO and monoclonal antibodies, both therapies result in loss of the expression of their target protein. ASO's block translation of its target protein and monoclonal antibodies result in degradation of soluble target proteins (114, 194). These therapies are successful in many cases, but their mechanisms of action restrict their use to nonessential target proteins. PPI modulators are advantageous in that they can target essential

proteins without resulting in complete loss of expression and represent the next generation of protein therapeutics.

There is a lot of potential for new PPI modulators for the treatment of hypertriglyceridemia (HTG). Blocking the interactions between LPL and its inhibitors could be a safe and efficacious way for lowering plasma TG levels and concomitantly raise HDL-cholesterol levels (130). More specifically, chapter 3 discussed the possibility that a PPI inhibitor of the LPL-ANGPTL4 interaction could mimic the cardioprotective phenotype observed in humans with a point mutation in ANGPTL4 that abolishes its interaction with LPL. Moreover, a PPI inhibitor of the LPL-ANGPTL3,8 interaction could offer unique advantages over the current anti-ANGPTL3 monoclonal antibody therapeutic, evinacumab. Evinacumab is well-tolerated and effectively lowers plasma TG, LDL-cholesterol, and HDL-cholesterol (64). Lowering TG and LDL-cholesterol is good; however, lowering HDL-cholesterol may not be ideal for every patient. As discussed in chapter 1, ANGPTL3 is an inhibitor for both LPL and endothelial lipase (EL). EL primarily hydrolyzes HDL-cholesterol, therefore, loss of ANGPTL3 enhances the pool of enzymatically active EL. ANGPTL3 can inhibit EL on its own but can only inhibit LPL when it is in complex with ANGPTL8 (62, 195, 196). Therefore, I would predict that LPL binds ANGPTL3 at a different site than EL and the LPL-ANGPTL3,8 interface could be targeted by a PPI inhibitor. A PPI inhibitor of the ANGPTL3,8 LPL complex that preserves the ability of ANGPTL3 to inhibit EL, could offer greater specificity in lowering TGs and LDL-cholesterol without lowering HDL-cholesterol levels. These are just two examples of how PPI modulators could be novel treatments for dyslipidemia. There are countless targets in the field of lipid metabolism and every novel approach could bring us closer to decreasing the global burden of cardiovascular disease.

5.3 Figures

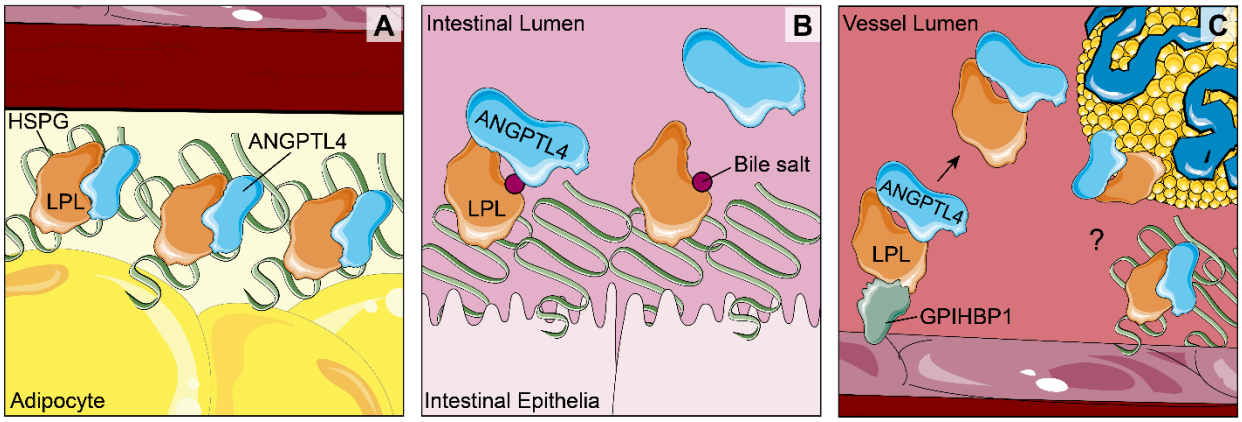

Figure 5.1 Potential mechanisms of LPL inhibition by ANGPTL4 in different cellular environments. A) LPL is anchored cell surface HSPGs in the interstitial space. Freshly secreted ANGPTL4 may bind HSPGs and form a ternary complex with LPL, resulting in potent inhibition via an HSPG-mediated template mechanism (153, 197). B) In environments rich in bile salts, like the small intestine, bile salt-bound LPL may be reversibly, noncompetitively inhibited by ANGPTL4 (198). C) In the vessel lumen, GPIHBP1-bound LPL binds ANGPTL4 and dissociates from GPIHBP1 (34, 199). The fate of the LPL-ANGPTL4 complex is not known, perhaps they bind downstream HSPG patches or associate with remnant lipoprotein particles to effect lipoprotein uptake (200).

REFERENCES

1. Gibbons, G. F., Wiggins, D., Brown, A.-M., and Hebbachi, A.-M. (2004) Synthesis and function of hepatic very-low-density lipoprotein. *Biochem. Soc. Trans.* **32**, 59–64

2. Wolska, A., Dunbar, R. L., Freeman, L. A., Ueda, M., Amar, M. J., Sviridov, D. O., and Remaley, A. T. (2017) Apolipoprotein C-II: New findings related to genetics, biochemistry, and role in triglyceride metabolism. *Atherosclerosis*. **267**, 49–60

3. Dash, S., Xiao, C., Morgantini, C., and Lewis, G. F. (2015) New Insights into the Regulation of Chylomicron Production. *Annu. Rev. Nutr.* **35**, 265–294

4. Bhatt-Wessel, B., Jordan, T. W., Miller, J. H., and Peng, L. (2018) Role of DGAT enzymes in triacylglycerol metabolism. *Arch. Biochem. Biophys.* **655**, 1–11

5. Kersten, S. (2014) Physiological regulation of lipoprotein lipase. *Biochim. Biophys. Acta - Mol. Cell Biol. Lipids*. **1841**, 919–933

6. Li, Y., He, P.-P., Zhang, D.-W., Zheng, X.-L., Cayabyab, F. S., Yin, W.-D., and Tang, C.-K. (2014) Lipoprotein lipase: From gene to atherosclerosis. *Atherosclerosis*. **237**, 597–608

7. Mead, J., Irvine, S., and Ramji, D. (2002) Lipoprotein lipase: structure, function, regulation, and role in disease. *J. Mol. Med.* **80**, 753–769

8. Allan, C. M., Larsson, M., Jung, R. S., Ploug, M., Bensadoun, A., Beigneux, A. P., Fong, L. G., and Young, S. G. (2017) Mobility of “HSPG-bound” LPL explains how LPL is able to reach GPIHBP1 on capillaries. *J. Lipid Res.* **58**, 216–225

9. Beigneux, A. P., Davies, B. S. J., Gin, P., Weinstein, M. M., Farber, E., Qiao, X., Peale, F., Bunting, S., Walzem, R. L., Wong, J. S., Blaner, W. S., Ding, Z.-M., Melford, K., Wongsiriroj, N., Shu, X., de Sauvage, F., Ryan, R. O., Fong, L. G., Bensadoun, A., and Young, S. G. (2007) Glycosylphosphatidylinositol-Anchored High-Density Lipoprotein-Binding Protein 1 Plays a Critical Role in the Lipolytic Processing of Chylomicrons. *Cell Metab.* **5**, 279–291

10. Sato, K., Okajima, F., Miyashita, K., Imamura, S., Kobayashi, J., Stanhope, K. L., Havel, P. J., Machida, T., Sumino, H., Murakami, M., Schaefer, E., and Nakajima, K. (2016) The majority of lipoprotein lipase in plasma is bound to remnant lipoproteins: A new definition of remnant lipoproteins. *Clin. Chim. Acta*. **461**, 114–125

11. Hayne, C. K., Lafferty, M. J., Eglinger, B. J., Kane, J. P., and Neher, S. B. (2017) Biochemical Analysis of the Lipoprotein Lipase Truncation Variant, LPL S447X , Reveals Increased Lipoprotein Uptake. *Biochemistry*. **56**, 525–533

12. Shetty, S. K., Walzem, R. L., and Davies, B. S. J. (2020) A novel NanoBiT-based assay monitors the interaction between lipoprotein lipase and GPIHBP1 in real time. *J. Lipid Res.* 10.1194/jlr.D119000388

13. Jensen, M. K., Rimm, E. B., Rader, D., Schmidt, E. B., Sørensen, T. I. A., Vogel, U., Overvad, K., and Mukamal, K. J. (2009) S447X variant of the lipoprotein lipase gene,

lipids, and risk of coronary heart disease in 3 prospective cohort studies. *Am. Heart J.* **157**, 384–390

14. Tenenbaum, A., Klempfner, R., and Fisman, E. Z. (2014) Hypertriglyceridemia: A too long unfairly neglected major cardiovascular risk factor. *Cardiovasc. Diabetol.* **13**, 1–10

15. Ramms, B., and Gordts, P. L. S. M. (2018) Apolipoprotein C-III in triglyceride-rich lipoprotein metabolism. *Curr. Opin. Lipidol.* **29**, 171–179
16. Laufs, U., Parhofer, K. G., Ginsberg, H. N., and Hegele, R. A. (2020) Clinical review on triglycerides. *Eur. Heart J.* **41**, 99-109c

17. Karalis, D. G. (2017) A Review of Clinical Practice Guidelines for the Management of Hypertriglyceridemia: A Focus on High Dose Omega-3 Fatty Acids. *Adv Ther*. **34**, 300–323

18. Wu, M. J., Wolska, A., Roberts, B. S., Pearson, E. M., Gutgsell, A. R., Remaley, A. T., and Neher, S. B. (2018) Co-expression of Novel Furin-Resistant LPL Variants with LMF1 Enhances LPL Secretion and Activity. *J. Lipid Res.* **1**, jlr.D086793

19. Birrane, G., Beigneux, A. P., Dwyer, B., Strack-Logue, B., Kristensen, K. K., Francone, O. L., Fong, L. G., Mertens, H. D. T., Pan, C. Q., Ploug, M., Young, S. G., and Meiyappan, M. (2019) Structure of the lipoprotein lipase–GPIHBP1 complex that mediates plasma triglyceride hydrolysis. *Proc. Natl. Acad. Sci.* **116**, 1723–1732

20. Arora, R., Nimonkar, A. V, Baird, D., Wang, C., Chiu, C., Horton, P. A., Hanrahan, S., Cubbon, R., Weldon, S., Tschantz, W. R., Mueller, S., Brunner, R., Lehr, P., Meier, P., Ottl, J., Voznesensky, A., Pandey, P., Smith, T. M., Stojanovic, A., Flyer, A., Benson, T. E., Romanowski, M. J., and Trauger, J. W. (2019) Structure of lipoprotein lipase in complex with GPIHBP1. *Proc. Natl. Acad. Sci.* **116**, 10360–10365

21. Iverius, P. H., and Ostlund-Lindqvist, A. M. (1976) Lipoprotein lipase from bovine milk. Isolation procedure, chemical characterization, and molecular weight analysis. *J. Biol. Chem.* **251**, 7791–5

22. Garfinkel, A. S., Kempner, E. S., Ben-Zeev, O., Nikazy, J., James, S. J., and Schotz, M. C. (1983) Lipoprotein lipase: size of the functional unit determined by radiation inactivation. *J. Lipid Res.* **24**, 775–80

23. Olivecrona, T., Bengtsson-Olivecrona, G., Osborne, J. C., and Kempner, E. S. (1985) Molecular size of bovine lipoprotein lipase as determined by radiation inactivation. *J. Biol. Chem.* **260**, 6888–91

24. Peterson, J., Ayyobi, A. F., Ma, Y., Henderson, H., Reina, M., Deeb, S. S., Santamarina-Fojo, S., Hayden, M. R., and Brunzell, J. D. (2002) Structural and functional consequences of missense mutations in exon 5 of the lipoprotein lipase gene. *J. Lipid Res.* **43**, 398–406

25. Osborne, J. C., Lee, N. S., Bengtsson-Olivecrona, G., and Olivecrona, T. (1985) Studies on Inactivation of Lipoprotein Lipase: Role of the Dimer to Monomer Dissociation. *Biochemistry*. **24**, 5606–5611

26. Vannier, C., and Ailhaud, G. (1989) Biosynthesis of lipoprotein lipase in cultured mouse adipocytes. II. Processing, subunit assembly, and intracellular transport. *J. Biol. Chem.* **264**, 13206–16

27. Olivecrona, T. and Bengtsson-Olivecrona, G. (1990) Lipoprotein lipase and hepatic lipase. *Curr. Opin. Lipidol.* **1**, 222–230

28. Lookene, A., and Bengtsson-Olivecrona, G. (1993) Chymotryptic cleavage of lipoprotein lipase. Identification of cleavage sites and functional studies of the truncated molecule. *Eur. J. Biochem.* **213**, 185–94

29. Wong, H., Davis, R. C., Thuren, T., Goers, J. W., Nikazy, J., Waite, M., and Schotz, M. C. (1994) Lipoprotein lipase domain function. *J. Biol. Chem.* **269**, 10319–23

30. Lookene, A., Skottova, N., and Olivecrona, G. (1994) Interactions of lipoprotein lipase with the active-site inhibitor tetrahydrolipstatin (Orlistat). *Eur. J. Biochem.* **222**, 395–403

31. Wong, H., Yang, D., Hill, J. S., Davis, R. C., Nikazy, J., and Schotz, M. C. (1997) A molecular biology-based approach to resolve the subunit orientation of lipoprotein lipase. *Proc. Natl. Acad. Sci.* **94**, 5594–5598

32. Kobayashi, Y., Nakajima, T., and Inoue, I. (2002) Molecular modeling of the dimeric structure of human lipoprotein lipase and functional studies of the carboxyl-terminal domain. *Eur. J. Biochem.* **269**, 4701–10

33. Beigneux, A. P., Allan, C. M., Sandoval, N. P., Cho, G. W., Heizer, P. J., Jung, R. S., Stanhope, K. L., Havel, P. J., Birrane, G., Meiyappan, M., Gill, J. E., Murakami, M., Miyashita, K., Nakajima, K., Ploug, M., Fong, L. G., and Young, S. G. (2019) Lipoprotein lipase is active as a monomer. *Proc. Natl. Acad. Sci. U. S. A.* **116**, 6319–6328

34. Nimonkar, A. V, Weldon, S., Godbout, K., Panza, D., Hanrahan, S., Cubbon, R., Xu, F., Trauger, J. W., Gao, J., and Voznesensky, A. (2020) A lipoprotein lipase-GPI-anchored high-density lipoprotein-binding protein 1 fusion lowers triglycerides in mice: Implications for managing familial chylomicronemia syndrome. *J. Biol. Chem.* **295**, 2900–2912

35. Brown, W. V, Levy, R. I., and Fredrickson, D. S. (1970) Further characterization of apolipoproteins from the human plasma very low density lipoproteins. *J. Biol. Chem.* **245**, 6588–94

36. LaRosa, J. C., Levy, R. I., Herbert, P., Lux, S. E., and Fredrickson, D. S. (1970) A specific apoprotein activator for lipoprotein lipase. *Biochem. Biophys. Res. Commun.* **41**, 57–62

37. Meyers, N. L., Larsson, M., Olivecrona, G., and Small, D. M. (2015) A Pressure-dependent Model for the Regulation of Lipoprotein Lipase by Apolipoprotein C-II. *J. Biol. Chem.* **290**, 18029–18044

38. Zdunek, J., Martinez, G. V., Schleucher, J., Lycksell, P. O., Yin, Y., Nilsson, S., Shen, Y., Olivecrona, G., and Wijmenga, S. (2003) Global structure and dynamics of human apolipoprotein CII in complex with micelles: evidence for increased mobility of the helix involved in the activation of lipoprotein lipase. *Biochemistry*. **42**, 1872–89

39. MacRaild, C. A., Hatters, D. M., Howlett, G. J., and Gooley, P. R. (2001) NMR structure

of human apolipoprotein C-II in the presence of sodium dodecyl sulfate. *Biochemistry*. **40**, 5414–21

40. MacPhee, C. E., Howlett, G. J., and Sawyer, W. H. (1999) Mass Spectrometry to Characterize the Binding of a Peptide to a Lipid Surface. *Anal. Biochem.* **275**, 22–29

41. Shen, Y., Lookene, A., Zhang, L., and Olivecrona, G. (2010) Site-directed mutagenesis of apolipoprotein CII to probe the role of its secondary structure for activation of lipoprotein lipase. *J. Biol. Chem.* **285**, 7484–92

42. Musliner, T. A., Herbert, P. N., and Church, E. C. (1979) Activation of lipoprotein lipase by native and acylated peptides of apolipoprotein C-II. *Biochim. Biophys. Acta*. **573**, 501–9

43. Vainio, P., Virtanen, J. A., Kinnunen, P. K. J., Gotto, A. M., Sparrow, J. T., Pattus, F., Bougis, P., and Verger, R. (1983) Action of lipoprotein lipase on mixed triacylglycerol/phosphatidylcholine monolayers. Activation by apolipoprotein C-II. *J. Biol. Chem.* **258**, 5477–82

44. McIlhargey, T. L., Yang, Y., Wong, H., and Hill, J. S. (2003) Identification of a lipoprotein lipase cofactor-binding site by chemical cross-linking and transfer of apolipoprotein C-II-responsive lipolysis from lipoprotein lipase to hepatic lipase. *J. Biol. Chem.* **278**, 23027–23035

45. Reimund, M., Kovrov, O., Olivecrona, G., and Lookene, A. (2017) Lipoprotein lipase activity and interactions studied in human plasma by isothermal titration calorimetry. *J. Lipid Res.* **58**, 279–288

46. Blom, D. J., O'Dea, L., Digenio, A., Alexander, V. J., Karwatowska-Prokopczuk, E., Williams, K. R., Hemphill, L., Muñiz-Grijalvo, O., Santos, R. D., Baum, S., and Witztum, J. L. (2018) Characterizing familial chylomicronemia syndrome: Baseline data of the APPROACH study. *J. Clin. Lipidol.* **12**, 1234-1243.e5

47. Chaudhry, R., Viljoen, A., and Wierzbicki, A. S. (2018) Pharmacological treatment options for severe hypertriglyceridemia and familial chylomicronemia syndrome. *Expert Rev. Clin. Pharmacol.* **11**, 589–598

48. Dallinga-Thie, G. M., Kroon, J., Boren, J., and Chapman, M. J. (2016) Triglyceride-Rich Lipoproteins and Remnants: Targets for Therapy? *Curr. Cardiol. Rep.* **18**, 1–9

49. Weinberg, R. B., Cook, V. R., Beckstead, J. A., Martin, D. D. O., Gallagher, J. W., Shelness, G. S., and Ryan, R. O. (2003) Structure and interfacial properties of human apolipoprotein A-V. *J. Biol. Chem.* **278**, 34438–44

50. Lookene, A., Beckstead, J. A., Nilsson, S., Olivecrona, G., and Ryan, R. O. (2005) Apolipoprotein A-V-heparin Interactions. *J. Biol. Chem.* **280**, 25383–25387

51. Gonzales, J. C., Gordts, P. L. S. M., Foley, E. M., and Esko, J. D. (2013) Apolipoproteins e and AV mediate lipoprotein clearance by hepatic proteoglycans. *J. Clin. Invest.* **123**, 2742–2751

52. Berbée, J. F. P., van der Hoogt, C. C., Sundararaman, D., Havekes, L. M., and Rensen,

P. C. N. (2005) Severe hypertriglyceridemia in human APOC1 transgenic mice is caused by apoC-I-induced inhibition of LPL. *J. Lipid Res.* **46**, 297–306

53. Berbée, J. F. P., Van Der Hoogt, C. C., Sundararaman, D., Havekes, L. M., and Rensen, P. C. N. (2005) Severe hypertriglyceridemia in human APOC1 transgenic mice is caused by apoC-I-induced inhibition of LPL. *J. Lipid Res.* **46**, 297–306

54. Larsson, M., Vorrsjo, E., Talmud, P., Lookene, A., and Olivecrona, G. (2013) Apolipoproteins C-I and C-III inhibit lipoprotein lipase activity by displacement of the enzyme from lipid droplets. *J. Biol. Chem.* **288**, 33997–34008

55. Eklund, L., Kangas, J., and Saharinen, P. (2017) Angiopoietin-Tie signalling in the cardiovascular and lymphatic systems. *Clin. Sci.* **131**, 87–103

56. Carbone, C., Piro, G., Merz, V., Simionato, F., Santoro, R., Zecchetto, C., Tortora, G., and Melisi, D. (2018) Angiopoietin-Like Proteins in Angiogenesis, Inflammation and Cancer. *Int. J. Mol. Sci.* **19**, 431

57. Kersten, S. (2019) New insights into angiopoietin-like proteins in lipid metabolism and cardiovascular disease risk. *Curr. Opin. Lipidol.* **30**, 205–211

58. Camenisch, G., Pisabarro, M. T., Sherman, D., Kowalski, J., Nagel, M., Hass, P., Xie, M. H., Gurney, A., Bodary, S., Liang, X. H., Clark, K., Beresini, M., Ferrara, N., and Gerber, H. P. (2002) ANGPTL3 stimulates endothelial cell adhesion and migration via integrin αvβ3 and induces blood vessel formation in vivo. *J. Biol. Chem.* **277**, 17281–17290

59. Ono, M., Shimizugawa, T., Shimamura, M., Yoshida, K., Noji-Sakikawa, C., Ando, Y., Koishi, R., and Furukawa, H. (2003) Protein Region Important for Regulation of Lipid Metabolism in Angiopoietin-like 3 (ANGPTL3): ANGPTL3 is cleaved and activated in vivo. *J. Biol. Chem.* **278**, 41804–41809

60. Quagliarini, F., Wang, Y., Kozlitina, J., Grishin, N. V., Hyde, R., Boerwinkle, E., Valenzuela, D. M., Murphy, A. J., Cohen, J. C., and Hobbs, H. H. (2012) Atypical angiopoietin-like protein that regulates ANGPTL3. *Proc. Natl. Acad. Sci.* **109**, 19751–19756

61. Chi, X., Britt, E. C., Shows, H. W., Hjelmaas, A. J., Shetty, S. K., Cushing, E. M., Li, W., Dou, A., Zhang, R., and Davies, B. S. J. (2017) ANGPTL8 promotes the ability of ANGPTL3 to bind and inhibit lipoprotein lipase. *Mol. Metab.* **6**, 1137–1149

62. Haller, J. F., Mintah, I. J., Shihanian, L. M., Stevis, P., Buckler, D., Alexa-Braun, C. A., Kleiner, S., Banfi, S., Cohen, J. C., Hobbs, H. H., Yancopoulos, G. D., Murphy, A. J., Gusarova, V., and Gromada, J. (2017) ANGPTL8 requires ANGPTL3 to inhibit lipoprotein lipase and plasma triglyceride clearance. *J. Lipid Res.* **58**, 1166–1173

63. Kovrov, O., Kristensen, K. K., Larsson, E., Ploug, M., and Olivecrona, G. (2019) On the mechanism of angiopoietin-like protein 8 for control of lipoprotein lipase activity. *J. Lipid Res.* **60**, 783–793

64. Dewey, F. E., Gusarova, V., Dunbar, R. L., O'Dushlaine, C., Schurmann, C., Gottesman, O., McCarthy, S., Van Hout, C. V., Bruse, S., Dansky, H. M., Leader, J. B., Murray, M. F.,

Ritchie, M. D., Kirchner, H. L., Habegger, L., Lopez, A., Penn, J., Zhao, A., Shao, W., Stahl, N., Murphy, A. J., Hamon, S., Bouzelmat, A., Zhang, R., Shumel, B., Pordy, R., Gipe, D., Herman, G. A., Sheu, W. H. H., Lee, I.-T., Liang, K.-W., Guo, X., Rotter, J. I., Chen, Y.-D. I., Kraus, W. E., Shah, S. H., Damrauer, S., Small, A., Rader, D. J., Wulff, A. B., Nordestgaard, B. G., Tybjærg-Hansen, A., van den Hoek, A. M., Princen, H. M. G., Ledbetter, D. H., Carey, D. J., Overton, J. D., Reid, J. G., Sasiela, W. J., Banerjee, P., Shuldiner, A. R., Borecki, I. B., Teslovich, T. M., Yancopoulos, G. D., Mellis, S. J., Gromada, J., and Baras, A. (2017) Genetic and Pharmacologic Inactivation of ANGPTL3 and Cardiovascular Disease. *N. Engl. J. Med.* **377**, 211–221

65. Stitziel, N. O., Khera, A. V., Wang, X., Bierhals, A. J., Vourakis, A. C., Sperry, A. E., Natarajan, P., Klarin, D., Emdin, C. A., Zekavat, S. M., Nomura, A., Erdmann, J., Schunkert, H., Samani, N. J., Kraus, W. E., Shah, S. H., Yu, B., Boerwinkle, E., Rader, D. J., Gupta, N., Frossard, P. M., Rasheed, A., Danesh, J., Lander, E. S., Gabriel, S., Saleheen, D., Musunuru, K., and Kathiresan, S. (2017) ANGPTL3 Deficiency and Protection Against Coronary Artery Disease. *J. Am. Coll. Cardiol.* **69**, 2054–2063

66. Musunuru, K., Pirruccello, J. P., Do, R., Peloso, G. M., Guiducci, C., Sougnez, C., Garimella, K. V, Fisher, S., Abreu, J., Barry, A. J., Fennell, T., Banks, E., Ambrogio, L., Cibulskis, K., Kernytsky, A., Gonzalez, E., Rudzicz, N., Engert, J. C., DePristo, M. A., Daly, M. J., Cohen, J. C., Hobbs, H. H., Altshuler, D., Schonfeld, G., Gabriel, S. B., Yue, P., and Kathiresan, S. (2010) Exome Sequencing, ANGPTL3 Mutations, and Familial Combined Hypolipidemia. *N. Engl. J. Med.* **363**, 2220–2227

67. Graham, M. J., Lee, R. G., Brandt, T. A., Tai, L.-J., Fu, W., Peralta, R., Yu, R., Hurh, E., Paz, E., McEvoy, B. W., Baker, B. F., Pham, N. C., Digenio, A., Hughes, S. G., Geary, R. S., Witztum, J. L., Crooke, R. M., and Tsimikas, S. (2017) Cardiovascular and Metabolic Effects of *ANGPTL3* Antisense Oligonucleotides. *N. Engl. J. Med.* **377**, 222–232

68. Gusarova, V., Alexa, C. a., Wang, Y., Rafique, A., Kim, J. H., Buckler, D., Mintah, I. J., Shihanian, L. M., Cohen, J. C., Hobbs, H. H., Xin, Y., Valenzuela, D. M., Murphy, A. J., Yancopoulos, G. D., and Gromada, J. (2015) ANGPTL3 blockade with a human monoclonal antibody reduces plasma lipids in dyslipidemic mice and monkeys. *J. Lipid Res.* **56**, 1308–17

69. Peloso, G. M., Auer, P. L., Bis, J. C., Voorman, A., Morrison, A. C., Stitziel, N. O., Brody, J. A., Khetarpal, S. A., Crosby, J. R., Fornage, M., Isaacs, A., Jakobsdottir, J., Feitosa, M. F., Davies, G., Huffman, J. E., Manichaikul, A., Davis, B., Lohman, K., Joon, A. Y., Smith, A. V., Grove, M. L., Zanoni, P., Redon, V., Demissie, S., Lawson, K., Peters, U., Carlson, C., Jackson, R. D., Ryckman, K. K., MacKey, R. H., Robinson, J. G., Siscovick, D. S., Schreiner, P. J., Mychaleckyj, J. C., Pankow, J. S., Hofman, A., Uitterlinden, A. G., Harris, T. B., Taylor, K. D., Stafford, J. M., Reynolds, L. M., Marioni, R. E., Dehghan, A., Franco, O. H., Patel, A. P., Lu, Y., Hindy, G., Gottesman, O., Bottinger, E. P., Melander, O., Orho-Melander, M., Loos, R. J. F., Duga, S., Merlini, P. A., Farrall, M., Goel, A., Asselta, R., Girelli, D., Martinelli, N., Shah, S. H., Kraus, W. E., Li, M., Rader, D. J., Reilly, M. P., McPherson, R., Watkins, H., Ardissino, D., Zhang, Q., Wang, J., Tsai, M. Y., Taylor, H. A., Correa, A., Griswold, M. E., Lange, L. A., Starr, J. M., Rudan, I., Eiriksdottir, G., Launer, L. J., Ordovas, J. M., Levy, D., Chen, Y. D. I., Reiner, A. P., Hayward, C., Polasek, O., Deary, I. J., Borecki, I. B., Liu, Y., Gudnason, V., Wilson, J. G., Van Duijn, C. M., Kooperberg, C., Rich, S. S., Psaty, B. M., Rotter, J. I., O'Donnell, C. J., Rice, K., Boerwinkle, E., Kathiresan, S., and Cupples, L. A. (2014) Association of low-frequency

and rare coding-sequence variants with blood lipids and coronary heart disease in 56,000 whites and blacks. *Am. J. Hum. Genet.* **94**, 223–232

70. Gusarova, V., Banfi, S., Alexa-Braun, C. A., Shihanian, L. M., Mintah, I. J., Lee, J. S., Xin, Y., Su, Q., Kamat, V., Cohen, J. C., Hobbs, H. H., Zambrowicz, B., Yancopoulos, G. D., Murphy, A. J., and Gromada, J. (2017) ANGPTL8 blockade with a monoclonal antibody promotes triglyceride clearance, energy expenditure, and weight loss in mice. *Endocrinology*. **158**, 1252–1259

71. Griffon, N., Budreck, E. C., Long, C. J., Broedl, U. C., Marchadier, D. H. L., Glick, J. M., and Rader, D. J. (2006) Substrate specificity of lipoprotein lipase and endothelial lipase: studies of lid chimeras. *J. Lipid Res.* **47**, 1803–1811

72. Zhu, P., Goh, Y. Y., Chin, H. F. A., Kersten, S., and Tan, N. S. (2012) Angiopoietin-like 4: a decade of research. *Biosci. Rep.* **32**, 211–219

73. Zhang, R. (2016) The ANGPTL3-4-8 model, a molecular mechanism for triglyceride trafficking. *Open Biol.* **6**, 150272

74. Gomez Perdiguero, E., Liabotis-Fontugne, A., Durand, M., Faye, C., Ricard-Blum, S., Simonutti, M., Augustin, S., Robb, B. M., Paques, M., Valenzuela, D. M., Murphy, A. J., Yancopoulos, G. D., Thurston, G., Galaup, A., Monnot, C., and Germain, S. (2016) ANGPTL4-αvβ3 interaction counteracts hypoxia-induced vascular permeability by modulating Src signalling downstream of vascular endothelial growth factor receptor 2. *J. Pathol.* **240**, 461–471

75. Goh, Y. Y., Pal, M., Chong, H. C., Zhu, P., Tan, M. J., Punugu, L., Tan, C. K., Huang, R. L., Sze, S. K., Tang, M. B. Y., Ding, J. L., Kersten, S., and Tan, N. S. (2010) Angiopoietin-like 4 interacts with matrix proteins to modulate wound healing. *J. Biol. Chem.* **285**, 32999–33009

76. Huang, R. L., Teo, Z., Chong, H. C., Zhu, P., Tan, M. J., Tan, C. K., Lam, C. R. I., Sng, M. K., Leong, D. T. W., Tan, S. M., Kersten, S., Ding, J. L., Li, H. Y., and Tan, N. S. (2011) ANGPTL4 modulates vascular junction integrity by integrin signaling and disruption of intercellular VE-cadherin and claudin-5 clusters. *Blood*. **118**, 3990–4002

77. Ge, H., Cha, J.-Y., Gopal, H., Harp, C., Yu, X., Repa, J. J., and Li, C. (2005) Differential regulation and properties of angiopoietin-like proteins 3 and 4. *J. Lipid Res.* **46**, 1484–1490

78. Sukonina, V., Lookene, A., Olivecrona, T., and Olivecrona, G. (2006) Angiopoietin-like protein 4 converts lipoprotein lipase to inactive monomers and modulates lipase activity in adipose tissue. *Proc. Natl. Acad. Sci. U. S. A.* **103**, 17450–5

79. Lafferty, M. J., Bradford, K. C., Erie, D. A., and Neher, S. B. (2013) Angiopoietin-like Protein 4 Inhibition of Lipoprotein Lipase. *J. Biol. Chem.* **288**, 28524–28534

80. Gunilla, B., and Olivecrona, T. (1985) Binding of active and inactive forms of lipoprotein lipase to heparin Effects of pH

81. Bengtsson, G., and Olivecrona, T. (1979) Binding of deoxycholate to lipoprotein lipase.

Biochim. Biophys. Acta (BBA)/Lipids Lipid Metab. **575**, 471–474

82. Sonnenburg, W. K., Yu, D., Lee, E.-C., Xiong, W., Gololobov, G., Key, B., Gay, J., Wilganowski, N., Hu, Y., Zhao, S., Schneider, M., Ding, Z.-M., Zambrowicz, B. P., Landes, G., Powell, D. R., and Desai, U. (2009) GPIHBP1 stabilizes lipoprotein lipase and prevents its inhibition by angiopoietin-like 3 and angiopoietin-like 4. *J. Lipid Res.* **50**, 2421–2429

83. Shan, L., Yu, X.-C., Liu, Z., Hu, Y., Sturgis, L. T., Miranda, M. L., and Liu, Q. (2009) The Angiopoietin-like Proteins ANGPTL3 and ANGPTL4 Inhibit Lipoprotein Lipase Activity through Distinct Mechanisms. *J. Biol. Chem.* **284**, 1419–1424

84. Robal, T., Larsson, M., Martin, M., Olivecrona, G., and Lookene, A. (2012) Fatty Acids Bind Tightly to the N-terminal Domain of Angiopoietin-like Protein 4 and Modulate Its Interaction with Lipoprotein Lipase. *J. Biol. Chem.* **287**, 29739–29752

85. Gutgsell, A. R., Ghodge, S. V., Bowers, A. A., and Neher, S. B. (2019) Mapping the sites of the lipoprotein lipase (LPL)–angiopoietin-like protein 4 (ANGPTL4) interaction provides mechanistic insight into LPL inhibition. *J. Biol. Chem.* **294**, 2678–2689

86. Goulbourne, C. N., Gin, P., Tatar, A., Nobumori, C., Hoenger, A., Jiang, H., Grovenor, C. R. M., Adeyo, O., Esko, J. D., Goldberg, I. J., Reue, K., Tontonoz, P., Bensadoun, A., Beigneux, A. P., Young, S. G., and Fong, L. G. (2014) The GPIHBP1-LPL complex is responsible for the margination of triglyceride-rich lipoproteins in capillaries. *Cell Metab.* **19**, 849–860

87. Mysling, S., Kristensen, K. K., Larsson, M., Kovrov, O., Bensadouen, A., Jørgensen, T. J., Olivecrona, G., Young, S. G., and Ploug, M. (2016) The angiopoietin-like protein ANGPTL4 catalyzes unfolding of the hydrolase domain in lipoprotein lipase and the endothelial membrane protein GPIHBP1 counteracts this unfolding. *Elife*. **5**, 1–18

88. Lichtenstein, L., Berbée, J. F. P., Van Dijk, S. J., Van Dijk, K. W., Bensadoun, A., Kema, I. P., Voshol, P. J., Müller, M., Rensen, P. C. N., and Kersten, S. (2007) Angptl4 upregulates cholesterol synthesis in liver via inhibition of LPL- and HL-dependent hepatic cholesterol uptake. *Arterioscler. Thromb. Vasc. Biol.* **27**, 2420–2427

89. Dewey, F. E., Gusarova, V., O'Dushlaine, C., Gottesman, O., Trejos, J., Hunt, C., Van Hout, C. V., Habegger, L., Buckler, D., Lai, K.-M. V., Leader, J. B., Murray, M. F., Ritchie, M. D., Kirchner, H. L., Ledbetter, D. H., Penn, J., Lopez, A., Borecki, I. B., Overton, J. D., Reid, J. G., Carey, D. J., Murphy, A. J., Yancopoulos, G. D., Baras, A., Gromada, J., and Shuldiner, A. R. (2016) Inactivating Variants in ANGPTL4 and Risk of Coronary Artery Disease. *N. Engl. J. Med.* **374**, 1123–1133

90. Romeo, S., Pennacchio, L. A., Fu, Y., Boerwinkle, E., Tybjaerg-Hansen, A., Hobbs, H. H., and Cohen, J. C. (2007) Population-based resequencing of ANGPTL4 uncovers variations that reduce triglycerides and increase HDL. *Nat. Genet.* **39**, 513–516

91. Desai, U., Lee, E. C., Chung, K., Gao, C., Gay, J., Key, B., Hansen, G., Machajewski, D., Platt, K. A., Sands, A. T., Schneider, M., Van Sligtenhorst, I., Suwanichkul, A., Vogel, P., Wilganowski, N., Wingert, J., Zambrowicz, B. P., Landes, G., and Powell, D. R. (2007) Lipid-lowering effects of anti-angiopoietin-like 4 antibody recapitulate the lipid phenotype found in angiopoietin-like 4 knockout mice. *Proc Natl Acad Sci U S A*. **104**, 11766–11771

92. Lichtenstein, L., Mattijssen, F., de Wit, N. J., Georgiadi, A., Hooiveld, G. J. G. J., van der Meer, R., He, Y., Qi, L., Köster, A., Tamsma, J. T., Tan, N. S. N. S., Müller, M., Kersten, S., Aterman, K., Remmele, W., Smith, M., Babaev, V. R., Fazio, S., Gleaves, L. A., Carter, K. J., Semenkovich, C. F., Linton, M. F., Backhed, F., Crawford, P. A., O'Donnell, D., Gordon, J. I., Borradaile, N. M., Han, X., Harp, J. D., Gale, S. E., Ory, D. S., Schaffer, J. E., Cani, P. D., Amar, J., Iglesias, M. A., Poggi, M., Knauf, C., Bastelica, D., Neyrinck, A. M., Fava, F., Tuohy, K. M., Chabo, C., al., et, Desai, U., Lee, E. C., Chung, K., Gao, C., Gay, J., Key, B., Hansen, G., Machajewski, D., Platt, K. A., Sands, A. T., al., et, Bosch, H. M. de V. den, Wit, N. J. de, Hooiveld, G. J. G. J., Vermeulen, H., Veen, J. N. van der, Houten, S. M., Kuipers, F., Muller, M., Meer, R. van der, Diakogiannaki, E., Welters, H. J., Morgan, N. G., Erbay, E., Babaev, V. R., Mayers, J. R., Makowski, L., Charles, K. N., Snitow, M. E., Fazio, S., Wiest, M. M., Watkins, S. M., Linton, M. F., al., et, Gale, N. W., Thurston, G., Hackett, S. F., Renard, R., Wang, Q., McClain, J., Martin, C., Witte, C., Witte, M. H., Jackson, D., al., et, Gianturco, S. H., Bradley, W. A., Gotto, A. M., Morrisett, J. D., Peavy, D. L., Harvey, N. L., Srinivasan, R. S., Dillard, M. E., Johnson, N. C., Witte, M. H., Boyd, K., Sleeman, M. W., Oliver, G., Hotamisligil, G. S., Jiang, H. Y., Wek, S. A., McGrath, B. C., Scheuner, D., Kaufman, R. J., Cavener, D. R., Wek, R. C., Kersten, S., Mandard, S., Tan, N. S. N. S., Escher, P., Metzger, D., Chambon, P., Gonzalez, F. J., Desvergne, B., Wahli, W., Koster, A., Chao, Y. B., Mosior, M., Ford, A., Gonzalez-DeWhitt, P. A., Hale, J. E., Li, D., Qiu, Y., Fraser, C. C., Yang, D. D., al., et, Lattin, J. E., Schroder, K., Su, A. I., Walker, J. R., Zhang, J., Wiltshire, T., Saijo, K., Glass, C. K., Hume, D. A., Kellie, S., al., et, Lee, J. Y., Sohn, K. H., Rhee, S. H., Hwang, D., Lichtenstein, L., Berbee, J. F., Dijk, S. J. van, Dijk, K. W. van, Bensadoun, A., Kema, I. P., Voshol, P. J., Muller, M., Rensen, P. C., Kersten, S., Mandard, S., Zandbergen, F., Straten, E. van, Wahli, W., Kuipers, F., Muller, M., Kersten, S., Martinon, F., Chen, X., Lee, A. H., Glimcher, L. H., Merkel, M., Eckel, R. H., Goldberg, I. J., Oike, Y., Akao, M., Yasunaga, K., Yamauchi, T., Morisada, T., Ito, Y., Urano, T., Kimura, Y., Kubota, Y., Maekawa, H., al., et, Ostlund-Lindqvist, A. M., Gustafson, S., Lindqvist, P., Witztum, J. L., Little, J. A., Romeo, S., Pennacchio, L. A., Fu, Y., Boerwinkle, E., Tybjaerg-Hansen, A., Hobbs, H. H., Cohen, J. C., Saraswathi, V., Hasty, A. H., Shan, L., Yu, X. C., Liu, Z., Hu, Y., Sturgis, L. T., Miranda, M. L., Liu, Q., Shi, H., Kokoeva, M. V., Inouye, K., Tzameli, I., Yin, H., Flier, J. S., Skarlatos, S. I., Dichek, H. L., Fojo, S. S., Brewer, H. B., Kruth, H. S., Sonnenburg, W. K., Yu, D., Lee, E. C., Xiong, W., Gololobov, G., Key, B., Gay, J., Wilganowski, N., Hu, Y., Zhao, S., al., et, Suganami, T., Tanimoto-Koyama, K., Nishida, J., Itoh, M., Yuan, X., Mizuarai, S., Kotani, H., Yamaoka, S., Miyake, K., Aoe, S., al., et, Tabata, M., Kadomatsu, T., Fukuhara, S., Miyata, K., Ito, Y., Endo, M., Urano, T., Zhu, H. J., Tsukano, H., Tazume, H., al., et, Urano, F., Wang, X., Bertolotti, A., Zhang, Y., Chung, P., Harding, H. P., Ron, D., Voshol, P. J., Rensen, P. C., Dijk, K. W. van, Romijn, J. A., Havekes, L. M., Wang, H., Eckel, R. H., Wei, Y., Wang, D., Topczewski, F., Pagliassotti, M. J., Woo, C. W., Cui, D., Arellano, J., Dorweiler, B., Harding, H. P., Fitzgerald, K. A., Ron, D., Tabas, I., Xu, A., Lam, M. C., Chan, K. W., Wang, Y., Zhang, J., Hoo, R. L., Xu, J. Y., Chen, B., Chow, W. S., Tso, A. W., al., et, Yang, L., Xue, Z., He, Y., Sun, S., Chen, H., Qi, L., Yin, B., Loike, J. D., Kako, Y., Weinstock, P. H., Breslow, J. L., Silverstein, S. C., Goldberg, I. J., Yin, W., Romeo, S., Chang, S., Grishin, N. V., Hobbs, H. H., Cohen, J. C., Yoon, J. C., Chickering, T. W., Rosen, E. D., Dussault, B., Qin, Y., Soukas, A., Friedman, J. M., Holmes, W. E., Spiegelman, B. M., Yoshida, K., Shimizugawa, T., Ono, M., and Furukawa, H. (2010) Angptl4 protects against severe proinflammatory effects of saturated fat by inhibiting fatty acid uptake into mesenteric lymph node macrophages. *Cell Metab.* **12**, 580–592

93. Gusarova, V., O'Dushlaine, C., Teslovich, T. M., Benotti, P. N., Mirshahi, T., Gottesman, O., Van Hout, C. V., Murray, M. F., Mahajan, A., Nielsen, J. B., Fritsche, L., Wulff, A. B., Gudbjartsson, D. F., Sjögren, M., Emdin, C. A., Scott, R. A., Lee, W.-J., Small, A., Kwee, L. C., Dwivedi, O. P., Prasad, R. B., Bruse, S., Lopez, A. E., Penn, J., Marcketta, A., Leader, J. B., Still, C. D., Kirchner, H. L., Mirshahi, U. L., Wardeh, A. H., Hartle, C. M., Habegger, L., Fetterolf, S. N., Tusie-Luna, T., Morris, A. P., Holm, H., Steinthorsdottir, V., Sulem, P., Thorsteinsdottir, U., Rotter, J. I., Chuang, L.-M., Damrauer, S., Birtwell, D., Brummett, C. M., Khera, A. V., Natarajan, P., Orho-Melander, M., Flannick, J., Lotta, L. A., Willer, C. J., Holmen, O. L., Ritchie, M. D., Ledbetter, D. H., Murphy, A. J., Borecki, I. B., Reid, J. G., Overton, J. D., Hansson, O., Groop, L., Shah, S. H., Kraus, W. E., Rader, D. J., Chen, Y.-D. I., Hveem, K., Wareham, N. J., Kathiresan, S., Melander, O., Stefansson, K., Nordestgaard, B. G., Tybjærg-Hansen, A., Abecasis, G. R., Altshuler, D., Florez, J. C., Boehnke, M., McCarthy, M. I., Yancopoulos, G. D., Carey, D. J., Shuldiner, A. R., Baras, A., Dewey, F. E., and Gromada, J. (2018) Genetic inactivation of ANGPTL4 improves glucose homeostasis and is associated with reduced risk of diabetes. *Nat. Commun.* **9**, 2252

94. Consortia, M. I. G. and Cardi. E. (2016) Coding Variation in ANGPTL4 , LPL , and SVEP1 and the Risk of Coronary Disease. *N. Engl. J. Med.* **374**, 1134–1144

95. Cushing, E. M., Chi, X., Sylvers, K. L., Shetty, S. K., Potthoff, M. J., and Davies, B. S. J. (2017) Angiopoietin-like 4 directs uptake of dietary fat away from adipose during fasting. *Mol. Metab.* **6**, 809–818

96. Kroupa, O., Vorrsjö, E., Stienstra, R., Mattijssen, F., Nilsson, S. K., Sukonina, V., Kersten, S., Olivecrona, G., and Olivecrona, T. (2012) Linking nutritional regulation of Angptl4, Gpihbp1, and Lmf1 to lipoprotein lipase activity in rodent adipose tissue. *BMC Physiol.* **12**, 13

97. Bergö, M., Wu, G., Ruge, T., and Olivecrona, T. (2002) Down-regulation of adipose tissue lipoprotein lipase during fasting requires that a gene, separate from the lipase gene, is switched on. *J. Biol. Chem.* **277**, 11927–11932

98. Dijk, W., Heine, M., Vergnes, L., Boon, M. R., Schaart, G., Hesselink, M. K. C., Reue, K., van Marken Lichtenbelt, W. D., Olivecrona, G., Rensen, P. C. N., Heeren, J., and Kersten, S. (2015) ANGPTL4 mediates shuttling of lipid fuel to brown adipose tissue during sustained cold exposure. *Elife*. **4**, 1–23

99. Catoire, M., Alex, S., Paraskevopulos, N., Mattijssen, F., Evers-van Gogh, I., Schaart, G., Jeppesen, J., Kneppers, A., Mensink, M., Voshol, P. J., Olivecrona, G., Tan, N. S., Hesselink, M. K. C., Berbee, J. F., Rensen, P. C. N., Kalkhoven, E., Schrauwen, P., and Kersten, S. (2014) Fatty acid-inducible ANGPTL4 governs lipid metabolic response to exercise. *Proc. Natl. Acad. Sci.* **111**, E1043–E1052

100. Ingerslev, B., Hansen, J. S., Hoffmann, C., Clemmesen, J. O., Secher, N. H., Scheler, M., Hrabě de Angelis, M., Häring, H. U., Pedersen, B. K., Weigert, C., and Plomgaard, P. (2017) Angiopoietin-like protein 4 is an exercise-induced hepatokine in humans, regulated by glucagon and cAMP. *Mol. Metab.* **6**, 1286–1295

101. McCamish, M., Yoon, W., and McKay, J. (2016) Biosimilars: biologics that meet patients' needs and healthcare economics. *Am. J. Manag. Care*. **22**, S439–S442

102. Watson, J. (2019) Biologics Market To Reach USD 625 . 6 Million By 2026 | Reports And Data CAGR of 11 . 9 %, Biologics Industry Trends – Product launches and research for advanced biologics . *Reports Data*. [online] https://www.globenewswire.com/news-release/2019/10/10/1928253/0/en/Biologics-Market-To-Reach-USD-625-6-Million-By-2026-Reports-And-Data.html (Accessed February 4, 2020)

103. Hegele, R. A., and Tsimikas, S. (2019) Lipid-Lowering Agents. *Circ. Res.* **124**, 386–404

104. Strilchuck, L., Fogacci, F., and Cicero, A. F. (2019) Safety and tolerability of injectable lipid-lowering drugs: an update of clinical data. *Expert Opin. Drug Saf.* **18**, 611–621

105. Reichert, J. M. (2015) Antibodies to watch in 2015. *MAbs*. **7**, 1–8

106. Chaudhary, R., Garg, J., Shah, N., and Sumner, A. (2017) PCSK9 inhibitors: A new era of lipid lowering therapy. *World J. Cardiol.* **9**, 76

107. Qamar, A., Khetarpal, S. A., Khera, A. V., Qasim, A., Rader, D. J., and Reilly, M. P. (2015) Plasma Apolipoprotein C-III Levels, Triglycerides, and Coronary Artery Calcification in Type 2 Diabetics. *Arterioscler. Thromb. Vasc. Biol.* **35**, 1880–1888

108. Crosby, J., Peloso, G. M., Auer, P. L., Crosslin, D. R., Stitziel, N. O., Lange, L. A., Lu, Y., Tang, Z. Z., Zhang, H., Hindy, G., Masca, N., Stirrups, K., Kanoni, S., Do, R., Jun, G., Hu, Y., Kang, H. M., Xue, C., Goel, A., Farrall, M., Duga, S., Merlini, P. A., Asselta, R., Girelli, D., Olivieri, O., Martinelli, N., Yin, W., Reilly, D., Speliotes, E., Fox, C. S., Hveem, K., Holmen, O. L., Nikpay, M., Farlow, D. N., Assimes, T. L., Franceschini, N., Robinson, J., North, K. E., Martin, L. W., DePristo, M., Gupta, N., Escher, S. A., Jansson, J. H., Van Zuydam, N., Palmer, C. N. A., Wareham, N., Koch, W., Meitinger, T., Peters, A., Lieb, W., Erbel, R., Konig, I. R., Kruppa, J., Degenhardt, F., Gottesman, O., Bottinger, E. P., O'Donnell, C. J., Psaty, B. M., Ballantyne, C. M., Abecasis, G., Ordovas, J. M., Melander, O., Watkins, H., Orho-Melander, M., Ardissino, D., Loos, R. J. F., McPherson, R., Willer, C. J., Erdmann, J., Hall, A. S., Samani, N. J., Deloukas, P., Schunkert, H., Wilson, J. G., Kooperberg, C., Rich, S. S., Tracy, R. P., Lin, D. Y., Altshuler, D., Gabriel, S., Nickerson, D. A., Jarvik, G. P., Cupples, L. A., Reiner, A. P., Boerwinkle, E., and Kathiresan, S. (2014) Loss-of-Function Mutations in APOC3, Triglycerides, and Coronary Disease. *N. Engl. J. Med.* **371**, 22–31

109. Witztum, J. L., Gaudet, D., Freedman, S. D., Alexander, V. J., Digenio, A., Williams, K. R., Yang, Q., Hughes, S. G., Geary, R. S., Arca, M., Stroes, E. S. G., Bergeron, J., Soran, H., Civeira, F., Hemphill, L., Tsimikas, S., Blom, D. J., O'Dea, L., and Bruckert, E. (2019) Volanesorsen and Triglyceride Levels in Familial Chylomicronemia Syndrome. *N. Engl. J. Med.* **381**, 531–542

110. Rhainds, D., Brodeur, M. R., and Tardif, J.-C. (2019) Investigational drugs in development for hypertriglyceridemia: a coming-of-age story. *Expert Opin. Investig. Drugs*. **28**, 1059–1079

111. Gordts, P. L. S. M., Nock, R., Son, N.-H., Ramms, B., Lew, I., Gonzales, J. C., Thacker, B. E., Basu, D., Lee, R. G., Mullick, A. E., Graham, M. J., Goldberg, I. J., Crooke, R. M., Witztum, J. L., and Esko, J. D. (2016) ApoC-III inhibits clearance of triglyceride-rich lipoproteins through LDL family receptors. *J. Clin. Invest.* **126**, 2855–66

112. Warden, B. A., and Duell, P. B. (2018) Volanesorsen for treatment of patients with familial chylomicronemia syndrome. *Drugs of Today*. **54**, 721

113. Mansoor, M., and Melendez, A. J. (2008) Advances in antisense oligonucleotide development for target identification, validation, and as novel therapeutics. *Gene Regul. Syst. Bio.* **2008**, 275–295

114. Shen, X., and Corey, D. R. (2018) Chemistry, mechanism and clinical status of antisense oligonucleotides and duplex RNAs. *Nucleic Acids Res.* **46**, 1584–1600

115. Gaudet, D., Gipe, D. A., Pordy, R., Ahmad, Z., Cuchel, M., Shah, P. K., Chyu, K.-Y., Sasiela, W. J., Chan, K.-C., Brisson, D., Khoury, E., Banerjee, P., Gusarova, V., Gromada, J., Stahl, N., Yancopoulos, G. D., and Hovingh, G. K. (2017) ANGPTL3 Inhibition in Homozygous Familial Hypercholesterolemia. *N. Engl. J. Med.* **377**, 296–297

116. FUJIMOTO, K., KOISHI, R., SHIMIZUGAWA, T., and ANDO, Y. (2006) Angptl3-null Mice Show Low Plasma Lipid Concentrations by Enhanced Lipoprotein Lipase Activity. *Exp. Anim.* **55**, 27–34

117. Wang, Y., Gusarova, V., Banfi, S., Gromada, J., Cohen, J. C., and Hobbs, H. H. (2015) Inactivation of ANGPTL3 reduces hepatic VLDL-triglyceride secretion. *J. Lipid Res.* **56**, 1296–307

118. Kaplon, H., Muralidharan, M., Schneider, Z., and Reichert, J. M. (2020) Antibodies to watch in 2020. *MAbs*. **12**, 1703531

119. Prakash, T. P., Graham, M. J., Yu, J., Carty, R., Low, A., Chappell, A., Schmidt, K., Zhao, C., Aghajan, M., Murray, H. F., Riney, S., Booten, S. L., Murray, S. F., Gaus, H., Crosby, J., Lima, W. F., Guo, S., Monia, B. P., Swayze, E. E., and Seth, P. P. (2014) Targeted delivery of antisense oligonucleotides to hepatocytes using triantennary N -acetyl galactosamine improves potency 10-fold in mice. *Nucleic Acids Res.* **42**, 8796–8807

120. Wolska, A., Lo, L., Sviridov, D. O., Pourmousa, M., Pryor, M., Ghosh, S. S., Kakkar, R., Davidson, M., Wilson, S., Pastor, R. W., Goldberg, I. J., Basu, D., Drake, S. K., Cougnoux, A., Wu, M. J., Neher, S. B., Freeman, L. A., Tang, J., Amar, M., Devalaraja, M., and Remaley, A. T. (2020) A dual apolipoprotein C-II mimetic-apolipoprotein C-III antagonist peptide lowers plasma triglycerides. *Sci. Transl. Med.* **12**, 1–14

121. Weil, T. (2014) The growing significance of peptide therapeutics. *BioRegion Ulm*

122. Ballinger, A. (2000) Orlistat in the treatment of obesity. *Expert Opin. Pharmacother.* **1**, 841–7

123. Liu, X., Men, P., Wang, Y., Zhai, S., Zhao, Z., and Liu, G. (2017) Efficacy and Safety of Lomitapide in Hypercholesterolemia. *Am. J. Cardiovasc. Drugs*. **17**, 299–309

124. Komatsu, T., Sakurai, T., Wolska, A., Amar, M. J., Sakurai, A., Vaisman, B. L., Sviridov, D., Demosky, S., Pryor, M., Ikewaki, K., and Remaley, A. T. (2019) Apolipoprotein C-II Mimetic Peptide Promotes the Plasma Clearance of Triglyceride-Rich Lipid Emulsion and the Incorporation of Fatty Acids into Peripheral Tissues of Mice. *J. Nutr. Metab.* 10.1155/2019/7078241

125. Kockx, M., and Kritharides, L. (2018) Triglyceride-Rich Lipoproteins. *Cardiol. Clin.* **36**, 265–275

126. Santamarina-Fojo, S., and Brewer Jr., H. B. (1994) Lipoprotein lipase: structure, function and mechanism of action. *Int. J. Clin. Lab. Res.* **24**, 143–147

127. Goldberg, I. J. (1996) Lipoprotein lipase and lipolysis: central roles in lipoprotein metabolism and atherogenesis. *J. Lipid Res.* **37**, 693–707

128. Brahm, A. J., and Hegele, R. A. (2015) Chylomicronaemia-current diagnosis and future therapies. *Nat. Rev. Endocrinol.* **11**, 352–362

129. Yuan, G., Al-Shali, K. Z., and Hegele, R. A. (2007) Hypertriglyceridemia: Its etiology, effects and treatment. *Cmaj*. **176**, 1113–1120

130. Rader, D. J. (2016) New therapeutic approaches to the treatment of dyslipidemia. *Cell Metab.* **23**, 405–412

131. Sniderman, A. D., Couture, P., Martin, S. S., DeGraaf, J., Lawler, P. R., Cromwell, W. C., Wilkins, J. T., and Thanassoulis, G. (2018) Hypertriglyceridemia and cardiovascular risk: a cautionary note about metabolic confounding. *J. Lipid Res.* **59**, 1266–1275

132. Peng, J., Luo, F., Ruan, G., Peng, R., and Li, X. (2017) Hypertriglyceridemia and atherosclerosis. *Lipids Health Dis.* **16**, 1–12

133. Sandoval, J. C., Nakagawa-Toyama, Y., Masuda, D., Tochino, Y., Nakaoka, H., Kawase, R., Yuasa-Kawase, M., Nakatani, K., Inagaki, M., Tsubakio-Yamamoto, K., Ohama, T., Matsuyama, A., Nishida, M., Ishigami, M., Komuro, I., and Yamashita, S. (2010) Molecular mechanisms of ezetimibe-induced attenuation of postprandial hypertriglyceridemia. *J. Atheroscler. Thromb.* **17**, 914–924

134. Karpe, F., Olivecrona, T., Olivecrona, G., Samra, J. S., Summers, L. K., Humphreys, S. M., and Frayn, K. N. (1998) Lipoprotein lipase transport in plasma: role of muscle and adipose tissues in regulation of plasma lipoprotein lipase concentrations. *J. Lipid Res.* **39**, 2387–93

135. Bergö, M., Olivecrona, G., and Olivecrona, T. (1996) Forms of lipoprotein lipase in rat tissues: in adipose tissue the proportion of inactive lipase increases on fasting. *Biochem. J.* **313**, 893–8

136. Li, Y., and Teng, C. (2014) Angiopoietin-like proteins 3, 4 and 8: regulating lipid metabolism and providing new hope for metabolic syndrome. *J. Drug Target.* **22**, 679–687

137. Lichtenstein, L., Mattijssen, F., de Wit, N. J., Georgiadi, A., Hooiveld, G. J., van der Meer, R., He, Y., Qi, L., Köster, A., Tamsma, J. T., Tan, N. S., Müller, M., and Kersten, S. (2010) Angptl4 Protects against Severe Proinflammatory Effects of Saturated Fat by Inhibiting Fatty Acid Uptake into Mesenteric Lymph Node Macrophages. *Cell Metab.* **12**, 580–592

138. Yin, W., Romeo, S., Chang, S., Grishin, N. V., Hobbs, H. H., and Cohen, J. C. (2009)

Genetic variation in ANGPTL4 provides insights into protein processing and function. *J. Biol. Chem.* **284**, 13213–13222

139. Biterova, E., Esmaeeli, M., Alanen, H. I., Saaranen, M., and Ruddock, L. W. (2018) Structures of Angptl3 and Angptl4, modulators of triglyceride levels and coronary artery disease. *Sci. Rep.* **8**, 1–12

140. Ge, H., Yang, G., Huang, L., Motola, D. L., Pourbahrami, T., and Li, C. (2004) Oligomerization and Regulated Proteolytic Processing of Angiopoietin-like Protein 4. *J. Biol. Chem.* **279**, 2038–2045
141. Miida, T., and Hirayama, S. (2010) Impacts of angiopoietin-like proteins on lipoprotein metabolism and cardiovascular events. *Curr. Opin. Lipidol.* **21**, 70–75

142. Lee, E.-C., Desai, U., Gololobov, G., Hong, S., Feng, X., Yu, X.-C., Gay, J., Wilganowski, N., Gao, C., Du, L.-L., Chen, J., Hu, Y., Zhao, S., Kirkpatrick, L., Schneider, M., Zambrowicz, B. P., Landes, G., Powell, D. R., and Sonnenburg, W. K. (2009) Identification of a New Functional Domain in Angiopoietin-like 3 (ANGPTL3) and Angiopoietin-like 4 (ANGPTL4) Involved in Binding and Inhibition of Lipoprotein Lipase (LPL). *J. Biol. Chem.* **284**, 13735–13745

143. Yau, M., Wang, Y., Lam, K. S. L., Zhang, J., Wu, D., and Xu, A. (2009) A Highly Conserved Motif within the NH 2 -terminal Coiled-coil Domain of Angiopoietin-like Protein 4 Confers Its Inhibitory Effects on Lipoprotein Lipase by Disrupting the Enzyme Dimerization. *J. Biol. Chem.* **284**, 11942–11952

144. Backhed, F., Crawford, P. A., O'Donnell, D., and Gordon, J. I. (2007) Postnatal lymphatic partitioning from the blood vasculature in the small intestine requires fasting-induced adipose factor. *Proc. Natl. Acad. Sci.* **104**, 606–611

145. Vadas, O., Jenkins, M. L., Dornan, G. L., and Burke, J. E. (2017) Using Hydrogen–Deuterium Exchange Mass Spectrometry to Examine Protein–Membrane Interactions. in *Methods in Enzymology*, 1st Ed., pp. 143–172, Elsevier Inc., **583**, 143–172

146. Oganesyan, I., Lento, C., and Wilson, D. J. (2018) Contemporary hydrogen deuterium exchange mass spectrometry. *Methods*. **144**, 27–42

147. Fang, J., Rand, K. D., Beuning, P. J., and Engen, J. R. (2011) False EX1 signatures caused by sample carryover during HX MS analyses. *Int. J. Mass Spectrom.* **302**, 19–25

148. Segel, I. (1993) Noncompetitive Inhibition. in *Enzyme Kinetics: Behavior and Analysis of Rapid Equilibrium and Steady-State Enzyme Systems*, Wiley Clas, pp. 125–136, Wiley, New York

149. Kearse, M., Moir, R., Wilson, A., Stones-Havas, S., Cheung, M., Sturrock, S., Buxton, S., Cooper, A., Markowitz, S., Duran, C., Thierer, T., Ashton, B., Meintjes, P., and Drummond, A. (2012) Geneious Basic: An integrated and extendable desktop software platform for the organization and analysis of sequence data. *Bioinformatics*. **28**, 1647–1649

150. Köster, A., Chao, Y. B., Mosior, M., Ford, A., Gonzalez-DeWhitt, P. A., Hale, J. E., Li, D., Qiu, Y., Fraser, C. C., Yang, D. D., Heuer, J. G., Jaskunas, S. R., and Eacho, P. (2005)

Transgenic angiopoietin-like (Angptl)4 overexpression and targeted disruption of Angptl4 and Angptl3: Regulation of triglyceride metabolism. *Endocrinology*. **146**, 4943–4950

151. Davis, R. C., Wong, H., Nikazy, J., Wang, K., Han, Q., and Schotz, M. C. (1992) Chimeras of hepatic lipase and lipoprotein lipase. Domain localization of enzyme-specific properties. *J. Biol. Chem.* **267**, 21499–504

152. Dugi, K. a, Dichek, H. L., Chem, J. B., Dichek, L., and Santamarina-fojo, S. (1995) Human Hepatic and Lipoprotein Lipase : The Loop Covering the Catalytic Site Mediates Lipase Substrate Specificity. **270**, 25396–25401

153. Dijk, W., Ruppert, P. M. M., Oost, L. J., and Kersten, S. (2018) Angiopoietin-like 4 promotes the intracellular cleavage of lipoprotein lipase by PCSK3/furin in adipocytes. *J. Biol. Chem.* **293**, 14134–14145

154. Dijk, W., Beigneux, A. P., Larsson, M., Bensadoun, A., Young, S. G., and Kersten, S. (2016) Angiopoietin-like 4 promotes intracellular degradation of lipoprotein lipase in adipocytes. *J. Lipid Res.* **57**, 1670–1683

155. Mysling, S., Kristensen, K. K., Larsson, M., Beigneux, A. P., Gårdsvoll, H., Loren, F. G., Bensadouen, A., Jørgensen, T. J. D., Young, S. G., and Ploug, M. (2016) The acidic domain of the endothelial membrane protein GPIHBP1 stabilizes lipoprotein lipase activity by preventing unfolding of its catalytic domain. *Elife*. **5**, 1–17

156. Neville, M. C., Waxman, L. J., Jensen, D., and Eckel, R. H. (1991) Lipoprotein lipase in human milk: compartmentalization and effect of fasting, insulin, and glucose. *J. Lipid Res.* **32**, 251–7

157. Nilsson, S. K., Anderson, F., Ericsson, M., Larsson, M., Makoveichuk, E., Lookene, A., Heeren, J., and Olivecrona, G. (2012) Triacylglycerol-rich lipoproteins protect lipoprotein lipase from inactivation by ANGPTL3 and ANGPTL4. *Biochim. Biophys. Acta - Mol. Cell Biol. Lipids*. **1821**, 1370–1378

158. Bengtsson-Olivecrona, G., and Olivecrona, T. (1991) Phospholipase Activity of Milk Lipoprotein Lipase. *Methods Enzymol.* **197**, 345–356

159. Pelay-Gimeno, M., Glas, A., Koch, O., and Grossmann, T. N. (2015) Structure-Based Design of Inhibitors of Protein-Protein Interactions: Mimicking Peptide Binding Epitopes. *Angew. Chemie - Int. Ed.* **54**, 8896–8927

160. Milroy, L.-G., Grossmann, T. N., Hennig, S., Brunsveld, L., and Ottmann, C. (2014) Modulators of Protein–Protein Interactions. *Chem. Rev.* **114**, 4695–4748

161. Moreira, I. S., Fernandes, P. A., and Ramos, M. J. (2007) Hot spots-A review of the protein-protein interface determinant amino-acid residues. *Proteins Struct. Funct. Bioinforma.* **68**, 803–812

162. Oteng, A.-B., Bhattacharya, A., Brodesser, S., Qi, L., Tan, N. S., and Kersten, S. (2017) Feeding Angptl4 −/− mice trans fat promotes foam cell formation in mesenteric lymph nodes without leading to ascites. *J. Lipid Res.* **58**, 1100–1113

163. Hamdan, T. A., Lang, P. A., and Lang, K. S. (2020) The Diverse Functions of the Ubiquitous Fcγ Receptors and Their Unique Constituent, FcRγ Subunit. *Pathog. (Basel, Switzerland)*. **9**, 1–12

164. Lawson, A. D. G. (2012) Antibody-enabled small-molecule drug discovery. *Nat. Rev. Drug Discov.* **11**, 519–525

165. Perdiguero, E. G., Galaup, A., Durand, M., Teillon, J., Philippe, J., Valenzuela, D. M., Murphy, A. J., Yancopoulos, G. D., Thurston, G., and Germain, S. (2011) Alteration of Developmental and Pathological Retinal Angiogenesis in angptl4 -deficient Mice. *J. Biol. Chem.* **286**, 36841–36851

166. Huang, Y., Wiedmann, M. M., and Suga, H. (2019) RNA Display Methods for the Discovery of Bioactive Macrocycles. *Chem. Rev.* **119**, 10360–10391

167. Suga, H. (2018) Max-Bergmann award lecture:A RaPID way to discover bioactive nonstandard peptides assisted by the flexizyme and FIT systems. *J. Pept. Sci.* **24**, 1–7

168. McMahon, C., Baier, A. S., Pascolutti, R., Wegrecki, M., Zheng, S., Ong, J. X., Erlandson, S. C., Hilger, D., Rasmussen, S. G. F., Ring, A. M., Manglik, A., and Kruse, A. C. (2018) Yeast surface display platform for rapid discovery of conformationally selective nanobodies. *Nat. Struct. Mol. Biol.* **25**, 289–296

169. Song, X., Lu, L., Passioura, T., and Suga, H. (2017) Macrocyclic peptide inhibitors for the protein–protein interaction of Zaire Ebola virus protein 24 and karyopherin alpha 5. *Org. Biomol. Chem.* **15**, 5155–5160

170. Wang, Y., McNutt, M. C., Banfi, S., Levin, M. G., Holland, W. L., Gusarova, V., Gromada, J., Cohen, J. C., and Hobbs, H. H. (2015) Hepatic ANGPTL3 regulates adipose tissue energy homeostasis. *Proc. Natl. Acad. Sci.* **112**, 11630–11635

171. Dijk, W., and Kersten, S. (2016) Regulation of lipid metabolism by angiopoietin-like proteins. *Curr. Opin. Lipidol.* **27**, 249–256

172. Essalmani, R., Susan-Resiga, D., Chamberland, A., Asselin, M. C., Canuel, M., Constam, D., Creemers, J. W., Day, R., Gauthier, D., Prat, A., and Seidah, N. G. (2013) Furin is the primary in vivo convertase of angiopoietin-like 3 and endothelial lipase in hepatocytes. *J. Biol. Chem.* **288**, 26410–26418

173. Lookene, A., Chevreuil, O., Østergaard, P., and Olivecrona, G. (1996) Interaction of Lipoprotein Lipase with Heparin Fragments and with Heparan Sulfate: Stoichiometry, Stabilization, and Kinetics †. *Biochemistry*. **35**, 12155–12163

174. Cazes, A., Galaup, A., Chomel, C., Bignon, M., Bréchot, N., Le Jan, S., Weber, H., Corvol, P., Muller, L., Germain, S., and Monnot, C. (2006) Extracellular Matrix–Bound Angiopoietin-Like 4 Inhibits Endothelial Cell Adhesion, Migration, and Sprouting and Alters Actin Cytoskeleton. *Circ. Res.* **99**, 1207–1215

175. Fischetti, R., Stepanov, S., Rosenbaum, G., Barrea, R., Black, E., Gore, D., Heurich, R., Kondrashkina, E., Kropf, A. J., Wang, S., Zhang, K., Irving, T. C., and Bunker, G. B. (2004) The BioCat undulator beamline 18ID: A facility for biological non-crystalline diffraction and X-ray absorption spectroscopy at the Advanced Photon Source. *J.*

Synchrotron Radiat. **11**, 399–405

176. Hopkins, J. B., Gillilan, R. E., and Skou, S. (2017) BioXTAS RAW : improvements to a free open-source program for small-angle X-ray scattering data reduction and analysis. *J. Appl. Crystallogr.* **50**, 1545–1553

177. Franke, D., Petoukhov, M. V., Konarev, P. V., Panjkovich, A., Tuukkanen, A., Mertens, H. D. T., Kikhney, A. G., Hajizadeh, N. R., Franklin, J. M., Jeffries, C. M., and Svergun, D. I. (2017) ATSAS 2.8: A comprehensive data analysis suite for small-angle scattering from macromolecular solutions. *J. Appl. Crystallogr.* **50**, 1212–1225

178. Franke, D., and Svergun, D. I. (2009) DAMMIF, a program for rapid ab-initio shape determination in small-angle scattering. *J. Appl. Crystallogr.* **42**, 342–346

179. Svergun, D. I. (1999) Restoring low resolution structure of biological macromolecules from solution scattering using simulated annealing. *Biophys. J.* **76**, 2879–86

180. Xu, Y., Chandarajoti, K., Zhang, X., Pagadala, V., Dou, W., Hoppensteadt, D. M., Sparkenbaugh, E. M., Cooley, B., Daily, S., Key, N. S., Severynse-Stevens, D., Fareed, J., Linhardt, R. J., Pawlinski, R., and Liu, J. (2017) Synthetic oligosaccharides can replace animal-sourced low-molecular weight heparins. *Sci. Transl. Med.* **9**, 1–21

181. Miller, C. M., Xu, Y., Kudrna, K. M., Hass, B. E., Kellar, B. M., Egger, A. W., Liu, J., and Harris, E. N. (2018) 3- O sulfation of heparin leads to hepatotropism and longer circulatory half-life. *Thromb. Res.* **167**, 80–87

182. Classen, S., Hura, G. L., Holton, J. M., Rambo, R. P., Rodic, I., McGuire, P. J., Dyer, K., Hammel, M., Meigs, G., Frankel, K. A., and Tainer, J. A. (2013) Implementation and performance of SIBYLS: a dual endstation small-angle X-ray scattering and macromolecular crystallography beamline at the Advanced Light Source. *J. Appl. Crystallogr.* **46**, 1–13

183. Trewhella, J., Duff, A. P., Durand, D., Gabel, F., Guss, J. M., Hendrickson, W. A., Hura, G. L., Jacques, D. A., Kirby, N. M., Kwan, A. H., Pérez, J., Pollack, L., Ryan, T. M., Sali, A., Schneidman-Duhovny, D., Schwede, T., Svergun, D. I., Sugiyama, M., Tainer, J. A., Vachette, P., Westbrook, J., and Whitten, A. E. (2017) 2017 publication guidelines for structural modelling of small-angle scattering data from biomolecules in solution: an update. *Acta Crystallogr. Sect. D Struct. Biol.* **73**, 710–728

184. Zhang, L., Lookene, A., Wu, G., and Olivecrona, G. (2005) Calcium triggers folding of lipoprotein lipase into active dimers. *J. Biol. Chem.* **280**, 42580–91

185. Bengtsson, G., and Olivecrona, T. (1977) Interaction of lipoprotein lipase with heparin-sepharose. Evaluation of conditions for affinity binding. *Biochem. J.* **167**, 109–119

186. Edwards, K., Chan, R. Y., and Sawyer, W. H. (1994) Interactions between fatty acids and lipoprotein lipase: specific binding and complex formation. *Biochemistry*. **33**, 13304–11

187. Hoylaerts, M., Owen, W. G., and Collen, D. (1984) Involvement of heparin chain length in the heparin-catalyzed inhibition of thrombin by antithrombin III. *J. Biol. Chem.* **259**, 5670–5677

188. Björk, I., and Lindahl, U. (1982) Mechanism of the anticoagulant action of heparin. *Mol. Cell. Biochem.* **48**, 161–182

189. Finley, A., and Greenberg, C. (2013) Heparin Sensitivity and Resistance: Management During Cardiopulmonary Bypass. *Anesth. Analg.* **116**, 1210–1222

190. Kristensen, K. K., Leth-Espensen, K. Z., Mertens, H. D. T., Birrane, G., Meiyappan, M., Olivecrona, G., Jørgensen, T. J. D., Young, S. G., and Ploug, M. (2020) Unfolding of monomeric lipoprotein lipase by ANGPTL4: Insight into the regulation of plasma triglyceride metabolism. *Proc. Natl. Acad. Sci.* 10.1073/pnas.1920202117

191. Liu, A. (2018) From old behemoth Lipitor to new king Humira: Best-selling U.S. drugs over 25 years | FiercePharma. *FiercePharma*

192. World Health Organization (2018) WHO - The top 10 causes of death. *World Heal. Organ.* [online] http://www.who.int/en/news-room/fact-sheets/detail/the-top-10-causes-of-death (Accessed March 2, 2020)

193. Nevola, L., and Giralt, E. (2015) Modulating protein-protein interactions: The potential of peptides. *Chem. Commun.* **51**, 3302–3315

194. Carter, P. J., and Lazar, G. A. (2018) Next generation antibody drugs: Pursuit of the “high-hanging fruit.” *Nat. Rev. Drug Discov.* **17**, 197–223

195. Kersten, S. (2017) Angiopoietin-like 3 in lipoprotein metabolism. *Nat. Rev. Endocrinol.* 10.1038/nrendo.2017.119

196. Shimamura, M., Matsuda, M., Yasumo, H., Okazaki, M., Fujimoto, K., Kono, K., Shimizugawa, T., Ando, Y., Koishi, R., Kohama, T., Sakai, N., Kotani, K., Komuro, R., Ishida, T., Hirata, K., Yamashita, S., Furukawa, H., and Shimomura, I. (2007) Angiopoietin-like protein3 regulates plasma HDL cholesterol through suppression of endothelial lipase. *Arterioscler. Thromb. Vasc. Biol.* **27**, 366–372

197. Chuang, Y.-J., Swanson, R., Raja, S. M., and Olson, S. T. (2001) Heparin Enhances the Specificity of Antithrombin for Thrombin and Factor Xa Independent of the Reactive Center Loop Sequence. *J. Biol. Chem.* **276**, 14961–14971

198. Mattijssen, F., Alex, S., Swarts, H. J., Groen, A. K., van Schothorst, E. M., and Kersten, S. (2014) Angptl4 serves as an endogenous inhibitor of intestinal lipid digestion. *Mol. Metab.* **3**, 135–144

199. Chi, X., Shetty, S. K., Shows, H. W., Hjelmaas, A. J., Malcolm, E. K., and Davies, B. S. J. (2015) Angiopoietin-like 4 modifies the interactions between lipoprotein lipase and its endothelial cell transporter GPIHBP1. *J. Biol. Chem.* **290**, 11865–11877

200. Lichtenstein, L., Berbée, J. F. P., Van Dijk, S. J., Van Dijk, K. W., Bensadoun, A., Kema, I. P., Voshol, P. J., Müller, M., Rensen, P. C. N., and Kersten, S. (2007) Angptl4 upregulates cholesterol synthesis in liver via inhibition of LPL- and HL-dependent hepatic cholesterol uptake. *Arterioscler. Thromb. Vasc. Biol.* **27**, 2420–2427